Training Dynamics of In-Context Learning in Linear Attention

Yedi Zhang[1], **Aaditya K. Singh**[1], **Peter E. Latham**[1,*], and **Andrew Saxe**[1,2,*]

[1]Gatsby Computational Neuroscience Unit, University College London
[2]Sainsbury Wellcome Centre, University College London
[*]Co-senior authors

Abstract

While attention-based models have demonstrated the remarkable ability of in-context learning, the theoretical understanding of how these models acquired this ability through gradient descent training is still preliminary. Towards answering this question, we study the gradient descent dynamics of multi-head linear self-attention trained for in-context linear regression. We examine two parametrizations of linear self-attention: one with the key and query weights merged as a single matrix (common in theoretical studies), and one with separate key and query matrices (closer to practical settings). For the merged parametrization, we show the training dynamics has two fixed points and the loss trajectory exhibits a single, abrupt drop. We derive an analytical time-course solution for a certain class of datasets and initialization. For the separate parametrization, we show the training dynamics has exponentially many fixed points and the loss exhibits saddle-to-saddle dynamics, which we reduce to scalar ordinary differential equations. During training, the model implements principal component regression in context with the number of principal components increasing over training time. Overall, we characterize how in-context learning abilities evolve during gradient descent training of linear attention, revealing dynamics of abrupt acquisition versus progressive improvements in models with different parametrizations.

1 Introduction

Self-attention-based models, such as transformers (Vaswani et al. 2017), exhibit a remarkable ability known as in-context learning (Brown et al. 2020). That is, these models can solve unseen tasks based on exemplars in the context of an input prompt. In-context learning is critical to the flexibility of large language models, allowing them to solve tasks not explicitly included in their training data. However, it remains unclear how architectures like self-attention acquire this ability through gradient descent training.

Seminal work by Olsson et al. (2022) identified an intriguing trait of the training dynamics of in-context learning: the in-context learning ability often emerges abruptly, coinciding with an abrupt drop in loss during training. This abrupt learning phase can reflect the formation of an induction head in the in-context learning setting (Olsson et al. 2022; Reddy 2024; Singh et al. 2024; Edelman et al. 2024), and also occur more broadly in transformer training dynamics, such as during grokking (Nanda et al. 2023), extracting syntactic relations (A. Chen et al. 2024), learning a new step in a multi-step task (Hoffmann et al. 2024), and learning a higher-order interaction among input tokens (Rende et al. 2024). Furthermore, Singh et al. (2023) found that in-context learning may often be a transient ability that the transformers acquire and then lose over the course of long training time, a phenomenon that has since been reproduced in many settings (He et al. 2024; Anand et al. 2024; B. Chan et al. 2024; Nguyen and Reddy 2024; Park et al. 2024). These findings underscore the importance of understanding not only the in-context learning ability in trained models, but also its full training dynamics.

This work aims to provide a theoretical description of how the in-context learning ability evolves in gradient descent training. To do so, we consider the increasingly common setup of linear self-attention[1] (Von Oswald et al. 2023) trained on an in-context linear regression task (Garg et al. 2022). The in-context linear regression task, in which the model needs to perform linear regression on the data in context, is a canonical instantiation of in-context learning (Garg et al. 2022; Akyürek et al. 2023; Von Oswald et al. 2023; Ahn et al. 2023). The linear attention model, which has been used in many prior studies (Schlag et al. 2021; Von Oswald et al. 2023; Ahn et al. 2023; Zhang et al. 2024a; Wu et al. 2024; Fu et al. 2024; Mahankali et al. 2024; Duraisamy 2024; Yingcong Li et al. 2024; Yau et al. 2024; Lu et al. 2024; Abedsoltan et al. 2024; Frei and Vardi 2024), reproduces key optimization properties of practical transformers (Ahn et al. 2024) and is more amenable to theoretical analysis. Importantly, despite its name, linear attention is a nonlinear model, as it removes the softmax operation but is still a nonlinear function of the input.

We study two common parametrizations of multi-head linear attention:

(i) $\mathsf{ATTN}_{\mathrm{M}}$, linear attention where the key and query matrices in each head are merged into a single matrix, a reparametrization procedure widely used in theoretical studies on transformers (Ahn et al. 2023; Tian et al. 2023; Ataee Tarzanagh et al. 2023; Zhang et al. 2024a,b; Siyu Chen et al. 2024a; Wu et al. 2024; Kim and Suzuki 2024; Y. Huang et al. 2024a; Ildiz et al. 2024; Ren et al. 2024; Tarzanagh et al. 2024; Vasudeva et al. 2024; Lu et al. 2024; Sitan Chen and Yuanzhi Li 2024; Julistiono et al. 2024; Yau et al. 2024; Anwar et al. 2024);

(ii) $\mathsf{ATTN}_{\mathrm{S}}$, linear attention with separate key and query matrices, which is closer to the implementation of attention in real-world transformers (Vaswani et al. 2017).

We specify the fixed points in the loss landscapes, as well as how gradient descent training dynamics traverses the landscape. Our findings are summarized as follows.

- We find two fixed points in the training dynamics of $\mathsf{ATTN}_{\mathrm{M}}$, and exponentially many fixed points in that of $\mathsf{ATTN}_{\mathrm{S}}$.
- We show a single, abrupt loss drop in training $\mathsf{ATTN}_{\mathrm{M}}$ from small initialization and derive an analytical time-course solution when the input token covariance is white. We show saddle-to-saddle training dynamics in training $\mathsf{ATTN}_{\mathrm{S}}$ from small initialization and reduce the high-dimensional training dynamics to scalar ordinary differential equations through an ansatz. We demonstrate the rank of the separate key and query weights affects the dynamics by shortening the duration of certain plateaus.
- We identify the in-context algorithm of the converged and early stopped models. When $\mathsf{ATTN}_{\mathrm{M}}$ and $\mathsf{ATTN}_{\mathrm{S}}$ are trained to convergence, they approximately implement least squares linear regression in context. When the training of $\mathsf{ATTN}_{\mathrm{S}}$ early stops during the $(m+1)$-th plateau of loss, it approximately implements principal component regression in context with the first m principal components.
- As a tool for our analysis, we show that when trained on in-context linear regression tasks, $\mathsf{ATTN}_{\mathrm{M}}$ is equivalent to a two-layer fully-connected linear network with a cubic feature map as input, and $\mathsf{ATTN}_{\mathrm{S}}$ is equivalent to a sum of three-layer convolutional linear networks with the same cubic feature map as input.

Comparing the two models, we find that the in-context learning ability evolves differently in them: $\mathsf{ATTN}_{\mathrm{M}}$ acquires the in-context linear regression ability through one abrupt loss drop, while $\mathsf{ATTN}_{\mathrm{S}}$ acquires this ability by *progressively improving* on in-context principal component regression. This makes a theoretical case for the progressive acquisition of in-context learning in gradient descent training. Our results also reveal how parametrization, such as merged versus separate key and query and the rank of the separate key and

[1]We will refer to linear self-attention as linear attention throughout this paper.

query weights, impacts the loss landscape and training dynamics. This motivates future research to take the parametrization factor into account when studying the landscape and dynamics of attention models.

2 Preliminaries

Notation. Non-bold small and capital symbols are scalars. Bold small symbols are column vectors. Bold capital symbols are matrices. $\|\cdot\|$ denotes the ℓ^2 norm of a vector or the Frobenius norm of a matrix. $\texttt{vec}(\cdot)$ represents flattening a matrix to a column vector by stacking its columns. For example, $\texttt{vec}\begin{bmatrix}1 & 3\\ 2 & 4\end{bmatrix} = \begin{bmatrix}1 & 2 & 3 & 4\end{bmatrix}^\top$. We use $i = 1, \cdots, H$ to denote the index of an attention head, $\mu = 1, \cdots, P$ to denote the index of a training sample, and $n = 1, \cdots, N$ to denote the index of a token within a sample.

2.1 In-Context Linear Regression Task

We study a standard in-context learning task of predicting the next token. The input is a sequence $\{\boldsymbol{x}_1, y_1, \boldsymbol{x}_2, y_2, \cdots, \boldsymbol{x}_N, y_N, \boldsymbol{x}_q\}$ and the desired output is y_q. We refer to $\boldsymbol{x}_q$ as the query token, $\{\boldsymbol{x}_1, y_1, \boldsymbol{x}_2, y_2, \cdots, \boldsymbol{x}_N, y_N\}$ as the context, and N as the context length. By convention (Ahn et al. 2023; Zhang et al. 2024a,b; Siyu Chen et al. 2024a; Y. Huang et al. 2024a), the input sequence is presented to the model as a matrix $\boldsymbol{X}$, defined as

$$\boldsymbol{X} = \begin{bmatrix}\boldsymbol{x}_1 & \boldsymbol{x}_2 & \cdots & \boldsymbol{x}_N & \boldsymbol{x}_q\\ y_1 & y_2 & \cdots & y_N & 0\end{bmatrix} \in \mathbb{R}^{(D+1)\times(N+1)}, \tag{1}$$

where $\boldsymbol{x}_1, \cdots, \boldsymbol{x}_N, \boldsymbol{x}_q \in \mathbb{R}^D$ and $y_1, \cdots, y_N \in \mathbb{R}$.

We are given a dataset $\{\boldsymbol{X}_\mu, y_{\mu,q}\}_{\mu=1}^P$ consisting of P samples. All $\boldsymbol{x}$ tokens are independently sampled from a D-dimensional zero-mean normal distribution with covariance $\boldsymbol{\Lambda}$,

$$\boldsymbol{x}_{\mu,n}, \boldsymbol{x}_{\mu,q} \sim N(\boldsymbol{0}, \boldsymbol{\Lambda}), \quad n = 1, \cdots, N,\ \mu = 1, \cdots, P. \tag{2}$$

We consider the in-context linear regression task, where the y_n in context and the target output y_q are generated as a linear map of the corresponding $\boldsymbol{x}_n$ and $\boldsymbol{x}_q$ (Garg et al. 2022). For each sequence $\boldsymbol{X}_\mu$, we independently sample a task vector $\boldsymbol{w}_\mu$ from a D-dimensional standard normal distribution

$$\boldsymbol{w}_\mu \sim \mathcal{N}(\boldsymbol{0}, \boldsymbol{I}), \quad \mu = 1, \cdots, P, \tag{3}$$

and generate

$$y_{\mu,n} = \boldsymbol{w}_\mu^\top \boldsymbol{x}_{\mu,n},\ y_{\mu,q} = \boldsymbol{w}_\mu^\top \boldsymbol{x}_{\mu,q}, \quad n = 1, \cdots, N,\ \mu = 1, \cdots, P. \tag{4}$$

Note that the task vector $\boldsymbol{w}_\mu$ is fixed for all tokens in one sample sequence but varies across different samples, and is independent of the tokens $\boldsymbol{x}_{\mu,1}, \cdots, \boldsymbol{x}_{\mu,N}, \boldsymbol{x}_{\mu,q}$.

2.2 Multi-Head Self-Attention

A standard multi-head softmax self-attention layer (Vaswani et al. 2017) takes matrix $\boldsymbol{X}$ as input and returns a matrix of the same size,

$$\mathsf{ATTN}(\boldsymbol{X}) = \boldsymbol{X} + \sum_{i=1}^H \boldsymbol{W}_i^V \boldsymbol{X} \mathsf{softmax}\left(\frac{\boldsymbol{X}^\top \boldsymbol{W}_i^{K\top} \boldsymbol{W}_i^Q \boldsymbol{X}}{\rho}\right), \tag{5}$$

where H is the number of heads, ρ is a scaling factor, and $\boldsymbol{W}_i^V, \boldsymbol{W}_i^K, \boldsymbol{W}_i^Q$ are the trainable value, key, and query matrices in the i-th head. The prediction for y_q is the bottom right entry of the output matrix:

$$\hat{y}_q = \mathsf{ATTN}(\boldsymbol{X})_{D+1,N+1}. \tag{6}$$

In this work, we consider multi-head linear self-attention, where we remove the softmax operation and take $\rho = N$. Specifically, we study two common parametrizations of linear attention: (i) linear attention with merged key and query introduced in Section 2.3 and analyzed in Section 3; (ii) linear attention with separate key and query introduced in Section 2.4 and analyzed in Section 4.

2.3 Multi-Head Linear Attention with Merged Key and Query

The multi-head linear attention ATTN_M with the key and query matrices merged as a single matrix $\boldsymbol{W}^{K\top}\boldsymbol{W}^Q = \boldsymbol{W}^{KQ}$ computes

$$\begin{aligned}\mathsf{ATTN}_\mathrm{M}(\boldsymbol{X}) &= \boldsymbol{X} + \sum_{i=1}^{H} \frac{1}{N}\boldsymbol{W}_i^V \boldsymbol{X}\boldsymbol{X}^\top \boldsymbol{W}_i^{KQ}\boldsymbol{X} \\ &= \boldsymbol{X} + \sum_{i=1}^{H} \begin{bmatrix} * & * \\ \boldsymbol{v}_i^\top & v_i \end{bmatrix} \begin{bmatrix} \frac{1}{N}\left(\boldsymbol{x}_q\boldsymbol{x}_q^\top + \sum_n \boldsymbol{x}_n\boldsymbol{x}_n^\top\right) & \frac{1}{N}\sum_n \boldsymbol{x}_n y_n \\ \frac{1}{N}\sum_n y_n \boldsymbol{x}_n^\top & \frac{1}{N}\sum_n y_n^2 \end{bmatrix} \begin{bmatrix} \boldsymbol{U}_i & * \\ \boldsymbol{u}_i^\top & * \end{bmatrix} \boldsymbol{X}\end{aligned}$$

where we write the value matrix $\boldsymbol{W}_i^V$ and the merged key-query matrix $\boldsymbol{W}_i^{KQ}$ as block matrices,

$$\boldsymbol{W}_i^V = \begin{bmatrix} * & * \\ \boldsymbol{v}_i^\top & v_i \end{bmatrix}, \; \boldsymbol{W}_i^{KQ} = \begin{bmatrix} \boldsymbol{U}_i & * \\ \boldsymbol{u}_i^\top & * \end{bmatrix}.$$

The blocks have dimensionalities $\boldsymbol{v}_i \in \mathbb{R}^D, v_i \in \mathbb{R}, \boldsymbol{U}_i \in \mathbb{R}^{D\times D}, \boldsymbol{u}_i \in \mathbb{R}^D$. The $*$ blocks denote entries that do not contribute to the computation of $\mathsf{ATTN}(\boldsymbol{X})_{D+1,N+1}$. With the block matrix notations, the bottom right entry of $\mathsf{ATTN}_\mathrm{M}(\boldsymbol{X})$ is

$$\mathsf{ATTN}_\mathrm{M}(\boldsymbol{X})_{D+1,N+1} = \sum_{i=1}^{H} \begin{bmatrix} \boldsymbol{v}_i^\top & v_i \end{bmatrix} \begin{bmatrix} \frac{1}{N}\left(\boldsymbol{x}_q\boldsymbol{x}_q^\top + \sum_n \boldsymbol{x}_n\boldsymbol{x}_n^\top\right) & \frac{1}{N}\sum_n \boldsymbol{x}_n y_n \\ \frac{1}{N}\sum_n y_n \boldsymbol{x}_n^\top & \frac{1}{N}\sum_n y_n^2 \end{bmatrix} \begin{bmatrix} \boldsymbol{U}_i \\ \boldsymbol{u}_i^\top \end{bmatrix} \begin{bmatrix} \boldsymbol{x}_q \\ 0 \end{bmatrix}. \tag{7}$$

Following Ahn et al. (2023), Zhang et al. (2024a), Kim and Suzuki (2024), and Y. Huang et al. (2024a), we initialize $\boldsymbol{v}_i, \boldsymbol{u}_i = \boldsymbol{0}$ as they are not required for this model to achieve global minimum loss on the in-context linear regression task. When $\boldsymbol{v}_i$ and $\boldsymbol{u}_i$ are initialized to zero, they will remain zero throughout training (see Appendix C.1). With the reduction $\boldsymbol{v}_i, \boldsymbol{u}_i = \boldsymbol{0}$, the multi-head linear attention with merged key and query matrices computes

$$\mathsf{ATTN}_\mathrm{M}(\boldsymbol{X})_{D+1,N+1} = \sum_{i=1}^{H} v_i \boldsymbol{\beta}^\top \boldsymbol{U}_i \boldsymbol{x}_q, \tag{M}$$

where $\boldsymbol{\beta}$ denotes the correlation between $\boldsymbol{x}_n$ and y_n in context,

$$\boldsymbol{\beta} \equiv \frac{1}{N}\sum_{n=1}^{N} y_n \boldsymbol{x}_n. \tag{8}$$

2.4 Multi-head Linear Attention with Separate Key and Query

In multi-head attention with separate key and query matrices, we follow the standard practice (Vaswani et al. 2017) of using low-rank key and query matrices where the rank $R \leq D$. Additionally, we enforce $RH \geq D$ to prevent expressivity limitations from affecting the behaviors we study.[2] The multi-head linear attention ATTN_S with separate rank-R key and query matrices computes

$$\begin{aligned}
\mathsf{ATTN}_\mathsf{S}(\boldsymbol{X}) &= \boldsymbol{X} + \sum_{i=1}^{H} \frac{1}{N} \boldsymbol{W}_i^V \boldsymbol{X}\boldsymbol{X}^\top \boldsymbol{W}_i^{K\top} \boldsymbol{W}_i^Q \boldsymbol{X} \\
&= \boldsymbol{X} + \sum_{i=1}^{H} \begin{bmatrix} * & * \\ \boldsymbol{v}_i^\top & v_i \end{bmatrix} \begin{bmatrix} \frac{1}{N}\left(\boldsymbol{x}_q\boldsymbol{x}_q^\top + \sum_n \boldsymbol{x}_n\boldsymbol{x}_n^\top\right) & \frac{1}{N}\sum_n \boldsymbol{x}_n y_n \\ \frac{1}{N}\sum_n y_n\boldsymbol{x}_n^\top & \frac{1}{N}\sum_n y_n^2 \end{bmatrix} \begin{bmatrix} \boldsymbol{k}_{i,1} & \cdots & \boldsymbol{k}_{i,R} \\ k_{i,1} & \cdots & k_{i,R} \end{bmatrix} \begin{bmatrix} \boldsymbol{q}_{i,1}^\top & * \\ \vdots & \vdots \\ \boldsymbol{q}_{i,R}^\top & * \end{bmatrix} \boldsymbol{X}
\end{aligned}$$

where we write the value, key, and query weights in block form,

$$\boldsymbol{W}_i^V = \begin{bmatrix} * & * \\ \boldsymbol{v}_i^\top & v_i \end{bmatrix}, \ \boldsymbol{W}_i^K = \begin{bmatrix} \boldsymbol{k}_{i,1}^\top & k_{i,1} \\ \vdots & \vdots \\ \boldsymbol{k}_{i,R}^\top & k_{i,R} \end{bmatrix}, \ \boldsymbol{W}_i^Q = \begin{bmatrix} \boldsymbol{q}_{i,1}^\top & * \\ \vdots & \vdots \\ \boldsymbol{q}_{i,R}^\top & * \end{bmatrix}.$$

The blocks have dimensionalities $v_i, k_{i,r} \in \mathbb{R}$ and $\boldsymbol{v}_i, \boldsymbol{k}_{i,r}, \boldsymbol{q}_{i,r} \in \mathbb{R}^D$. Similarly to the case with merged key and query, we initialize $\boldsymbol{v}_i = \boldsymbol{0}, k_{i,r} = 0$; they will remain zero throughout training (see Appendix E.1). With $\boldsymbol{v}_i = \boldsymbol{0}$ and $k_{i,r} = 0$, the multi-head linear attention with separate rank-one key and query matrices computes

$$\mathsf{ATTN}_\mathsf{S}(\boldsymbol{X})_{D+1,N+1} = \sum_{i=1}^{H} v_i \boldsymbol{\beta}^\top \begin{bmatrix} \boldsymbol{k}_{i,1} & \cdots & \boldsymbol{k}_{i,R} \end{bmatrix} \begin{bmatrix} \boldsymbol{q}_{i,1}^\top \\ \vdots \\ \boldsymbol{q}_{i,R}^\top \end{bmatrix} \boldsymbol{x}_q = \sum_{i=1}^{H}\sum_{r=1}^{R} v_i \boldsymbol{\beta}^\top \boldsymbol{k}_{i,r} \boldsymbol{q}_{i,r}^\top \boldsymbol{x}_q, \tag{S}$$

where $\boldsymbol{\beta}$ is the input-output correlation in context defined in Equation (8). The expression of Equation (S) already reveals interesting insight. It implies that linear attention with H heads and rank-R key and query differs from linear attention with RH heads and rank-one key and query only in the sharing of certain value weights.

2.5 Gradient Flow Training Dynamics

We train the multi-head linear attention model with gradient descent on mean square error loss. We consider the population loss, that is the limit of infinite training samples, $P \to \infty$,

$$\mathcal{L} = \lim_{P\to\infty} \frac{1}{P} \sum_{\mu=1}^{P} (y_{\mu,q} - \hat{y}_{\mu,q})^2 = \mathbb{E}(y_q - \hat{y}_q)^2 \,. \tag{9}$$

We analyze the gradient flow dynamics on the loss, given by

$$\tau \frac{\mathrm{d}\boldsymbol{W}}{\mathrm{d}t} = -\frac{1}{2}\frac{\partial \mathcal{L}}{\partial \boldsymbol{W}} = \mathbb{E}\left[(y_q - \hat{y}_q)\frac{\partial \hat{y}_q}{\partial \boldsymbol{W}}\right], \tag{10}$$

where τ is the time constant. The gradient flow dynamics captures the behavior of gradient descent in the limit of an infinitesimal learning rate.

[2] In practice, usually $RH = D$.

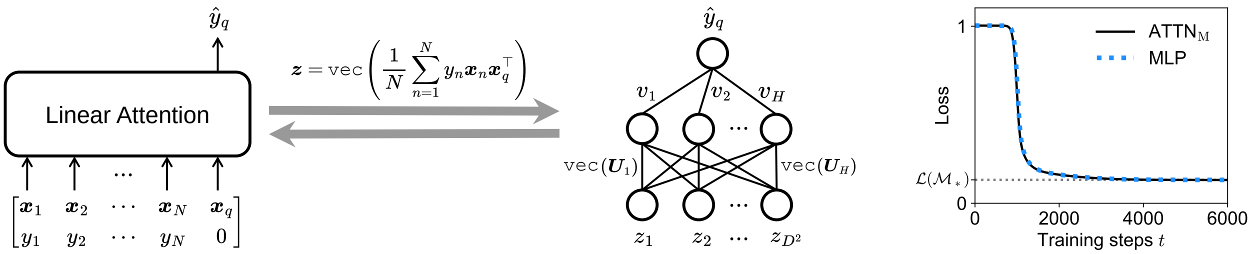

Figure 1: Multi-head linear attention with merged key and query $\mathsf{ATTN}_\mathsf{M}(\boldsymbol{X})_{D+1,N+1}$ is equivalent to a two-layer fully-connected linear network with cubic feature input $\mathsf{MLP}(\boldsymbol{z})$. *Left*: Schematic of the equivalence. *Right*: Loss trajectories of linear attention and the fully-connected linear network match well. The two models are trained with the same data and initialization. Both exhibit the characteristic abrupt loss drop documented by prior work on the in-context learning dynamics in linear (Von Oswald et al. 2023) and softmax attention (Singh et al. 2024). Here $D = 4, N = 32, H = 8$.

3 Linear Attention with Merged Key and Query

We first study multi-head linear attention with the key and query matrices merged as a single matrix, as described by Equation (M).

3.1 Equivalence to Two-Layer Fully-Connected Linear Networks

The H-head linear attention with input sequence $\boldsymbol{X}$ defined in Equation (M) can be viewed as a two-layer width-H fully-connected linear network with a cubic feature $\boldsymbol{z}(\boldsymbol{X})$ as input,

$$\mathsf{ATTN}_\mathsf{M}(\boldsymbol{X})_{D+1,N+1} = \sum_{i=1}^{H} v_i \boldsymbol{\beta}^\top \boldsymbol{U}_i \boldsymbol{x}_q = \sum_{i=1}^{H} v_i \mathtt{vec}(\boldsymbol{U}_i)^\top \mathtt{vec}\left(\boldsymbol{\beta}\boldsymbol{x}_q^\top\right) = \boldsymbol{w}_2^\top \boldsymbol{W}_1 \boldsymbol{z} = \mathsf{MLP}(\boldsymbol{z}), \quad (11)$$

where

$$\boldsymbol{w}_2 = \begin{bmatrix} v_1 \\ v_2 \\ \vdots \\ v_H \end{bmatrix}, \boldsymbol{W}_1 = \begin{bmatrix} \mathtt{vec}(\boldsymbol{U}_1)^\top \\ \mathtt{vec}(\boldsymbol{U}_2)^\top \\ \vdots \\ \mathtt{vec}(\boldsymbol{U}_H)^\top \end{bmatrix}, \boldsymbol{z}(\boldsymbol{X}) = \mathtt{vec}\left(\boldsymbol{\beta}\boldsymbol{x}_q^\top\right). \quad (12)$$

The blue expression in Equation (11) can be understood through the definition of the quadratic form $\boldsymbol{\beta}^\top \boldsymbol{U}_i \boldsymbol{x}_q$. The feature $\boldsymbol{z} \in \mathbb{R}^{D^2}$, whose entries are cubic functions of the entries in the original sequence $\boldsymbol{X}$, is the input to the equivalent two-layer fully-connected linear network. The stacked value weights correspond to the second-layer weights $\boldsymbol{w}_2 \in \mathbb{R}^H$ of the fully-connected linear network. The stacked merged key-query weights correspond to the first-layer weights $\boldsymbol{W}_1 \in \mathbb{R}^{H \times D^2}$ of the fully-connected linear network. A schematic of this equivalence is given in Figure 1.

The somewhat surprising and useful fact here is that the linear attention in this regime is equivalent to a *fully-connected* linear network (with cubic features of $\boldsymbol{X}$ as input). It is evident that the linear attention is a cubic function of $\boldsymbol{X}$ given its definition in Equation (M), while it is less evident that the cubic function is a fully-connected linear network of $\boldsymbol{z}(\boldsymbol{X})$. This equivalence draws a connection between the well-established fully-connected linear network and the more recent attention model, enabling us to apply the theoretical machinery of the former to the latter.

3.2 Loss Landscape: Two Fixed Points

The gradient flow training dynamics of the linear attention or the equivalent two-layer fully-connected linear network given in Equation (11) is

$$\tau \dot{\boldsymbol{W}}_1 = \boldsymbol{w}_2 \left(\mathbb{E}\left(y_q \boldsymbol{z}^\top \right) - \boldsymbol{w}_2^\top \boldsymbol{W}_1 \mathbb{E}\left(\boldsymbol{z}\boldsymbol{z}^\top \right) \right), \tag{13a}$$

$$\tau \dot{\boldsymbol{w}}_2 = \boldsymbol{W}_1 \left(\mathbb{E}\left(y_q \boldsymbol{z}^\top \right) - \boldsymbol{w}_2^\top \boldsymbol{W}_1 \mathbb{E}\left(\boldsymbol{z}\boldsymbol{z}^\top \right) \right)^\top. \tag{13b}$$

There are two manifolds of fixed points in this dynamical system: one is the unstable fixed point at zero, denoted $\mathcal{M}_0$, and the other is a manifold of stable fixed points at the global minimum, denoted $\mathcal{M}_*$,

$$\mathcal{M}_0 = \{\boldsymbol{w}_2 = \boldsymbol{0}, \boldsymbol{W}_1 = \boldsymbol{0}\} \tag{14a}$$

$$\mathcal{M}_* = \left\{ \boldsymbol{w}_2, \boldsymbol{W}_1 \middle| \boldsymbol{w}_2^\top \boldsymbol{W}_1 = \mathbb{E}\left(y_q \boldsymbol{z}^\top \right) \mathbb{E}\left(\boldsymbol{z}\boldsymbol{z}^\top \right)^{-1} \right\} \tag{14b}$$

3.3 Training Dynamics: An Abrupt Drop in the Loss

We have shown the linear attention defined in Equation (M) is equivalent to a fully-connected linear network with cubic feature input. Since this equivalence holds at the level of the computation of the model, the equivalence applies to the training dynamics with any initialization and optimizer. Here we discuss the training dynamics of gradient flow from small initialization, commonly referred to as the rich learning regime (Woodworth et al. 2020).

With small initialization, the network is initially near the unstable fixed point, $\mathcal{M}_0$, at zero. As training progresses, the network escapes from the unstable fixed point, and subsequently converges to a stable fixed point on the global minimum manifold, $\mathcal{M}_*$. The time it takes to escape from the unstable fixed point is approximately $\frac{\tau}{\|\boldsymbol{\Lambda}^2\|} \ln \frac{1}{w_{\text{init}}}$, where the initialization scale w_{init} is the initial ℓ^2 norm of a layer (see Appendix C.6.1). Because the time to escape from the unstable fixed point starting from small initialization is long, the loss exhibits an initial plateau followed by an abrupt drop, as validated by simulations in Figure 1. In particular, when the input token covariance is white $\boldsymbol{\Lambda} = \boldsymbol{I}$ and the initialization is infinitesimally small, we derive an analytical time-course solution in Appendix C.5 exploiting the equivalence between linear attention and linear networks (Saxe et al. 2014) and obtain

$$\mathsf{ATTN}_{\mathrm{M}}(\boldsymbol{X}; t)_{D+1,N+1} = \sigma(t) \boldsymbol{\beta}^\top \boldsymbol{x}_q, \quad \text{where } \sigma(t) = \frac{e^{2\sqrt{D}\frac{t}{\tau}}}{\left(1 + \frac{1+D}{N}\right)\left(e^{2\sqrt{D}\frac{t}{\tau}} - 1\right) + \frac{\sqrt{D}}{w_{\text{init}}^2}}. \tag{15}$$

Since $\sigma(t)$ is a rescaled and shifted sigmoid function, the weights and the loss trajectories have sigmoidal shapes, characterized by a plateau followed by a rapid drop.

3.4 In-Context Algorithm: Least Squares Regression

When the linear attention model converges to the global minimum manifold $\mathcal{M}_*$ at the end of training, the model implements

$$\mathsf{ATTN}_{\mathrm{M}}(\boldsymbol{X})_{D+1,N+1} = \mathbb{E}\left(y_q \boldsymbol{z}^\top \right) \mathbb{E}\left(\boldsymbol{z}\boldsymbol{z}^\top \right)^{-1} \boldsymbol{z} = \boldsymbol{\beta}^\top \left(\boldsymbol{\Lambda} + \frac{\boldsymbol{\Lambda} + \mathtt{tr}(\boldsymbol{\Lambda})\boldsymbol{I}}{N} \right)^{-1} \boldsymbol{x}_q, \tag{16}$$

where the first equality follows directly from Equations (11) and (14b) and the second equality is proved in Appendix C.4. Equation (16) reveals an intriguing duality: the linear regression solution in the cubic feature space of $\boldsymbol{z}$ is the in-context linear regression solution in the original space of the $\boldsymbol{x}_n, y_n$ token pairs in a sequence $\boldsymbol{X}$. The middle expression in Equation (16) is the linear regression solution of fitting $y_{\mu,q}$ with $\boldsymbol{z}_\mu$ for all training sequences $\mu = 1, \cdots, P$. The last expression in Equation (16) is approximately the in-context linear regression solution, which fits $y_{\mu,n}$ with $\boldsymbol{x}_{\mu,n}(n = 1, \cdots, N)$ for each sequence $\boldsymbol{X}_\mu$. The approximation is exact when the sequence length N is large:

$$\lim_{N\to\infty} \boldsymbol{\beta}^\top \left(\boldsymbol{\Lambda} + \frac{\boldsymbol{\Lambda} + \mathtt{tr}(\boldsymbol{\Lambda})\boldsymbol{I}}{N} \right)^{-1} \boldsymbol{x}_q = \boldsymbol{\beta}^\top \boldsymbol{\Lambda}^{-1} \boldsymbol{x}_q.$$

Here $\boldsymbol{\beta}$ is the $\boldsymbol{x}, y$ correlation in a sequence $\boldsymbol{X}$, and $\boldsymbol{\Lambda}$ is the covariance of all $\boldsymbol{x}$ tokens in all training sequences, which approximates the covariance of $\boldsymbol{x}$ in each individual sequence.

3.5 Conservation Law: All Heads Are Parallel

The weights in a fully-connected linear network are known to obey a conservation law during training (Fukumizu 1998; Saxe et al. 2014; Du et al. 2018; Ji and Telgarsky 2019)

$$\frac{\mathrm{d}}{\mathrm{d}t} \left(\boldsymbol{w}_2 \boldsymbol{w}_2^\top - \boldsymbol{W}_1 \boldsymbol{W}_1^\top \right) = \boldsymbol{0}, \tag{17}$$

which follows directly from the gradient flow dynamics in Equation (13). Under small initialization, the quantity $\boldsymbol{w}_2 \boldsymbol{w}_2^\top - \boldsymbol{W}_1 \boldsymbol{W}_1^\top \approx \boldsymbol{0}$ is small at initialization and remains small throughout training. Since the vector $\boldsymbol{w}_2$ is rank-one, the conservation law forces $\boldsymbol{W}_1$ to also be approximately rank-one, which means that the rows of $\boldsymbol{W}_1$ are approximately parallel. Since each row of $\boldsymbol{W}_1$ is the vectorized merged key-query matrix of a head, $\mathtt{vec}(\boldsymbol{U}_i)$, a rank-one $\boldsymbol{W}_1$ implies that the key-query weight matrices of all heads are parallel, differing only in scale. As shown in Figure 6, simulations indeed show that the key-query weights in different heads are parallel.

4 Linear Attention with Separate Rank-One Key and Query

We now study multi-head linear attention with separate low-rank key and query matrices. Because the rank-one case captures most of the behaviors of the general rank-R case, we focus on the rank-one case in this section and defer the rank-R case to Section 5. When $R = 1$, the model definition in Equation (S) simplifies to

$$\mathsf{ATTN}_\mathsf{S}(\boldsymbol{X})_{D+1,N+1} = \sum_{i=1}^{H} v_i \boldsymbol{\beta}^\top \boldsymbol{k}_i \boldsymbol{q}_i^\top \boldsymbol{x}_q. \tag{18}$$

4.1 Equivalence to Three-Layer Convolutional Linear Networks

The single-head linear attention with separate rank-one key and query can be viewed as a convolutional linear network with the cubic feature $\boldsymbol{z}$ defined in Equation (12) as input, and the multi-head case is a sum of such convolutional linear networks. Specifically, Equation (18) can be rewritten as a sum of H three-layer convolutional linear networks

$$\mathsf{ATTN}_\mathsf{S}(\boldsymbol{X})_{D+1,N+1} = \sum_{i=1}^{H} v_i \boldsymbol{q}_i^\top \boldsymbol{K}_i \boldsymbol{z}, \quad \text{where } \boldsymbol{K}_i = \begin{bmatrix} \boldsymbol{k}_i^\top & \boldsymbol{0}_D^\top & \dots & \boldsymbol{0}_D^\top \\ \boldsymbol{0}_D^\top & \boldsymbol{k}_i^\top & \dots & \boldsymbol{0}_D^\top \\ \vdots & \vdots & \ddots & \vdots \\ \boldsymbol{0}_D^\top & \boldsymbol{0}_D^\top & \dots & \boldsymbol{k}_i^\top \end{bmatrix} \in \mathbb{R}^{D \times D^2}.$$

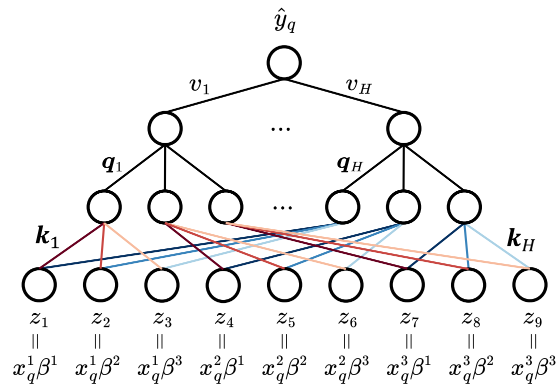

Figure 2: Multi-head linear attention with separate rank-one key and query $\mathsf{ATTN}_\mathrm{S}(\boldsymbol{X})_{D+1,N+1}$ is a sum of H (number of heads) three-layer convolutional linear networks with the cubic feature $\boldsymbol{z}$ as input. Here we take $D = 3$ to avoid clutter. Entries in the vectors are denoted as $\boldsymbol{x}_q = \left[x_q^1, x_q^2, x_q^3\right]^\top, \boldsymbol{\beta} = \left[\beta^1, \beta^2, \beta^3\right]^\top$.

The matrix $\boldsymbol{K}_i$ is a convolutional matrix with kernel size D and stride D. A schematic of this three-layer convolutional linear network is provided in Figure 2. We do not explicitly use the equivalence to linear convolutional networks in our derivations, but it provides intuition and may be of independent interest to studies on the geometry of linear convolutional networks (Kohn et al. 2022, 2024a,b) and attention (Henry et al. 2024).

When the number of heads satisfies $H \geq D$, the linear attention with separate rank-one key and query, $\mathsf{ATTN}_\mathrm{S}(\boldsymbol{X})$, can express any linear map of $\boldsymbol{z}(\boldsymbol{X})$ and has the same expressivity as linear attention with merged key and query, $\mathsf{ATTN}_\mathrm{M}(\boldsymbol{X})$. However, the two models, ATTN_M and ATTN_S, correspond to multi-layer linear networks with different connectivity and depths, resulting in different loss landscape (Kohn et al. 2022, 2024a) and training dynamics (Saxe et al. 2014, 2019), which we discuss next.

4.2 Loss Landscape: Exponential Number of Fixed Points

The gradient flow training dynamics of linear attention with separate rank-one key and query, derived in Appendix D.2, is given by

$$\tau \dot{v}_i = \boldsymbol{k}_i^\top \left(\boldsymbol{\Lambda}^2 - \mathbb{E}\left(\hat{\boldsymbol{\Lambda}}^2\right) \sum_{i'=1}^H v_{i'} \boldsymbol{k}_{i'} \boldsymbol{q}_{i'}^\top \boldsymbol{\Lambda} \right) \boldsymbol{q}_i, \tag{19a}$$

$$\tau \dot{\boldsymbol{k}}_i = v_i \left(\boldsymbol{\Lambda}^2 - \mathbb{E}\left(\hat{\boldsymbol{\Lambda}}^2\right) \sum_{i'=1}^H v_{i'} \boldsymbol{k}_{i'} \boldsymbol{q}_{i'}^\top \boldsymbol{\Lambda} \right) \boldsymbol{q}_i, \tag{19b}$$

$$\tau \dot{\boldsymbol{q}}_i = v_i \left(\boldsymbol{\Lambda}^2 - \boldsymbol{\Lambda} \sum_{i'=1}^H v_{i'} \boldsymbol{k}_{i'} \boldsymbol{q}_{i'}^\top \mathbb{E}\left(\hat{\boldsymbol{\Lambda}}^2\right) \right) \boldsymbol{k}_i, \tag{19c}$$

where $\hat{\boldsymbol{\Lambda}}$ represents the covariance of tokens $\{\boldsymbol{x}_n\}_{n=1}^N$ in context and the expectation of $\hat{\boldsymbol{\Lambda}}^2$ is

$$\mathbb{E}\left(\hat{\boldsymbol{\Lambda}}^2\right) \equiv \mathbb{E}\left(\frac{1}{N}\sum_{n=1}^N \boldsymbol{x}_n \boldsymbol{x}_n^\top\right)^2 = \boldsymbol{\Lambda}^2 + \frac{\boldsymbol{\Lambda} + \mathtt{tr}(\boldsymbol{\Lambda})\boldsymbol{I}}{N}\boldsymbol{\Lambda} \tag{20}$$

This dynamical system contains 2^D fixed points in the function space of $\mathsf{ATTN}_\mathrm{S}(\boldsymbol{X})_{D+1,N+1}$. We specify the fixed points below and prove the validity of them in Appendix D.3.

Let $\lambda_1, \cdots, \lambda_D$ be the eigenvalues of covariance matrix $\boldsymbol{\Lambda}$ arranged in descending order, and $\boldsymbol{e}_1, \cdots, \boldsymbol{e}_D$ be the corresponding normalized eigenvectors. We use $\mathcal{M}(\mathcal{S}_m)$ to denote a set of fixed points that correspond to learning m ($m = 0, 1, \cdots, D$) out of the D eigenvectors,

$$\mathcal{M}(\mathcal{S}_m) = \left\{ v_{1:H}, \boldsymbol{k}_{1:H}, \boldsymbol{q}_{1:H} \middle| \text{conditions (C1)-(C3) are met} \right\}, \tag{21}$$

where the set $\mathcal{S}_m$ specifies the indices of the learned eigenvectors,

$$\mathcal{S}_m \subseteq \{1, 2, \cdots, D\}, \; |\mathcal{S}_m| = m. \tag{22}$$

The three conditions for Equation (21) are:

(C1) The heads sum up to fit the eigenvectors with indices in set $\mathcal{S}_m$

$$\sum_{i=1}^{H} v_i \boldsymbol{k}_i \boldsymbol{q}_i^\top = \sum_{d \in \mathcal{S}_m} \lambda_d^{-1} \left(1 + \frac{1 + \mathtt{tr}(\boldsymbol{\Lambda})/\lambda_d}{N} \right)^{-1} \boldsymbol{e}_d \boldsymbol{e}_d^\top. \tag{23}$$

(C2) For heads with a nonzero value weight, $v_i \neq 0$, both $\boldsymbol{k}_i$ and $\boldsymbol{q}_i$ lie in the span of $\{\boldsymbol{e}_d\}_{d \in \mathcal{S}_m}$.

(C3) For heads with a zero value weight, $v_i = 0$, at least one of $\boldsymbol{k}_i$ or $\boldsymbol{q}_i$ lies in the span of $\{\boldsymbol{e}_d\}_{d \in \mathcal{S}_m}$.

Since there are $\binom{D}{m}$ possible ways of choosing m out of D indices to define $\mathcal{S}_m$ in Equation (22), the total number of possible choices summed over $m = 0, \cdots, D$ is $\sum_{m=0}^{D} \binom{D}{m} = 2^D$. Each choice corresponds to a different condition (C1) in Equation (23) and thus a different function, $\mathsf{ATTN}_\mathsf{S}(\boldsymbol{X})_{D+1,N+1}$. Therefore, the gradient flow dynamics in Equation (19) has 2^D fixed points in the function space.

In comparison with Section 3.2 where there were two fixed points in the dynamics of linear attention with merged key and query, there are now 2^D fixed points for linear attention with separate key and query. The two fixed points for linear attention with merged key and query in Equation (14) are contained in the 2^D fixed points in the separate case: the zero fixed point in Equation (14a) corresponds to $\mathcal{M}(\mathcal{S}_0)$, i.e., learning no eigenvector; the global minimum fixed point in Equation (14b) corresponds to $\mathcal{M}(\mathcal{S}_D)$, i.e., learning all D eigenvectors.

4.3 Training Dynamics: Saddle-to-Saddle Dynamics

Building on the exponentially many fixed points we have identified, we now analyze which fixed points are actually visited in gradient flow training and in what order. We find that starting from small initialization, the model visits $(D+1)$ out of the 2^D fixed points and exhibits saddle-to-saddle dynamics.

With small initialization, the model is initially near the unstable zero fixed point, $\mathcal{M}_0 = \mathcal{M}(\varnothing)$. As training progresses, the model sequentially visits the fixed points in $\mathcal{M}_1, \mathcal{M}_2, \cdots, \mathcal{M}_D$ where

$$\begin{aligned} \mathcal{M}_1 &= \mathcal{M}(\{1\}), \\ \mathcal{M}_2 &= \mathcal{M}(\{1, 2\}), \\ &\cdots \\ \mathcal{M}_D &= \mathcal{M}(\{1, 2, \cdots, D\}). \end{aligned}$$

That is, the model trained from small initialization sequentially learns to fit the first eigenvector (the eigenvector of $\boldsymbol{\Lambda}$ with the largest eigenvalue), the second eigenvector, and so on. As shown in Figure 3a, the loss goes through D abrupt drops in training, each corresponding to the transition from one fixed point to the next. The abrupt drops of loss are separated by plateaus, during which the model lingers in an unstable fixed

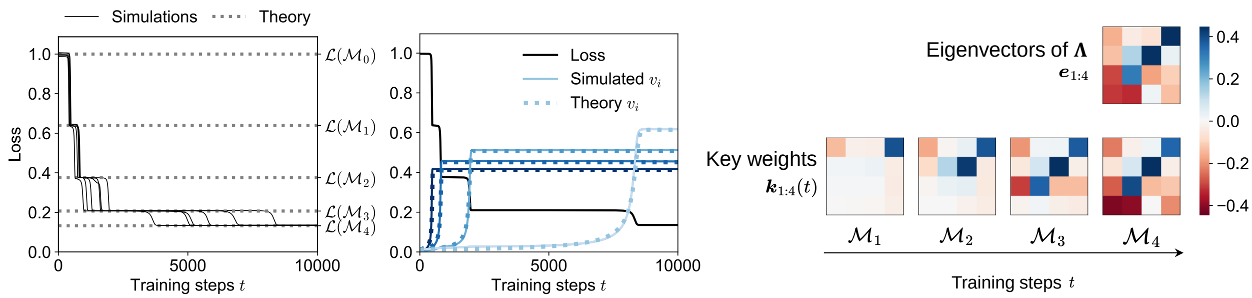

(a) Loss (b) Loss and value weights (c) Key weights and eigenvectors of $\mathbf{\Lambda}$

Figure 3: Multi-head linear attention with separate rank-one key and query exhibits saddle-to-saddle dynamics. (a) The loss trajectory has D abrupt drops, separated by plateaus (six runs from different random initialization are plotted). The loss at each plateau matches our theoretical prediction in Equation (24) (dashed gray lines). (b) The value weight v_i in each head for one of the runs in (a) is plotted in solid blue curves. The numerical solutions of v_i from Equation (26) are plotted in dashed blue curves and match the simulations well. The shades of blue distinguish different heads. (c) The key weights during the loss plateau are plotted in color. When the model moves from one fixed point to the next, the key weight in a head $\boldsymbol{k}_i$ aligns with a new eigenvector of the input token covariance $\mathbf{\Lambda}$. The key weights $\boldsymbol{k}_{1:4}$ and the eigenvectors $\boldsymbol{e}_{1:4}$ are rows in the heatmaps. A video of the dynamics is provided at URL. Here $D = 4, N = 32, H = 5$, and $\mathbf{\Lambda}$ has eigenvalues $0.4, 0.3, 0.2, 0.1$ and eigenvectors as plotted in (c).

point. Because the time required for a head to learn the eigenvector $\boldsymbol{e}_d$ from small initialization scales with λ_d^{-2} (see Appendix D.6), an eigenvector associated with a larger eigenvalue is learned faster. This explains why the model learns to fit the eigenvectors sequentially in descending order of the eigenvalues, as well as why we empirically see the later plateaus last longer in Figure 3a.

When the model is at a fixed point in $\mathcal{M}_m$, we compute the loss in Appendix D.4 and obtain

$$\mathcal{L}(\mathcal{M}_m) = \mathtt{tr}(\mathbf{\Lambda}) - \sum_{d=1}^{m} \lambda_d \left(1 + \frac{1 + \mathtt{tr}(\mathbf{\Lambda})/\lambda_d}{N}\right)^{-1}. \tag{24}$$

Equation (24) is highly interpretable in the limit of a large sequence length N. The loss, $\mathcal{L}(\mathcal{M}_m)$, is the sum of the eigenvalues associated with the remaining unlearned eigenvectors

$$\lim_{N\to\infty} \mathcal{L}(\mathcal{M}_m) = \mathtt{tr}(\mathbf{\Lambda}) - \sum_{d=1}^{m} \lambda_d = \sum_{d=m+1}^{D} \lambda_d.$$

Thus, the loss decreases by the amount of approximately λ_m during the m-th abrupt loss drop. We plot Equation (24) as dashed gray lines in Figure 3a and find they match the plateaus of simulated loss trajectories well.

When the model reaches $\mathcal{M}_m$ from small initialization, its weights take on a highly structured form, which is a specific instance of the general definition in Equation (21). As shown in Figure 3c, the key and query weights in a head grow in scale and align with a new eigenvector of the input token covariance $\mathbf{\Lambda}$ during each abrupt loss drop. Based on simulations in Figure 3 and derivations in Appendices D.5 and D.6, we propose an ansatz that during the $(m + 1)$-th plateau and the subsequent abrupt drop of loss $(0 \leq m < D)$, the weights are approximately given by[3]

$$\boldsymbol{k}_i = \boldsymbol{q}_i = v_i \boldsymbol{e}_i,\ v_i = \lambda_i^{-\frac{1}{3}} \left(1 + \frac{1 + \mathtt{tr}(\boldsymbol{\Lambda})/\lambda_i}{N}\right)^{-\frac{1}{3}}, \quad 1 \le i \le m, \tag{25a}$$

$$\boldsymbol{k}_i = \boldsymbol{q}_i = v_i(t) \boldsymbol{e}_{m+1}, \quad i = m+1, \tag{25b}$$

$$\boldsymbol{k}_i = \boldsymbol{q}_i = \boldsymbol{0}, v_i = 0, \quad m+2 \le i \le H, \tag{25c}$$

where $v_{m+1}(t)$ is small during the $(m+1)$-th loss plateau and will grow during the $(m+1)$-th abrupt loss drop. Equation (25) implies that the ℓ^2 norms of $v_i, \boldsymbol{k}_i, \boldsymbol{q}_i$ in a head are equal, which is a consequence of small initialization and the conservation law in Equation (79). With this ansatz, the high-dimensional training dynamics during the $(m+1)$-th plateau and the subsequent abrupt drop of loss reduces to an ordinary differential equation about $v_{m+1}(t)$:

$$\tau \dot{v}_i = \lambda_{m+1}^2 v_i^2 - \lambda_{m+1}^3 \left(1 + \frac{1 + \mathtt{tr}(\boldsymbol{\Lambda})/\lambda_{m+1}}{N}\right) v_i^5, \quad i = m+1. \tag{26}$$

Equation (26) is a separable differential equation but does not admit a general analytical solution of $v_{m+1}(t)$ in terms of t (see Equation (67)). Nonetheless, it greatly simplifies the high-dimensional dynamics in Equation (19) and provides a good approximation of the true dynamics: during each plateau and the subsequent abrupt loss drop, weights in one of the heads grow in scale with the key and query weights aligning with the next eigenvector, while the rest of the heads remain approximately unchanged. In Figure 3b, we compare the numerical solution of Equation (26) with the value weights trajectories in the simulation and find excellent agreement.

In summary, the loss trajectory of linear attention with separate rank-one key and query trained from small initialization exhibits D abrupt drops, each followed by a plateau. The amount of the m-th abrupt loss drop $(1 \le m \le D)$ is approximately the eigenvalue λ_m, during which the key and query weights in an attention head grow in scale and align with the eigenvector $\boldsymbol{e}_m$.

4.4 In-Context Algorithm: Principal Component Regression

When the linear attention model is at a fixed point in $\mathcal{M}_m$, based on Equation (23), the model implements

$$\mathsf{ATTN}_{\mathsf{S}}(\boldsymbol{X})_{D+1,N+1} = \boldsymbol{\beta}^\top \sum_{d=1}^{m} \lambda_d^{-1} \left(1 + \frac{1 + \mathtt{tr}(\boldsymbol{\Lambda})/\lambda_d}{N}\right)^{-1} \boldsymbol{e}_d \boldsymbol{e}_d^\top \boldsymbol{x}_q. \tag{27}$$

In the limit of a large sequence length N, Equation (27) simplifies and can be interpreted as principal component regression in context with m principal components

$$\lim_{N\to\infty} \mathsf{ATTN}_{\mathsf{S}}(\boldsymbol{X})_{D+1,N+1} = \boldsymbol{w}^\top \boldsymbol{\Lambda} \sum_{d=1}^{m} \lambda_d^{-1} \boldsymbol{e}_d \boldsymbol{e}_d^\top \boldsymbol{x}_q = \boldsymbol{w}^\top \sum_{d=1}^{m} \boldsymbol{e}_d \boldsymbol{e}_d^\top \boldsymbol{x}_q.$$

Here $\boldsymbol{w}$ is the task vector for the sequence $\boldsymbol{X}$, and $\sum_{d=1}^{m} \boldsymbol{e}_d \boldsymbol{e}_d^\top \boldsymbol{x}_q$ is query input $\boldsymbol{x}_q$ projected onto the first m principal components. Hence, if training stops during the $(m+1)$-th plateau, the linear attention approximately implements the principal component regression algorithm in context with m principal components.

[3] We trivially permute the heads so that the head aligned with the d-th eigenvector have index d. The signs of any two among $v_i, \boldsymbol{k}_i, \boldsymbol{q}_i$ can be flipped with trivial effect on the analysis.

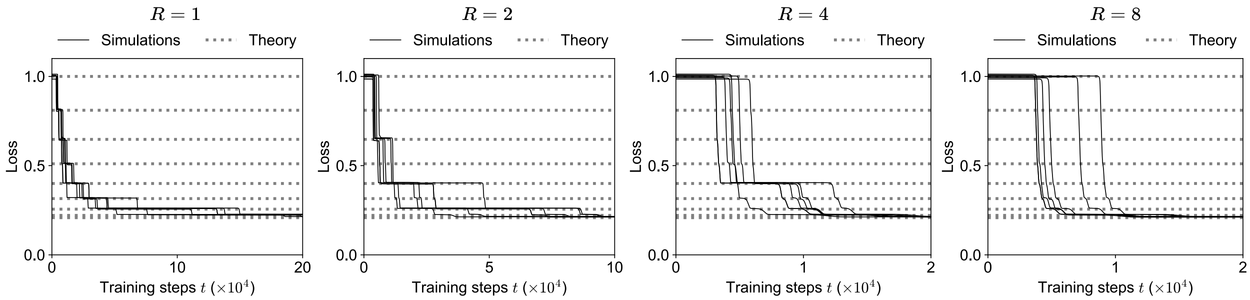

Figure 4: Multi-head linear attention with separate low-rank key and query exhibits saddle-to-saddle dynamics, with the duration of plateaus depending on the rank R. Solid black curves are loss trajectories from six random initializations. Dashed gray lines mark the loss values predicted by Equation (24) at nine fixed points, which are $\mathcal{L}(\mathcal{M}_0), \mathcal{L}(\mathcal{M}_1), \cdots, \mathcal{L}(\mathcal{M}_8)$ from top to bottom. The four panels differ only in the rank of the key and query weights. Here $D = 8, N = 32, H = 9$, $\mathbf{\Lambda}$ has trace 1 and eigenvalues $\lambda_d \propto d^{-1}$.

After the model has undergone D plateaus, it converges to the global minimum fixed point, $\mathcal{M}_D$, and approximately implements principal component regression in context with all D components, which is least square regression. Thus, the linear attention model with either merged or separate key and query undergoes different training dynamics but converges to the same global minimum solution.

5 Linear Attention with Separate Low-Rank Key and Query

The linear attention model with separate rank-R key and query shares many behaviors with its rank-one counterpart. For loss landscape, linear attention with rank-R key and query has the same 2^D fixed points in the function space as its linear counterpart, corresponding to the model implementing in-context principal component regression with a subset of all D principal components (see Appendix E.3).

For training dynamics, the loss trajectories differ slightly depending on the rank R. We plot the loss trajectories with input token dimension $D = 8$ and different ranks $R = 1, 2, 4, 8$ in Figure 4. For $R = 1$, the loss exhibits plateaus at eight values $\mathcal{L}(\mathcal{M}_m)\,(m = 0, 1, \cdots, 7)$. For $R = 2$, the loss exhibits plateaus at four values $\mathcal{L}(\mathcal{M}_m)\,(m = 0, 2, 4, 6)$, and either brief plateaus or no plateau at the other four values. For $R = 4$, the loss exhibits conspicuous plateaus at only two values $\mathcal{L}(\mathcal{M}_m)\,(m = 0, 4)$. To summarize, with rank-R key and query, the loss trajectory exhibits conspicuous plateaus at value $\mathcal{L}(\mathcal{M}_m)$ for m that divides R.

The difference in the loss trajectories arises from the structure of the model defined in Equation (S). Each attention head has a single value weight v_i that is associated with all R pairs of key and query weights in that head, $\boldsymbol{k}_{i,r}, \boldsymbol{q}_{i,r}\ (r = 1, \cdots, R)$. During a conspicuous plateau, a new value weight escapes from the unstable zero fixed point and grows in scale. Once the value weight has grown, it leads to larger gradient updates for all the key and query weights in that head, speeding up their escape from the zero fixed point. Hence, in the rank-R case, a conspicuous plateau occurs when m divides R, corresponding to learning a new head from small initialization. Brief or no plateau occurs when m does not divide R, corresponding to learning a new pair of key and query weights in a head whose value weight has already grown, as shown in Figure 8. See Appendix E.4 for more details.

6 Related Work

6.1 Theory of Linear Attention

Recent theoretical research on linear attention has investigated its expressivity (Vladymyrov et al. 2024; Gatmiry et al. 2024), learnability (Yau et al. 2024), loss landscape (Mahankali et al. 2024; Yingcong Li et al. 2024), convergence (Zhang et al. 2024a,b; Ren et al. 2024; Fu et al. 2024), and generalization (Wu et al. 2024; Mahankali et al. 2024; Duraisamy 2024; Lu et al. 2024; Abedsoltan et al. 2024; Frei and Vardi 2024). The seminal work by Zhang et al. (2024a) analyzed the gradient flow training dynamics of linear attention to prove convergence guarantees, showing what the model converges to at the end of training. Our work also analyzes the gradient flow training dynamics but goes beyond existing convergence results to describe the entire training process. Moreover, we study multi-head attention with merged or separate key and query weights, while Zhang et al. (2024a) focused on single-head attention with merged key and query.

6.2 Theory of Training Dynamics In Attention Models

Another line of recent research studied the training dynamics of softmax attention models, revealing stage-wise dynamics that reflects various phenomena across different settings. These phenomena include the increasing rank of weights (Boix-Adsera et al. 2023), the formation of an induction head (Nichani et al. 2024; Siyu Chen et al. 2024b; Wang et al. 2024), shifting attention to tokens with high co-occurrence with the query (Tian et al. 2023), learning new tasks in a multi-task dataset (Siyu Chen et al. 2024a), learning features with different probabilities of appearance in the dataset (Y. Huang et al. 2024a), or learning higher-order interactions among input tokens (Rende et al. 2024; Edelman et al. 2024). Given the intractability of softmax attention training dynamics in general, these studies made certain assumptions to enable theoretical analyses, including restricted weights (Boix-Adsera et al. 2023; Siyu Chen et al. 2024a; Rende et al. 2024; Edelman et al. 2024), specifically chosen datasets (Y. Huang et al. 2024a), and a simpler layer-wise training algorithm in place of standard gradient descent (Tian et al. 2023; Nichani et al. 2024; Siyu Chen et al. 2024b; Wang et al. 2024). In comparison, our work leverages the linear attention model without softmax operation, enabling us to study in fine detail the dynamics of standard gradient descent training without restrictions on weights. Namely, we derive an analytical time-course solution and a reduction of high-dimensional dynamics to a one-dimensional ordinary differential equation for the two models we study. Furthermore, we characterize how parametrization (i.e., merged or separate key and query, and rank of the separate key and query weights) impacts the loss landscape and training dynamics, an aspect not previously examined.

7 Discussion

We studied the gradient flow training dynamics of multi-head linear attention and demonstrated how it acquires in-context learning abilities in training. We begin with a simple setting of linear attention with merged key and query trained for in-context linear regression, following the setting in seminal works (Von Oswald et al. 2023; Ahn et al. 2023; Zhang et al. 2024a). We show an abrupt loss drop in training and give an analytical time-course solution in the case of a white input token covariance and small initialization.

However, a single abrupt loss drop does not fully capture the development of in-context learning abilities in training practical transformers, where the abilities continue to develop throughout training (Xia et al. 2023; Park et al. 2024). We thus extend our analysis to a parametrization closer to the attention in practical transformers, that is attention with separate key and query. In the separate case, we find that the loss exhibits saddle-to-saddle dynamics with multiple abrupt drops. The in-context learning ability evolves progressively, manifesting as implementing a principal component regression algorithm in context with the number of principal components increasing over time. Building on prior findings showing that transformers

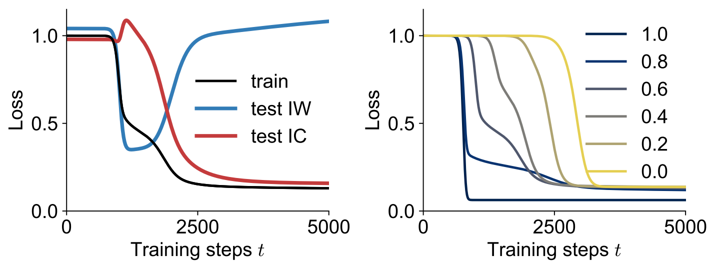

Figure 5: Dynamics of in-context and in-weight learning in linear attention. The training set is the same as the in-context linear regression described in Section 2.1 except that we fix a certain portion of the task vectors $\boldsymbol{w}$ to elicit in-weight learning. The model is multi-head linear attention with merged key and query. *Left*: Training loss, in-weight learning test loss, and in-context learning test loss of linear attention trained on a dataset with 60% of task vectors fixed. *Right*: Training loss of linear attention on datasets with different portions of fixed task vectors. The portion is denoted by color and labeled in the legend. Corresponding test loss trajectories are provided in Figure 10. Here $D = 4, N = 32, H = 8, \boldsymbol{\Lambda} = \boldsymbol{I}/D$.

can implement different forms of in-context learning (Bai et al. 2023; Lampinen et al. 2024), we show that different forms of in-context learning can indeed emerge in gradient descent training. By identifying the in-context algorithm at different times in training, we characterize how the linear attention model develops increasingly sophisticated in-context learning abilities over time.

7.1 Future Direction: Training Dynamics of In-Context and In-Weight Learning

In this work, we focused on the training dynamics of in-context learning abilities. Other than in-context learning, attention models can also learn in weight, that is solving the task by memorizing the map between the query input and the target output without using the information in context. The arbitration between in-context and in-weight learning may depend on the properties of the training data (S. Chan et al. 2022). To focus on the dynamics of in-context learning, we considered a purely in-context learning task, which is in-context linear regression with the task vector sampled from a zero-mean standard normal distribution, $\boldsymbol{w} \sim \mathcal{N}(\boldsymbol{0}, \boldsymbol{I})$. Since memorizing any particular task vector does not effectively decrease the loss, linear attention develops only in-context learning ability during training, as shown in Figure 10a.

If the task vector $\boldsymbol{w}$ follows a different distribution, the training dynamics involves the development of both in-context and in-weight learning abilities. When fixing a portion of the task vectors and sampling the rest from $\mathcal{N}(\boldsymbol{0}, \boldsymbol{I})$, we find that the linear attention model first learns in weight and then learns in context, as shown in Figure 5 (left). We vary the portion of fixed task vectors and plot the training loss trajectories in Figure 5 (right) and the test loss trajectories in Figure 10. The larger the portion of fixed task vectors, the lower the loss the model can achieve by memorizing the fixed task vector in weight. We indeed observe the training loss and in-weight learning test loss are lower right after the first abrupt loss drop when the portion is larger. Future research can build on our findings on the dynamics of in-context learning and explore its interactions with in-weight learning.

7.2 Implications for Future Theory

In our analysis, we draw connections between linear attention and multi-layer linear networks, which allow us to employ the rich theoretical machinery built for linear networks (Baldi and Hornik 1989; Fukumizu 1998; Saxe et al. 2014, 2019; Arora et al. 2018; Ji and Telgarsky 2019; Atanasov et al. 2022) to help understand linear attention. We mainly leverage these connections to understand the training dynamics of linear attention. Beyond training dynamics, many other theoretical results for linear networks can be readily applied to linear attention through the equivalence we draw. For example, the convergence guarantee for multi-head linear attention trained on in-context linear regression tasks can be obtained from the convergence proofs for deep linear networks (Arora et al. 2019; Shamir 2019). In contrast, without the equivalence, Zhang et al. (2024a) previously obtained a convergence guarantee for single-head linear attention, which required highly non-trivial derivations. Hence, we believe the connections we draw are useful in enabling the applications of theory from one architecture to the other.

Additionally, our results on linear attention with merged versus separate key and query reveal that the parametrization choice significantly impacts the loss landscape and training dynamics. This comparison can motivate future research concerning landscape and dynamics to examine how the phenomena may or may not be influenced by the parametrization choice.

Acknowledgement

We thank Jin Hwa Lee for feedback on the draft and William Tong for an inspirational conversation. We thank the following funding sources: Gatsby Charitable Foundation (GAT3850) to YZ, AKS, PEL, and AS; Wellcome Trust (110114/Z/15/Z) to PEL; Sainsbury Wellcome Centre Core Grant from Wellcome (219627/Z/19/Z) to AS; Schmidt Science Polymath Award to AS. AS is a CIFAR Azrieli Global Scholar in the Learning in Machines & Brains program.

References

Abedsoltan, Amirhesam, Adityanarayanan Radhakrishnan, Jingfeng Wu, and Mikhail Belkin (2024). *Context-Scaling versus Task-Scaling in In-Context Learning*. arXiv: `2410.12783 [cs.LG]`. URL: `https://arxiv.org/abs/2410.12783`.

Ahn, Kwangjun, Xiang Cheng, Hadi Daneshmand, and Suvrit Sra (2023). "Transformers learn to implement preconditioned gradient descent for in-context learning". In: *Advances in Neural Information Processing Systems*. Ed. by A. Oh, T. Naumann, A. Globerson, K. Saenko, M. Hardt, and S. Levine. Vol. 36. Curran Associates, Inc., pp. 45614–45650. URL: `https://proceedings.neurips.cc/paper_files/paper/2023/file/8ed3d610ea4b68e7afb30ea7d01422c6-Paper-Conference.pdf`.

Ahn, Kwangjun, Xiang Cheng, Minhak Song, Chulhee Yun, Ali Jadbabaie, and Suvrit Sra (2024). "Linear attention is (maybe) all you need (to understand Transformer optimization)". In: *The Twelfth International Conference on Learning Representations*. URL: `https://openreview.net/forum?id=0uI5415ry7`.

Akyürek, Ekin, Dale Schuurmans, Jacob Andreas, Tengyu Ma, and Denny Zhou (2023). "What learning algorithm is in-context learning? Investigations with linear models". In: *The Eleventh International Conference on Learning Representations*. URL: `https://openreview.net/forum?id=0g0X4H8yN4I`.

Anand, Suraj, Michael A. Lepori, Jack Merullo, and Ellie Pavlick (May 2024). *Dual Process Learning: Controlling Use of In-Context vs. In-Weights Strategies with Weight Forgetting*. arXiv:2406.00053 [cs] version: 1. DOI: `10.48550/arXiv.2406.00053`. URL: `http://arxiv.org/abs/2406.00053` (visited on 09/26/2024).

Anwar, Usman, Johannes Von Oswald, Louis Kirsch, David Krueger, and Spencer Frei (2024). *Adversarial Robustness of In-Context Learning in Transformers for Linear Regression*. arXiv: `2411.05189 [cs.LG]`. URL: `https://arxiv.org/abs/2411.05189`.

Arora, Sanjeev, Nadav Cohen, Noah Golowich, and Wei Hu (2019). "A Convergence Analysis of Gradient Descent for Deep Linear Neural Networks". In: *International Conference on Learning Representations*. URL: https://openreview.net/forum?id=SkMQg3C5K7.

Arora, Sanjeev, Nadav Cohen, and Elad Hazan (Oct. 2018). "On the Optimization of Deep Networks: Implicit Acceleration by Overparameterization". In: *Proceedings of the 35th International Conference on Machine Learning*. Ed. by Jennifer Dy and Andreas Krause. Vol. 80. Proceedings of Machine Learning Research. PMLR, pp. 244–253. URL: https://proceedings.mlr.press/v80/arora18a.html.

Ataee Tarzanagh, Davoud, Yingcong Li, Xuechen Zhang, and Samet Oymak (2023). "Max-Margin Token Selection in Attention Mechanism". In: *Advances in Neural Information Processing Systems*. Ed. by A. Oh, T. Naumann, A. Globerson, K. Saenko, M. Hardt, and S. Levine. Vol. 36. Curran Associates, Inc., pp. 48314–48362. URL: https://proceedings.neurips.cc/paper_files/paper/2023/file/970f59b22f4c72aec75174aae63c7459-Paper-Conference.pdf.

Atanasov, Alexander, Blake Bordelon, and Cengiz Pehlevan (2022). "Neural Networks as Kernel Learners: The Silent Alignment Effect". In: *International Conference on Learning Representations*. URL: https://openreview.net/forum?id=1NvflqAdoom.

Bai, Yu, Fan Chen, Huan Wang, Caiming Xiong, and Song Mei (2023). "Transformers as Statisticians: Provable In-Context Learning with In-Context Algorithm Selection". In: *Advances in Neural Information Processing Systems*. Ed. by A. Oh, T. Naumann, A. Globerson, K. Saenko, M. Hardt, and S. Levine. Vol. 36. Curran Associates, Inc., pp. 57125–57211. URL: https://proceedings.neurips.cc/paper_files/paper/2023/file/b2e63e36c57e153b9015fece2352a9f9-Paper-Conference.pdf.

Baldi, Pierre and Kurt Hornik (1989). "Neural networks and principal component analysis: Learning from examples without local minima". In: *Neural Networks* 2.1, pp. 53–58. ISSN: 0893-6080. DOI: https://doi.org/10.1016/0893-6080(89)90014-2. URL: https://www.sciencedirect.com/science/article/pii/0893608089900142.

Boix-Adsera, Enric, Etai Littwin, Emmanuel Abbe, Samy Bengio, and Joshua Susskind (2023). "Transformers learn through gradual rank increase". In: *Advances in Neural Information Processing Systems*. Ed. by A. Oh, T. Naumann, A. Globerson, K. Saenko, M. Hardt, and S. Levine. Vol. 36. Curran Associates, Inc., pp. 24519–24551. URL: https://proceedings.neurips.cc/paper_files/paper/2023/file/4d69c1c057a8bd570ba4a7b71aae8331-Paper-Conference.pdf.

Bordelon, Blake, Hamza Tahir Chaudhry, and Cengiz Pehlevan (2024). "Infinite Limits of Multi-head Transformer Dynamics". In: *Advances in Neural Information Processing Systems*. URL: https://openreview.net/forum?id=p0BBKhD5aI.

Brown, Tom et al. (2020). "Language Models are Few-Shot Learners". In: *Advances in Neural Information Processing Systems*. Ed. by H. Larochelle, M. Ranzato, R. Hadsell, M.F. Balcan, and H. Lin. Vol. 33. Curran Associates, Inc., pp. 1877–1901. URL: https://proceedings.neurips.cc/paper_files/paper/2020/file/1457c0d6bfcb4967418bfb8ac142f64a-Paper.pdf.

Chan, Bryan, Xinyi Chen, András György, and Dale Schuurmans (2024). *Toward Understanding In-context vs. In-weight Learning*. arXiv: 2410.23042 [cs.LG]. URL: https://arxiv.org/abs/2410.23042.

Chan, Stephanie, Adam Santoro, Andrew Lampinen, Jane Wang, Aaditya Singh, Pierre Richemond, James McClelland, and Felix Hill (2022). "Data Distributional Properties Drive Emergent In-Context Learning in Transformers". In: *Advances in Neural Information Processing Systems*. Ed. by S. Koyejo, S. Mohamed, A. Agarwal, D. Belgrave, K. Cho, and A. Oh. Vol. 35. Curran Associates, Inc., pp. 18878–18891. URL: https://proceedings.neurips.cc/paper_files/paper/2022/file/77c6ccacfd9962e2307fc64680fc5ace-Paper-Conference.pdf.

Chen, Angelica, Ravid Shwartz-Ziv, Kyunghyun Cho, Matthew L Leavitt, and Naomi Saphra (2024). "Sudden Drops in the Loss: Syntax Acquisition, Phase Transitions, and Simplicity Bias in MLMs". In: *The Twelfth International Conference on Learning Representations*. URL: https://openreview.net/forum?id=MO5PiKHELW.

Chen, Sitan and Yuanzhi Li (2024). *Provably learning a multi-head attention layer*. arXiv: 2402.04084 [cs.LG]. URL: https://arxiv.org/abs/2402.04084.

Chen, Siyu, Heejune Sheen, Tianhao Wang, and Zhuoran Yang (30 Jun–03 Jul 2024a). "Training Dynamics of Multi-Head Softmax Attention for In-Context Learning: Emergence, Convergence, and Optimality". In: *Proceedings of Thirty Seventh Conference on Learning Theory*. Ed. by Shipra Agrawal and Aaron Roth. Vol. 247. Proceedings of Machine Learning Research. PMLR, pp. 4573–4573. URL: https://proceedings.mlr.press/v247/siyu24a.html.

Chen, Siyu, Heejune Sheen, Tianhao Wang, and Zhuoran Yang (2024b). "Unveiling Induction Heads: Provable Training Dynamics and Feature Learning in Transformers". In: *Advances in Neural Information Processing Systems*. URL: https://openreview.net/forum?id=4fN2REs0Ma.

Du, Simon S, Wei Hu, and Jason D Lee (2018). "Algorithmic Regularization in Learning Deep Homogeneous Models: Layers are Automatically Balanced". In: *Advances in Neural Information Processing Systems*. Ed. by S. Bengio, H. Wallach, H. Larochelle, K. Grauman, N. Cesa-Bianchi, and R. Garnett. Vol. 31. Curran Associates, Inc. URL: https://proceedings.neurips.cc/paper_files/paper/2018/file/fe131d7f5a6b38b23cc967316c13dae2-Paper.pdf.

Duraisamy, Karthik (2024). *Finite Sample Analysis and Bounds of Generalization Error of Gradient Descent in In-Context Linear Regression*. arXiv: 2405.02462 [math.ST]. URL: https://arxiv.org/abs/2405.02462.

Edelman, Ezra, Nikolaos Tsilivis, Benjamin L. Edelman, eran malach, and Surbhi Goel (2024). "The Evolution of Statistical Induction Heads: In-Context Learning Markov Chains". In: *Advances in Neural Information Processing Systems*. URL: https://openreview.net/forum?id=qaRT6QTIqJ.

Frei, Spencer and Gal Vardi (2024). *Trained Transformer Classifiers Generalize and Exhibit Benign Overfitting In-Context*. arXiv: 2410.01774 [cs.LG]. URL: https://arxiv.org/abs/2410.01774.

Fu, Deqing, Tian-qi Chen, Robin Jia, and Vatsal Sharan (2024). "Transformers Learn to Achieve Second-Order Convergence Rates for In-Context Linear Regression". In: *Advances in Neural Information Processing Systems*. URL: https://openreview.net/forum?id=L8h6cozcbn.

Fukumizu, Kenji (1998). "Effect of batch learning in multilayer neural networks". In: *Gen* 1.04, 1E–03.

Garg, Shivam, Dimitris Tsipras, Percy S Liang, and Gregory Valiant (2022). "What Can Transformers Learn In-Context? A Case Study of Simple Function Classes". In: *Advances in Neural Information Processing Systems*. Ed. by S. Koyejo, S. Mohamed, A. Agarwal, D. Belgrave, K. Cho, and A. Oh. Vol. 35. Curran Associates, Inc., pp. 30583–30598. URL: https://proceedings.neurips.cc/paper_files/paper/2022/file/c529dba08a146ea8d6cf715ae8930cbe-Paper-Conference.pdf.

Gatmiry, Khashayar, Nikunj Saunshi, Sashank J. Reddi, Stefanie Jegelka, and Sanjiv Kumar (2024). *On the Role of Depth and Looping for In-Context Learning with Task Diversity*. arXiv: 2410.21698 [cs.LG]. URL: https://arxiv.org/abs/2410.21698.

He, Tianyu, Darshil Doshi, Aritra Das, and Andrey Gromov (2024). "Learning to grok: Emergence of in-context learning and skill composition in modular arithmetic tasks". In: *Advances in Neural Information Processing Systems*. URL: https://openreview.net/forum?id=aVh9KRZdRk.

Henry, Nathan W., Giovanni Luca Marchetti, and Kathlén Kohn (2024). *Geometry of Lightning Self-Attention: Identifiability and Dimension*. arXiv: 2408.17221 [cs.LG]. URL: https://arxiv.org/abs/2408.17221.

Hoffmann, David T, Simon Schrodi, Jelena Bratulić, Nadine Behrmann, Volker Fischer, and Thomas Brox (21–27 Jul 2024). "Eureka-Moments in Transformers: Multi-Step Tasks Reveal Softmax Induced Optimization Problems". In: *Proceedings of the 41st International Conference on Machine Learning*. Ed. by Ruslan Salakhutdinov, Zico Kolter, Katherine Heller, Adrian Weller, Nuria Oliver, Jonathan Scarlett, and Felix Berkenkamp. Vol. 235. Proceedings of Machine Learning Research. PMLR, pp. 18409–18438. URL: https://proceedings.mlr.press/v235/hoffmann24a.html.

Huang, Ruiquan, Yingbin Liang, and Jing Yang (2024). "Non-asymptotic Convergence of Training Transformers for Next-token Prediction". In: *Advances in Neural Information Processing Systems*. URL: https://openreview.net/forum?id=NfOFbPpYII.

Huang, Yu, Yuan Cheng, and Yingbin Liang (21–27 Jul 2024a). "In-context Convergence of Transformers". In: *Proceedings of the 41st International Conference on Machine Learning*. Ed. by Ruslan Salakhutdinov, Zico Kolter, Katherine Heller, Adrian Weller, Nuria Oliver, Jonathan Scarlett, and Felix Berkenkamp. Vol. 235. Proceedings of Machine Learning Research. PMLR, pp. 19660–19722. URL: https://proceedings.mlr.press/v235/huang24d.html.

Huang, Yu, Zixin Wen, Yuejie Chi, and Yingbin Liang (2024b). *How Transformers Learn Diverse Attention Correlations in Masked Vision Pretraining*. arXiv: 2403.02233 [cs.LG]. URL: https://arxiv.org/abs/2403.02233.

Ildiz, Muhammed Emrullah, Yixiao Huang, Yingcong Li, Ankit Singh Rawat, and Samet Oymak (21–27 Jul 2024). "From Self-Attention to Markov Models: Unveiling the Dynamics of Generative Transformers". In: *Proceedings of the 41st International Conference on Machine Learning*. Ed. by Ruslan Salakhutdinov, Zico Kolter, Katherine Heller, Adrian Weller, Nuria Oliver, Jonathan Scarlett, and Felix Berkenkamp. Vol. 235. Proceedings of Machine Learning Research. PMLR, pp. 20955–20982. URL: https://proceedings.mlr.press/v235/ildiz24a.html.

Jang, Uijeong, Jason D. Lee, and Ernest K. Ryu (21–27 Jul 2024). "LoRA Training in the NTK Regime has No Spurious Local Minima". In: *Proceedings of the 41st International Conference on Machine Learning*. Ed. by Ruslan Salakhutdinov, Zico Kolter, Katherine Heller, Adrian Weller, Nuria Oliver, Jonathan Scarlett, and Felix Berkenkamp. Vol. 235. Proceedings of Machine Learning Research. PMLR, pp. 21306–21328. URL: https://proceedings.mlr.press/v235/jang24d.html.

Jelassi, Samy, Michael Sander, and Yuanzhi Li (2022). "Vision Transformers provably learn spatial structure". In: *Advances in Neural Information Processing Systems*. Ed. by S. Koyejo, S. Mohamed, A. Agarwal, D. Belgrave, K. Cho, and A. Oh. Vol. 35. Curran Associates, Inc., pp. 37822–37836. URL: https://proceedings.neurips.cc/paper_files/paper/2022/file/f69707de866eb0805683d3521756b73f-Paper-Conference.pdf.

Ji, Ziwei and Matus Telgarsky (2019). "Gradient descent aligns the layers of deep linear networks". In: *International Conference on Learning Representations*. URL: https://openreview.net/forum?id=HJflg30qKX.

Jiang, Jiarui, Wei Huang, Miao Zhang, Taiji Suzuki, and Liqiang Nie (2024). "Unveil Benign Overfitting for Transformer in Vision: Training Dynamics, Convergence, and Generalization". In: *Advances in Neural Information Processing Systems*. URL: https://openreview.net/forum?id=FGJb0peY4R.

Julistiono, Aaron Alvarado Kristanto, Davoud Ataee Tarzanagh, and Navid Azizan (2024). *Optimizing Attention with Mirror Descent: Generalized Max-Margin Token Selection*. arXiv: 2410.14581 [cs.LG]. URL: https://arxiv.org/abs/2410.14581.

Kim, Juno and Taiji Suzuki (21–27 Jul 2024). "Transformers Learn Nonlinear Features In Context: Nonconvex Mean-field Dynamics on the Attention Landscape". In: *Proceedings of the 41st International Conference on Machine Learning*. Ed. by Ruslan Salakhutdinov, Zico Kolter, Katherine Heller, Adrian Weller, Nuria Oliver, Jonathan Scarlett, and Felix Berkenkamp. Vol. 235. Proceedings of Machine Learning Research. PMLR, pp. 24527–24561. URL: https://proceedings.mlr.press/v235/kim24af.html.

Kohn, Kathlén, Thomas Merkh, Guido Montúfar, and Matthew Trager (2022). "Geometry of Linear Convolutional Networks". In: *SIAM Journal on Applied Algebra and Geometry* 6.3, pp. 368–406. DOI: 10.11

37/21M1441183. eprint: https://doi.org/10.1137/21M1441183. URL: https://doi.org/10.1137/21M1441183.

Kohn, Kathlén, Guido Montúfar, Vahid Shahverdi, and Matthew Trager (2024a). "Function Space and Critical Points of Linear Convolutional Networks". In: *SIAM Journal on Applied Algebra and Geometry* 8.2, pp. 333–362. DOI: 10.1137/23M1565504. eprint: https://doi.org/10.1137/23M1565504. URL: https://doi.org/10.1137/23M1565504.

Kohn, Kathlén, Anna-Laura Sattelberger, and Vahid Shahverdi (2024b). *Geometry of Linear Neural Networks: Equivariance and Invariance under Permutation Groups*. arXiv: 2309.13736 [cs.LG]. URL: https://arxiv.org/abs/2309.13736.

Lampinen, Andrew Kyle, Stephanie C. Y. Chan, Aaditya K. Singh, and Murray Shanahan (2024). *The broader spectrum of in-context learning*. arXiv: 2412.03782 [cs.CL]. URL: https://arxiv.org/abs/2412.03782.

Li, Yingcong, Ankit Singh Rawat, and Samet Oymak (2024). "Fine-grained Analysis of In-context Linear Estimation: Data, Architecture, and Beyond". In: *Advances in Neural Information Processing Systems*. URL: https://openreview.net/forum?id=lYPAYmfQqm.

Lu, Yue M., Mary I. Letey, Jacob A. Zavatone-Veth, Anindita Maiti, and Cengiz Pehlevan (2024). *Asymptotic theory of in-context learning by linear attention*. arXiv: 2405.11751 [stat.ML]. URL: https://arxiv.org/abs/2405.11751.

Mahankali, Arvind V., Tatsunori Hashimoto, and Tengyu Ma (2024). "One Step of Gradient Descent is Provably the Optimal In-Context Learner with One Layer of Linear Self-Attention". In: *The Twelfth International Conference on Learning Representations*. URL: https://openreview.net/forum?id=8p3fu56lKc.

Makkuva, Ashok Vardhan, Marco Bondaschi, Adway Girish, Alliot Nagle, Hyeji Kim, Michael Gastpar, and Chanakya Ekbote (2024). "Local to Global: Learning Dynamics and Effect of Initialization for Transformers". In: *Advances in Neural Information Processing Systems*. URL: https://openreview.net/forum?id=OX4yll3X53.

Nanda, Neel, Lawrence Chan, Tom Lieberum, Jess Smith, and Jacob Steinhardt (2023). "Progress measures for grokking via mechanistic interpretability". In: *The Eleventh International Conference on Learning Representations*. URL: https://openreview.net/forum?id=9XFSbDPmdW.

Nguyen, Alex and Gautam Reddy (2024). *Differential learning kinetics govern the transition from memorization to generalization during in-context learning*. arXiv: 2412.00104 [cs.LG]. URL: https://arxiv.org/abs/2412.00104.

Nichani, Eshaan, Alex Damian, and Jason D. Lee (21–27 Jul 2024). "How Transformers Learn Causal Structure with Gradient Descent". In: *Proceedings of the 41st International Conference on Machine Learning*. Ed. by Ruslan Salakhutdinov, Zico Kolter, Katherine Heller, Adrian Weller, Nuria Oliver, Jonathan Scarlett, and Felix Berkenkamp. Vol. 235. Proceedings of Machine Learning Research. PMLR, pp. 38018–38070. URL: https://proceedings.mlr.press/v235/nichani24a.html.

Olsson, Catherine et al. (2022). *In-context Learning and Induction Heads*. arXiv: 2209.11895 [cs.LG]. URL: https://arxiv.org/abs/2209.11895.

Park, Core Francisco, Ekdeep Singh Lubana, Itamar Pres, and Hidenori Tanaka (2024). *Competition Dynamics Shape Algorithmic Phases of In-Context Learning*. arXiv: 2412.01003 [cs.LG]. URL: https://arxiv.org/abs/2412.01003.

Reddy, Gautam (2024). "The mechanistic basis of data dependence and abrupt learning in an in-context classification task". In: *The Twelfth International Conference on Learning Representations*. URL: https://openreview.net/forum?id=aN4Jf6Cx69.

Ren, Yunwei, Zixuan Wang, and Jason D. Lee (2024). "Learning and Transferring Sparse Contextual Bigrams with Linear Transformers". In: *Advances in Neural Information Processing Systems*. URL: https://openreview.net/forum?id=PukaVAwYBo.

Rende, Riccardo, Federica Gerace, Alessandro Laio, and Sebastian Goldt (2024). "A distributional simplicity bias in the learning dynamics of transformers". In: *Advances in Neural Information Processing Systems*. URL: https://openreview.net/forum?id=GgV6UczIWM.

Saxe, Andrew M, James L McClelland, and Surya Ganguli (2014). "Exact solutions to the nonlinear dynamics of learning in deep linear neural networks". In: *The Second International Conference on Learning Representations*. URL: https://openreview.net/forum?id=_wzZwKpTDF_9C.

Saxe, Andrew M, James L McClelland, and Surya Ganguli (2019). "A mathematical theory of semantic development in deep neural networks". In: *Proceedings of the National Academy of Sciences* 116.23, pp. 11537–11546. DOI: 10.1073/pnas.1820226116. eprint: https://www.pnas.org/doi/pdf/10.1073/pnas.1820226116. URL: https://www.pnas.org/doi/abs/10.1073/pnas.1820226116.

Schlag, Imanol, Kazuki Irie, and Jürgen Schmidhuber (18–24 Jul 2021). "Linear Transformers Are Secretly Fast Weight Programmers". In: *Proceedings of the 38th International Conference on Machine Learning*. Ed. by Marina Meila and Tong Zhang. Vol. 139. Proceedings of Machine Learning Research. PMLR, pp. 9355–9366. URL: https://proceedings.mlr.press/v139/schlag21a.html.

Shamir, Ohad (25–28 Jun 2019). "Exponential Convergence Time of Gradient Descent for One-Dimensional Deep Linear Neural Networks". In: *Proceedings of the Thirty-Second Conference on Learning Theory*. Ed. by Alina Beygelzimer and Daniel Hsu. Vol. 99. Proceedings of Machine Learning Research. PMLR, pp. 2691–2713. URL: https://proceedings.mlr.press/v99/shamir19a.html.

Sheen, Heejune, Siyu Chen, Tianhao Wang, and Harrison H. Zhou (2024). *Implicit Regularization of Gradient Flow on One-Layer Softmax Attention*. arXiv: 2403.08699 [cs.LG]. URL: https://arxiv.org/abs/2403.08699.

Singh, Aaditya K, Stephanie Chan, Ted Moskovitz, Erin Grant, Andrew Saxe, and Felix Hill (2023). "The Transient Nature of Emergent In-Context Learning in Transformers". In: *Advances in Neural Information Processing Systems*. Ed. by A. Oh, T. Naumann, A. Globerson, K. Saenko, M. Hardt, and S. Levine. Vol. 36. Curran Associates, Inc., pp. 27801–27819. URL: https://proceedings.neurips.cc/paper_files/paper/2023/file/58692a1701314e09cbd7a5f5f3871cc9-Paper-Conference.pdf.

Singh, Aaditya K, Ted Moskovitz, Felix Hill, Stephanie C.Y. Chan, and Andrew M Saxe (21–27 Jul 2024). "What needs to go right for an induction head? A mechanistic study of in-context learning circuits and their formation". In: *Proceedings of the 41st International Conference on Machine Learning*. Ed. by Ruslan Salakhutdinov, Zico Kolter, Katherine Heller, Adrian Weller, Nuria Oliver, Jonathan Scarlett, and Felix Berkenkamp. Vol. 235. Proceedings of Machine Learning Research. PMLR, pp. 45637–45662. URL: https://proceedings.mlr.press/v235/singh24c.html.

Song, Bingqing, Boran Han, Shuai Zhang, Jie Ding, and Mingyi Hong (2024). "Unraveling the Gradient Descent Dynamics of Transformers". In: *Advances in Neural Information Processing Systems*. URL: https://openreview.net/forum?id=XswQeLjJo5.

Tarzanagh, Davoud Ataee, Yingcong Li, Christos Thrampoulidis, and Samet Oymak (2024). *Transformers as Support Vector Machines*. arXiv: 2308.16898 [cs.LG]. URL: https://arxiv.org/abs/2308.16898.

Tian, Yuandong, Yiping Wang, Beidi Chen, and Simon S Du (2023). "Scan and Snap: Understanding Training Dynamics and Token Composition in 1-layer Transformer". In: *Advances in Neural Information Processing Systems*. Ed. by A. Oh, T. Naumann, A. Globerson, K. Saenko, M. Hardt, and S. Levine. Vol. 36. Curran Associates, Inc., pp. 71911–71947. URL: https://proceedings.neurips.cc/paper_files/paper/2023/file/e359ebe56ba306b674e8952349c6049e-Paper-Conference.pdf.

Vasudeva, Bhavya, Puneesh Deora, and Christos Thrampoulidis (2024). *Implicit Bias and Fast Convergence Rates for Self-attention*. arXiv: 2402.05738 [cs.LG]. URL: https://arxiv.org/abs/2402.05738.

Vaswani, Ashish, Noam Shazeer, Niki Parmar, Jakob Uszkoreit, Llion Jones, Aidan N Gomez, Łukasz Kaiser, and Illia Polosukhin (2017). "Attention is All you Need". In: *Advances in Neural Information Processing Systems*. Ed. by I. Guyon, U. Von Luxburg, S. Bengio, H. Wallach, R. Fergus, S. Vishwanathan, and R. Garnett. Vol. 30. Curran Associates, Inc. URL: https://proceedings.neurips.cc/paper_files/paper/2017/file/3f5ee243547dee91fbd053c1c4a845aa-Paper.pdf.

Vladymyrov, Max, Johannes Von Oswald, Mark Sandler, and Rong Ge (2024). "Linear Transformers are Versatile In-Context Learners". In: *Advances in Neural Information Processing Systems*. URL: https://openreview.net/forum?id=p1ft33Mu3J.

Von Oswald, Johannes, Eyvind Niklasson, Ettore Randazzo, Joao Sacramento, Alexander Mordvintsev, Andrey Zhmoginov, and Max Vladymyrov (23–29 Jul 2023). "Transformers Learn In-Context by Gradient Descent". In: *Proceedings of the 40th International Conference on Machine Learning*. Ed. by Andreas Krause, Emma Brunskill, Kyunghyun Cho, Barbara Engelhardt, Sivan Sabato, and Jonathan Scarlett. Vol. 202. Proceedings of Machine Learning Research. PMLR, pp. 35151–35174. URL: https://proceedings.mlr.press/v202/von-oswald23a.html.

Wang, Mingze, Ruoxi Yu, Weinan E, and Lei Wu (2024). *How Transformers Implement Induction Heads: Approximation and Optimization Analysis*. arXiv: 2410.11474 [cs.LG]. URL: https://arxiv.org/abs/2410.11474.

Woodworth, Blake, Suriya Gunasekar, Jason D. Lee, Edward Moroshko, Pedro Savarese, Itay Golan, Daniel Soudry, and Nathan Srebro (Sept. 2020). "Kernel and Rich Regimes in Overparametrized Models". In: *Proceedings of Thirty Third Conference on Learning Theory*. Ed. by Jacob Abernethy and Shivani Agarwal. Vol. 125. Proceedings of Machine Learning Research. PMLR, pp. 3635–3673. URL: https://proceedings.mlr.press/v125/woodworth20a.html.

Wu, Jingfeng, Difan Zou, Zixiang Chen, Vladimir Braverman, Quanquan Gu, and Peter Bartlett (2024). "How Many Pretraining Tasks Are Needed for In-Context Learning of Linear Regression?" In: *The Twelfth International Conference on Learning Representations*. URL: https://openreview.net/forum?id=vSh5ePa0ph.

Xia, Mengzhou, Mikel Artetxe, Chunting Zhou, Xi Victoria Lin, Ramakanth Pasunuru, Danqi Chen, Luke Zettlemoyer, and Veselin Stoyanov (July 2023). "Training Trajectories of Language Models Across Scales". In: *Proceedings of the 61st Annual Meeting of the Association for Computational Linguistics (Volume 1: Long Papers)*. Ed. by Anna Rogers, Jordan Boyd-Graber, and Naoaki Okazaki. Toronto, Canada: Association for Computational Linguistics, pp. 13711–13738. DOI: 10.18653/v1/2023.acl-long.767. URL: https://aclanthology.org/2023.acl-long.767.

Yau, Morris, Ekin Akyürek, Jiayuan Mao, Joshua B. Tenenbaum, Stefanie Jegelka, and Jacob Andreas (2024). *Learning Linear Attention in Polynomial Time*. arXiv: 2410.10101 [cs.LG]. URL: https://arxiv.org/abs/2410.10101.

Zhang, Ruiqi, Spencer Frei, and Peter L. Bartlett (2024a). "Trained Transformers Learn Linear Models In-Context". In: *Journal of Machine Learning Research* 25.49, pp. 1–55. URL: http://jmlr.org/papers/v25/23-1042.html.

Zhang, Ruiqi, Jingfeng Wu, and Peter Bartlett (2024b). "In-Context Learning of a Linear Transformer Block: Benefits of the MLP Component and One-Step GD Initialization". In: *Advances in Neural Information Processing Systems*. URL: https://openreview.net/forum?id=Thou1rKdpZ.

Contents

1 Introduction **1**

2 Preliminaries **3**
2.1 In-Context Linear Regression Task 3
2.2 Multi-Head Self-Attention 3
2.3 Multi-Head Linear Attention with Merged Key and Query 4
2.4 Multi-head Linear Attention with Separate Key and Query 5
2.5 Gradient Flow Training Dynamics 5

3 Linear Attention with Merged Key and Query **6**
3.1 Equivalence to Two-Layer Fully-Connected Linear Networks 6
3.2 Loss Landscape: Two Fixed Points 7
3.3 Training Dynamics: An Abrupt Drop in the Loss 7
3.4 In-Context Algorithm: Least Squares Regression 7
3.5 Conservation Law: All Heads Are Parallel 8

4 Linear Attention with Separate Rank-One Key and Query **8**
4.1 Equivalence to Three-Layer Convolutional Linear Networks 8
4.2 Loss Landscape: Exponential Number of Fixed Points 9
4.3 Training Dynamics: Saddle-to-Saddle Dynamics 10
4.4 In-Context Algorithm: Principal Component Regression 12

5 Linear Attention with Separate Low-Rank Key and Query **13**

6 Related Work **14**
6.1 Theory of Linear Attention 14
6.2 Theory of Training Dynamics In Attention Models 14

7 Discussion **14**
7.1 Future Direction: Training Dynamics of In-Context and In-Weight Learning 15
7.2 Implications for Future Theory 15

A Additional Related Work **25**

B Additional Preliminaries **25**
B.1 Data Statistics 25
B.2 Initialization 26
B.3 Kronecker Product 26

C Linear Attention with Merged Key and Query **27**
C.1 Justification for Zero Blocks Assumption 27
C.2 Gradient Flow Equations 28
C.3 Fixed Points 28
C.4 Duality of the Global Minimum Solution 28
C.5 Analytical Time-Course Solution for White Covariance 29
C.6 Training Dynamics for General Covariance 31

D Linear Attention with Separate Rank-One Key and Query **32**
D.1 Justification for Zero Blocks Assumption . . . 32
D.2 Gradient Flow Equations . . . 32
D.3 Validity of Fixed Points . . . 33
D.4 Loss Value at A Fixed Point . . . 35
D.5 Saddle-to-Saddle Dynamics: From $\mathcal{M}_0$ to $\mathcal{M}_1$ . . . 36
D.6 Saddle-to-Saddle Dynamics: From $\mathcal{M}_m$ to $\mathcal{M}_{m+1}$ . . . 39
D.7 Weight Configuration with Minimal L2 Norm . . . 41
D.8 Conservation Law . . . 43

E Linear Attention with Separate Low-Rank Key and Query **44**
E.1 Justification for Zero Blocks Assumption . . . 44
E.2 Gradient Flow Equations . . . 45
E.3 Fixed Points . . . 45
E.4 Saddle-to-Saddle Dynamics . . . 46
E.5 Conservation Law . . . 47

F Training Dynamics of In-Context and In-Weight Learning **48**

Appendix

A Additional Related Work

A broader body of theoretical literature have explored the transformers training dynamics but addressed different problem from ours, such as the effect of initialization (Makkuva et al. 2024), convergence results (Song et al. 2024; R. Huang et al. 2024), sample complexity guarantees (Ildiz et al. 2024), scaling limits (Bordelon et al. 2024), and implicit regularization (Ataee Tarzanagh et al. 2023; Tarzanagh et al. 2024; Julistiono et al. 2024; Vasudeva et al. 2024; Sheen et al. 2024). Other studies considered special training regimes, such as the neural tangent kernel regime (Jang et al. 2024) and the mean-field regime (Kim and Suzuki 2024). A few works focused on vision transformers (Jelassi et al. 2022; Jiang et al. 2024; Y. Huang et al. 2024b). In contrast, our works focuses on characterizing the process of training and the development of in-context learning abilities over time.

B Additional Preliminaries

B.1 Data Statistics

Recall that we use $\boldsymbol{\beta}$ to denote the in-context correlation between $\boldsymbol{x}_n$ and y_n in a sequence $\boldsymbol{X}$, as defined in Equation (8). We additionally denote the in-context covariance of $\boldsymbol{x}_n$ in a sequence as $\hat{\boldsymbol{\Lambda}}$

$$\hat{\boldsymbol{\Lambda}} \equiv \frac{1}{N}\sum_{n=1}^{N} \boldsymbol{x}_n \boldsymbol{x}_n^\top. \tag{28}$$

We can thus write $\boldsymbol{X}\boldsymbol{X}^\top/N$ as a block matrix

$$\frac{1}{N}\boldsymbol{X}\boldsymbol{X}^\top = \begin{bmatrix} \frac{1}{N}\left(\boldsymbol{x}_q\boldsymbol{x}_q^\top + \sum_n \boldsymbol{x}_n\boldsymbol{x}_n^\top\right) & \frac{1}{N}\sum_n \boldsymbol{x}_n y_n \\ \frac{1}{N}\sum_n y_n \boldsymbol{x}_n^\top & \frac{1}{N}\sum_n y_n^2 \end{bmatrix} = \begin{bmatrix} \frac{1}{N}\boldsymbol{x}_q\boldsymbol{x}_q^\top + \hat{\boldsymbol{\Lambda}} & \boldsymbol{\beta} \\ \boldsymbol{\beta}^\top & \boldsymbol{w}^\top\hat{\boldsymbol{\Lambda}}\boldsymbol{w} \end{bmatrix}. \tag{29}$$

Due to the definition of the in-context linear regression task, we have that

$$\boldsymbol{\beta} = \hat{\boldsymbol{\Lambda}}\boldsymbol{w}. \tag{30}$$

We will need a second-order statistics of $\hat{\boldsymbol{\Lambda}}$,

$$\begin{aligned}
\mathbb{E}\left(\hat{\boldsymbol{\Lambda}}^2\right) &= \mathbb{E}\left(\frac{1}{N}\sum_{n=1}^{N}\boldsymbol{x}_n\boldsymbol{x}_n^\top\right)^2 \\
&= \frac{1}{N^2}\mathbb{E}\left(\sum_{n\neq n'}\boldsymbol{x}_n\boldsymbol{x}_n^\top\boldsymbol{x}_{n'}\boldsymbol{x}_{n'}^\top + \sum_{n=1}^{N}\boldsymbol{x}_n\boldsymbol{x}_n^\top\boldsymbol{x}_n\boldsymbol{x}_n^\top\right) \\
&= \frac{N-1}{N}\mathbb{E}\left(\boldsymbol{x}_n\boldsymbol{x}_n^\top\right)\mathbb{E}\left(\boldsymbol{x}_{n'}\boldsymbol{x}_{n'}^\top\right) + \frac{1}{N}\mathbb{E}\left(\boldsymbol{x}_n\boldsymbol{x}_n^\top\boldsymbol{x}_n\boldsymbol{x}_n^\top\right) \\
&= \frac{N-1}{N}\boldsymbol{\Lambda}^2 + \frac{1}{N}\left(2\boldsymbol{\Lambda}^2 + \mathtt{tr}(\boldsymbol{\Lambda})\boldsymbol{\Lambda}\right) \\
&= \boldsymbol{\Lambda}^2 + \frac{\boldsymbol{\Lambda} + \mathtt{tr}(\boldsymbol{\Lambda})\boldsymbol{I}}{N}\boldsymbol{\Lambda}.
\end{aligned} \tag{31}$$

We note that the eigenvectors of $\mathbb{E}\left(\hat{\boldsymbol{\Lambda}}^2\right)$ are the same as those of $\boldsymbol{\Lambda}$, which are $\boldsymbol{e}_1, \cdots, \boldsymbol{e}_D$,

$$\mathbb{E}\left(\hat{\boldsymbol{\Lambda}}^2\right)\boldsymbol{e}_d = \left(1+\frac{1}{N}\right)\boldsymbol{\Lambda}^2\boldsymbol{e}_d + \frac{\mathtt{tr}(\boldsymbol{\Lambda})}{N}\boldsymbol{\Lambda}\boldsymbol{e}_d = \left[\left(1+\frac{1}{N}\right)\lambda_d^2 + \frac{\mathtt{tr}(\boldsymbol{\Lambda})}{N}\lambda_d\right]\boldsymbol{e}_d.$$

We denote the eigenvalues of $\mathbb{E}(\hat{\mathbf{\Lambda}}^2)$ corresponding to eigenvectors $\boldsymbol{e}_1, \cdots, \boldsymbol{e}_D$ as $a_1, \cdots, a_D$. These eigenvalues are given by

$$a_d = \left[\left(1 + \frac{1}{N}\right) \lambda_d^2 + \frac{\mathtt{tr}(\mathbf{\Lambda})}{N} \lambda_d \right] = \lambda_d^2 \left(1 + \frac{1 + \mathtt{tr}(\mathbf{\Lambda})/\lambda_d}{N}\right). \tag{32}$$

The matrix $\mathbb{E}(\hat{\mathbf{\Lambda}}^2)$ can be expressed through its eigen-decomposition, which will be useful in later derivations:

$$\mathbb{E}\left(\hat{\mathbf{\Lambda}}^2\right) = \sum_{d=1}^{D} a_d \boldsymbol{e}_d \boldsymbol{e}_d^\top. \tag{33}$$

B.2 Initialization

For linear attention with merged key and query, we initialize the entries of the value and the merged key-query weights as

$$v_i \sim \mathcal{N}(0, w_{\text{init}}^2/H), \quad U_i^{d,d'} \sim \mathcal{N}(0, w_{\text{init}}^2/HD^2). \tag{34}$$

At initialization, the following ℓ^2 norms are

$$\sqrt{\sum_{i=1}^{H} v_i^2}, \sqrt{\sum_{i=1}^{H} \|\boldsymbol{U}_i\|^2} \sim O(w_{\text{init}}). \tag{35}$$

For linear attention with separate rank-R key and query, we initialize the entries of the value, key, and query weights as

$$v_i \sim \mathcal{N}(0, w_{\text{init}}^2/H), \quad k_{i,r}^d \sim \mathcal{N}(0, w_{\text{init}}^2/HRD), \quad q_{i,r}^d \sim \mathcal{N}(0, w_{\text{init}}^2/HRD). \tag{36}$$

At initialization, the following ℓ^2 norms are

$$\sqrt{\sum_{i=1}^{H} v_i^2}, \sqrt{\sum_{i=1}^{H}\sum_{r=1}^{R} \|\boldsymbol{k}_{i,r}\|^2}, \sqrt{\sum_{i=1}^{H}\sum_{r=1}^{R} \|\boldsymbol{q}_{i,r}\|^2} \sim O(w_{\text{init}}). \tag{37}$$

B.3 Kronecker Product

The Kronecker product, denoted as $\otimes$, is defined for two matrices of arbitrary sizes. The Kronecker product of the matrix $\boldsymbol{A} \in \mathbb{R}^{p\times q}$ and the matrix $\boldsymbol{B} \in \mathbb{R}^{r\times s}$ is a block matrix of shape $pr \times qs$

$$\boldsymbol{A} \otimes \boldsymbol{B} = \begin{bmatrix} a_{11} & \cdots & a_{1q} \\ \vdots & \ddots & \vdots \\ a_{p1} & \cdots & a_{pq} \end{bmatrix} \otimes \boldsymbol{B} = \begin{bmatrix} a_{11}\boldsymbol{B} & \cdots & a_{1q}\boldsymbol{B} \\ \vdots & \ddots & \vdots \\ a_{p1}\boldsymbol{B} & \cdots & a_{pq}\boldsymbol{B} \end{bmatrix}.$$

Based on the definition, it holds for any pair of column vectors $\boldsymbol{a}$ and $\boldsymbol{b}$

$$\boldsymbol{a} \otimes \boldsymbol{b} = \mathtt{vec}(\boldsymbol{b}\boldsymbol{a}^\top).$$

We quote some properties of the Kronecker product to be used in our derivations:

$$(c\boldsymbol{A}) \otimes \boldsymbol{B} = \boldsymbol{A} \otimes (c\boldsymbol{B}) = c(\boldsymbol{A} \otimes \boldsymbol{B}) \quad \text{for any scalar } c, \tag{38a}$$

$$(\boldsymbol{A} \otimes \boldsymbol{B})^\top = \boldsymbol{A}^\top \otimes \boldsymbol{B}^\top \quad \text{for any matrices } \boldsymbol{A}, \boldsymbol{B}, \tag{38b}$$

$$(\boldsymbol{A} \otimes \boldsymbol{B})^{-1} = \boldsymbol{A}^{-1} \otimes \boldsymbol{B}^{-1} \quad \text{for invertible matrices } \boldsymbol{A}, \boldsymbol{B}, \tag{38c}$$

$$(\boldsymbol{A} \otimes \boldsymbol{B})(\boldsymbol{C} \otimes \boldsymbol{D}) = (\boldsymbol{A}\boldsymbol{C}) \otimes (\boldsymbol{B}\boldsymbol{D}) \quad \text{for compatible matrices } \boldsymbol{A}, \boldsymbol{B}, \boldsymbol{C}, \boldsymbol{D}, \tag{38d}$$

$$(\boldsymbol{B}^\top \otimes \boldsymbol{A})\mathtt{vec}(\boldsymbol{M}) = \mathtt{vec}(\boldsymbol{A}\boldsymbol{M}\boldsymbol{B}) \quad \text{for compatible matrices } \boldsymbol{A}, \boldsymbol{B}, \boldsymbol{M}. \tag{38e}$$

C Linear Attention with Merged Key and Query

C.1 Justification for Zero Blocks Assumption

We prove our claim that $\boldsymbol{v}_i$ and $\boldsymbol{u}_i$ in Equation (7) remain zero throughout training if their initialization is zero.

Proof. The bottom right entry of $\mathsf{ATTN}_{\mathrm{M}}(\boldsymbol{X})$ is given by Equation (7), which is

$$\hat{y}_q = \sum_{i=1}^{H} \left(\boldsymbol{v}_i^\top \left(\hat{\boldsymbol{\Lambda}} + \frac{1}{N} \boldsymbol{x}_q \boldsymbol{x}_q^\top \right) \boldsymbol{U}_i + v_i \boldsymbol{\beta}^\top \boldsymbol{U}_i + \boldsymbol{v}_i^\top \boldsymbol{\beta} \boldsymbol{u}_i^\top + v_i \boldsymbol{w}^\top \hat{\boldsymbol{\Lambda}} \boldsymbol{w} \boldsymbol{u}_i^\top \right) \boldsymbol{x}_q$$

If we initialize $\boldsymbol{v}_i, \boldsymbol{u}_i = \boldsymbol{0}$, $\hat{y}_q$ is

$$\hat{y}_q = \sum_{i=1}^{H} v_i \boldsymbol{\beta}^\top \boldsymbol{U}_i \boldsymbol{x}_q = \boldsymbol{w}^\top \hat{\boldsymbol{\Lambda}} \sum_{i=1}^{H} v_i \boldsymbol{U}_i \boldsymbol{x}_q.$$

We now calculate the gradient updates of $\boldsymbol{v}_i, \boldsymbol{u}_i$ and prove their gradients are zero if their initialization is zero. The gradient update of $\boldsymbol{v}_i$ contains $\mathbb{E}(\boldsymbol{w})$, which is zero as defined in Equation (3). Specifically, we have, from Equation (10),

$$\begin{aligned}
\tau \dot{\boldsymbol{v}}_i &= \mathbb{E}\left[(y_q - \hat{y}_q) \left(\left(\hat{\boldsymbol{\Lambda}} + \frac{1}{N} \boldsymbol{x}_q \boldsymbol{x}_q^\top \right) \boldsymbol{U}_i + \boldsymbol{\beta} \boldsymbol{u}_i^\top \right) \boldsymbol{x}_q \right] \\
&= \mathbb{E}\left[\left(\boldsymbol{w}^\top \boldsymbol{x}_q - \boldsymbol{w}^\top \hat{\boldsymbol{\Lambda}} \sum_{i=1}^{H} v_i \boldsymbol{U}_i \boldsymbol{x}_q \right) \left(\hat{\boldsymbol{\Lambda}} + \frac{1}{N} \boldsymbol{x}_q \boldsymbol{x}_q^\top \right) \boldsymbol{U}_i \boldsymbol{x}_q \right] \\
&= \mathbb{E}_{\boldsymbol{w}}(\boldsymbol{w})^\top \mathbb{E}\left[\left(\boldsymbol{x}_q - \hat{\boldsymbol{\Lambda}} \sum_{i=1}^{H} v_i \boldsymbol{U}_i \boldsymbol{x}_q \right) \left(\hat{\boldsymbol{\Lambda}} + \frac{1}{N} \boldsymbol{x}_q \boldsymbol{x}_q^\top \right) \boldsymbol{U}_i \boldsymbol{x}_q \right] \\
&= \boldsymbol{0}.
\end{aligned} \tag{39}$$

Note that we separated the expectation of $\boldsymbol{w}$ because of the independence between $\boldsymbol{w}$ and all $\boldsymbol{x}$ tokens.

The gradient update of $\boldsymbol{v}_i$ contains $\mathbb{E}_{\boldsymbol{w}}\left(\boldsymbol{w}^\top \hat{\boldsymbol{\Lambda}} \boldsymbol{w} \boldsymbol{w}^\top \right)$, whose entries are linear combinations of third moments of the zero-mean normal random variable $\boldsymbol{w}$, and are thus zero. Specifically, we have

$$\begin{aligned}
\tau \dot{\boldsymbol{u}}_i &= \mathbb{E}\left[\left(\boldsymbol{v}_i^\top \boldsymbol{\beta} + v_i \boldsymbol{w}^\top \hat{\boldsymbol{\Lambda}} \boldsymbol{w} \right) (y_q - \hat{y}_q) \boldsymbol{x}_q \right] \\
&= \mathbb{E}\left[v_i \boldsymbol{w}^\top \hat{\boldsymbol{\Lambda}} \boldsymbol{w} \left(\boldsymbol{w}^\top \boldsymbol{x}_q - \boldsymbol{w}^\top \hat{\boldsymbol{\Lambda}} \sum_{i=1}^{H} v_i \boldsymbol{U}_i \boldsymbol{x}_q \right) \boldsymbol{x}_q \right] \\
&= \mathbb{E}_{\boldsymbol{w}} \left(\boldsymbol{w}^\top \hat{\boldsymbol{\Lambda}} \boldsymbol{w} \boldsymbol{w}^\top \right) \mathbb{E}\left[v_i \left(\boldsymbol{x}_q - \hat{\boldsymbol{\Lambda}} \sum_{i=1}^{H} v_i \boldsymbol{U}_i \boldsymbol{x}_q \right) \boldsymbol{x}_q \right] \\
&= \boldsymbol{0}.
\end{aligned} \tag{40}$$

■

C.2 Gradient Flow Equations

We here derive the gradient flow dynamics for linear attention with merged key and query given in Equation (13).

For linear attention with merged key and query, the prediction for the query output can be written as $\hat{y}_q = \boldsymbol{w}_2^\top \boldsymbol{W}_1 \boldsymbol{z}$ due to Equation (11). Based on the gradient flow training rule in Equation (10), the gradient flow dynamics is

$$\begin{aligned}\tau \dot{\boldsymbol{W}}_1 &= \mathbb{E}\left[\boldsymbol{w}_2\left(y_q - \boldsymbol{w}_2^\top \boldsymbol{W}_1 \boldsymbol{z}\right)\boldsymbol{z}^\top\right] = \boldsymbol{w}_2\left(\mathbb{E}\left(y_q \boldsymbol{z}^\top\right) - \boldsymbol{w}_2^\top \boldsymbol{W}_1 \mathbb{E}\left(\boldsymbol{z}\boldsymbol{z}^\top\right)\right), \\ \tau \dot{\boldsymbol{w}}_2 &= \mathbb{E}\left[\boldsymbol{W}_1\left(y_q - \boldsymbol{w}_2^\top \boldsymbol{W}_1 \boldsymbol{z}\right)\boldsymbol{z}\right] = \boldsymbol{W}_1\left(\mathbb{E}\left(y_q \boldsymbol{z}^\top\right) - \boldsymbol{w}_2^\top \boldsymbol{W}_1 \mathbb{E}\left(\boldsymbol{z}\boldsymbol{z}^\top\right)\right)^\top,\end{aligned}$$

which was introduced in Equation (13) in the main text.

C.3 Fixed Points

To find the fixed points, we set the gradients in Equation (13) to zero

$$\begin{aligned}\tau \dot{\boldsymbol{W}}_1 &= \boldsymbol{w}_2\left(\mathbb{E}\left(y_q \boldsymbol{z}^\top\right) - \boldsymbol{w}_2^\top \boldsymbol{W}_1 \mathbb{E}\left(\boldsymbol{z}\boldsymbol{z}^\top\right)\right) \overset{\text{set}}{=} \boldsymbol{0}, \\ \tau \dot{\boldsymbol{w}}_2 &= \boldsymbol{W}_1\left(\mathbb{E}\left(y_q \boldsymbol{z}^\top\right) - \boldsymbol{w}_2^\top \boldsymbol{W}_1 \mathbb{E}\left(\boldsymbol{z}\boldsymbol{z}^\top\right)\right)^\top \overset{\text{set}}{=} \boldsymbol{0},\end{aligned}$$

which yield the two manifolds of fixed points introduced in Equation (14) in the main text:

$$\begin{aligned}\boldsymbol{w}_2 = \boldsymbol{0},\, \boldsymbol{W}_1 = \boldsymbol{0} \quad &\Rightarrow \quad \mathcal{M}_0 = \{\boldsymbol{w}_2 = \boldsymbol{0}, \boldsymbol{W}_1 = \boldsymbol{0}\}, \\ \mathbb{E}\left(y_q \boldsymbol{z}^\top\right) - \boldsymbol{w}_2^\top \boldsymbol{W}_1 \mathbb{E}\left(\boldsymbol{z}\boldsymbol{z}^\top\right) = \boldsymbol{0} \quad &\Rightarrow \quad \mathcal{M}_* = \left\{\boldsymbol{w}_2, \boldsymbol{W}_1 \middle| \boldsymbol{w}_2^\top \boldsymbol{W}_1 = \mathbb{E}\left(y_q \boldsymbol{z}^\top\right)\mathbb{E}\left(\boldsymbol{z}\boldsymbol{z}^\top\right)^{-1}\right\}.\end{aligned}$$

C.4 Duality of the Global Minimum Solution

We here prove the second equality in Equation (16), that is

$$\mathbb{E}\left(y_q \boldsymbol{z}^\top\right)\mathbb{E}\left(\boldsymbol{z}\boldsymbol{z}^\top\right)^{-1}\boldsymbol{z} = \boldsymbol{\beta}^\top\left(\boldsymbol{\Lambda} + \frac{\boldsymbol{\Lambda} + \mathtt{tr}(\boldsymbol{\Lambda})\boldsymbol{I}}{N}\right)^{-1}\boldsymbol{x}_q.$$

This equality implies the intriguing duality that the linear regression solution in the cubic feature space of $\boldsymbol{z}$ is the in-context linear regression solution in the $\boldsymbol{x}_n, y_n$ token space for each sequence.

Proof. We first calculate the input and input-output correlations in the cubic feature space. We denote $\boldsymbol{\Lambda}_q \equiv \mathbb{E}\left(\boldsymbol{x}_q \boldsymbol{x}_q^\top\right)$. While $\boldsymbol{\Lambda}_q = \boldsymbol{\Lambda}$, this equality is not used in this proof.

We substitute in $\boldsymbol{z} = \boldsymbol{x}_q \otimes \boldsymbol{\beta}, \boldsymbol{\beta} = \hat{\boldsymbol{\Lambda}}\boldsymbol{w}$ and use the properties of the Kronecker product listed in Appendix B.3 to obtain

$$\begin{aligned}\mathbb{E}\left(y_q \boldsymbol{z}^\top\right) &= \mathbb{E}\left[\boldsymbol{x}_q^\top \boldsymbol{w}(\boldsymbol{x}_q^\top \otimes \boldsymbol{\beta}^\top)\right] \\ &= \mathbb{E}\left(\boldsymbol{x}_q^\top \otimes \boldsymbol{x}_q^\top \boldsymbol{w}\boldsymbol{w}^\top \hat{\boldsymbol{\Lambda}}\right) \\ &= \mathbb{E}\left(\boldsymbol{x}_q^\top \otimes \boldsymbol{x}_q^\top \hat{\boldsymbol{\Lambda}}\right) \\ &= \mathbb{E}\mathtt{vec}\left(\hat{\boldsymbol{\Lambda}}\boldsymbol{x}_q \boldsymbol{x}_q^\top\right)^\top \\ &= \mathtt{vec}(\boldsymbol{\Lambda}\boldsymbol{\Lambda}_q)^\top.\end{aligned} \tag{41}$$

Similarly, we have

$$\begin{aligned}
\mathbb{E}\left(\boldsymbol{z}\boldsymbol{z}^\top\right) &= \mathbb{E}\left[(\boldsymbol{x}_q \otimes \boldsymbol{\beta})(\boldsymbol{x}_q^\top \otimes \boldsymbol{\beta}^\top)\right] \\
&= \mathbb{E}\left[(\boldsymbol{x}_q\boldsymbol{x}_q^\top) \otimes (\boldsymbol{\beta}\boldsymbol{\beta}^\top)\right] \\
&= \mathbb{E}(\boldsymbol{x}_q\boldsymbol{x}_q^\top) \otimes \mathbb{E}(\hat{\boldsymbol{\Lambda}}\boldsymbol{w}\boldsymbol{w}^\top\hat{\boldsymbol{\Lambda}}) \\
&= \boldsymbol{\Lambda}_q \otimes \mathbb{E}\left(\hat{\boldsymbol{\Lambda}}^2\right) \\
&= \boldsymbol{\Lambda}_q \otimes \left(\boldsymbol{\Lambda}^2 + \frac{\boldsymbol{\Lambda} + \mathtt{tr}(\boldsymbol{\Lambda})\boldsymbol{I}}{N}\boldsymbol{\Lambda}\right), \qquad (42)
\end{aligned}$$

where we substituted in $\mathbb{E}\left(\hat{\boldsymbol{\Lambda}}^2\right)$ obtained from Equation (31) into the last equality. Using Equation (38c), the inverse of $\mathbb{E}\left(\boldsymbol{z}\boldsymbol{z}^\top\right)$ is

$$\mathbb{E}\left(\boldsymbol{z}\boldsymbol{z}^\top\right)^{-1} = \boldsymbol{\Lambda}_q^{-1} \otimes \left(\boldsymbol{\Lambda} + \frac{\boldsymbol{\Lambda} + \mathtt{tr}(\boldsymbol{\Lambda})\boldsymbol{I}}{N}\right)\boldsymbol{\Lambda}^{-1} \qquad (43)$$

Multiplying Equations (41) and (43) finishes the proof

$$\begin{aligned}
\mathbb{E}\left(y_q\boldsymbol{z}^\top\right)\mathbb{E}\left(\boldsymbol{z}\boldsymbol{z}^\top\right)^{-1}\boldsymbol{z} &= \mathtt{vec}(\boldsymbol{\Lambda}\boldsymbol{\Lambda}_q)^\top\boldsymbol{\Lambda}_q^{-1} \otimes \left(\boldsymbol{\Lambda} + \frac{\boldsymbol{\Lambda} + \mathtt{tr}(\boldsymbol{\Lambda})\boldsymbol{I}}{N}\right)\boldsymbol{\Lambda}^{-1}(\boldsymbol{x}_q \otimes \boldsymbol{\beta}) \\
&= \mathtt{vec}\left[\left(\boldsymbol{\Lambda} + \frac{\boldsymbol{\Lambda} + \mathtt{tr}(\boldsymbol{\Lambda})\boldsymbol{I}}{N}\right)\boldsymbol{\Lambda}^{-1}\boldsymbol{\Lambda}\boldsymbol{\Lambda}_q\boldsymbol{\Lambda}_q^{-1}\right]^\top(\boldsymbol{x}_q \otimes \boldsymbol{\beta}) \\
&= \mathtt{vec}\left[\left(\boldsymbol{\Lambda} + \frac{\boldsymbol{\Lambda} + \mathtt{tr}(\boldsymbol{\Lambda})\boldsymbol{I}}{N}\right)^{-1}\right]^\top(\boldsymbol{x}_q \otimes \boldsymbol{\beta}) \\
&= \boldsymbol{\beta}^\top\left(\boldsymbol{\Lambda} + \frac{\boldsymbol{\Lambda} + \mathtt{tr}(\boldsymbol{\Lambda})\boldsymbol{I}}{N}\right)^{-1}\boldsymbol{x}_q.
\end{aligned}$$

■

C.5 Analytical Time-Course Solution for White Covariance

We include a derivation of the time-course solution of two-layer fully-connected linear network with white input covariance and vanishing initialization following Saxe et al. (2014), and then apply it to linear attention. With vanishing initialization, the conserved quantity given in Equation (17) is exactly zero throughout learning,

$$\boldsymbol{w}_2\boldsymbol{w}_2^\top - \boldsymbol{W}_1\boldsymbol{W}_1^\top = \boldsymbol{0}.$$

Hence, there exists a unit norm vector $\boldsymbol{m}$ such that $\boldsymbol{W}_1 = \boldsymbol{w}_2\boldsymbol{m}^\top$. With the assumption of white covariance, $\mathbb{E}\left(\boldsymbol{z}\boldsymbol{z}^\top\right) = \alpha\boldsymbol{I}_{D^2}$, Saxe et al. (2014) and Atanasov et al. (2022) have shown that the unit norm vector $\boldsymbol{m}$ is parallel with the correlation between y_q and $\boldsymbol{z}$ throughout training, that is

$$\boldsymbol{W}_1 = \boldsymbol{w}_2\boldsymbol{m}^\top, \quad \text{where } \boldsymbol{m} = \frac{\mathbb{E}(y_q\boldsymbol{z})}{\|\mathbb{E}(y_q\boldsymbol{z})\|}. \qquad (44)$$

We substitute Equation (44) and the white covariance assumption, $\mathbb{E}\left(\boldsymbol{z}\boldsymbol{z}^\top\right) = \alpha\boldsymbol{I}_{D^2}$, into the gradient flow dynamics given in Equation (13) and obtain

$$\tau\dot{\boldsymbol{w}}_2 = \boldsymbol{w}_2\boldsymbol{m}^\top\left(\mathbb{E}(y_q\boldsymbol{z}) - \alpha\boldsymbol{w}_2^\top\boldsymbol{w}_2\boldsymbol{m}\right) = \boldsymbol{w}_2\left(\gamma - \alpha\boldsymbol{w}_2^\top\boldsymbol{w}_2\right), \quad \text{where } \gamma \equiv \|\mathbb{E}(y_q\boldsymbol{z})\|.$$

Notice that the square of the ℓ^2 norm of $\boldsymbol{w}_2$ follows a solvable ordinary differential equation. Let $s = \boldsymbol{w}_2^\top \boldsymbol{w}_2$. The dynamics of $s(t)$ is

$$\tau \dot{s} = 2\boldsymbol{w}_2^\top \tau \dot{\boldsymbol{w}}_2 = 2\boldsymbol{w}_2^\top \boldsymbol{w}_2 \left(\gamma - \alpha \boldsymbol{w}_2^\top \boldsymbol{w}_2\right) = 2s(\gamma - \alpha s). \tag{45}$$

We can solve this differential equation by separating variables and integrating both sides,

$$\int_{s(0)}^{s(t)} \frac{1}{s(\gamma - \alpha s)} \mathrm{d}s = \int_0^t \frac{2}{\tau} \mathrm{d}t \quad \Rightarrow \quad \frac{1}{\gamma} \ln \frac{s(t)(\gamma - \alpha s(0))}{s(0)(\gamma - \alpha s(t))} = \frac{2}{\tau} t.$$

The solution of $s(t)$ is given by

$$s(t) = \frac{\gamma e^{2\gamma \frac{t}{\tau}}}{\alpha \left(e^{2\gamma \frac{t}{\tau}} - 1\right) + \frac{\gamma}{s(0)}}.$$

The time-course of the total weights is given by

$$\boldsymbol{w}_2^\top \boldsymbol{W}_1 = s(t) \boldsymbol{m}^\top = s(t) \frac{\mathbb{E}(y_q \boldsymbol{z})^\top}{\|\mathbb{E}(y_q \boldsymbol{z})^\top\|}. \tag{46}$$

We now apply this solution to linear attention. If the input token covariance is identity, $\boldsymbol{\Lambda} = \boldsymbol{I}_D$, we calculate the input and input-output correlations in the cubic feature space according to Equations (41) and (42) and get

$$\begin{aligned}
\mathbb{E}\left(y_q \boldsymbol{z}^\top\right) &= \mathtt{vec}(\boldsymbol{I}_D)^\top, \\
\mathbb{E}\left(\boldsymbol{z}\boldsymbol{z}^\top\right) &= \boldsymbol{I}_D \otimes \left(1 + \frac{1+D}{N}\right) \boldsymbol{I}_D = \left(1 + \frac{1+D}{N}\right) \boldsymbol{I}_{D^2}.
\end{aligned}$$

The parameters in the dynamics of the equivalent two-layer fully-connected linear network are

$$\alpha = 1 + \frac{1+D}{N}, \, \gamma = \|\mathtt{vec}(\boldsymbol{I}_D)\| = \sqrt{D}. \tag{47}$$

Substituting Equation (47) into Equation (46), we obtain

$$\boldsymbol{w}^\top \boldsymbol{W}_1(t) = s(t) \frac{\mathtt{vec}(\boldsymbol{I}_D)^\top}{\sqrt{D}}, \quad \text{where } s(t) = \frac{\sqrt{D} e^{2\sqrt{D}\frac{t}{\tau}}}{\left(1 + \frac{1+D}{N}\right)\left(e^{2\sqrt{D}\frac{t}{\tau}} - 1\right) + \frac{\sqrt{D}}{s(0)}}.$$

Due to the equivalence between linear attention and the two-layer fully-connected linear network given in Equation (11), we obtain

$$\mathsf{ATTN}_{\mathrm{M}}(\boldsymbol{X}; t)_{D+1,N+1} = \boldsymbol{w}_2^\top \boldsymbol{W}_1 \boldsymbol{z} = s(t) \frac{\mathtt{vec}(\boldsymbol{I}_D)^\top}{\sqrt{D}} \boldsymbol{x}_q \otimes \boldsymbol{\beta} = \frac{1}{\sqrt{D}} s(t) \boldsymbol{\beta}^\top \boldsymbol{I}_D \boldsymbol{x}_q = \frac{1}{\sqrt{D}} s(t) \boldsymbol{\beta}^\top \boldsymbol{x}_q.$$

which is Equation (15) in the main text where we have rewritten $\sigma(t) = s(t)/\sqrt{D}$.

The time-course of loss can also be expressed in terms of $\sigma(t)$ as

$$\mathcal{L}(t) = \left(1 - 2\sigma(t) + \left(1 + \frac{1+D}{N}\right)\sigma(t)^2\right) D. \tag{48}$$

C.6 Training Dynamics for General Covariance

C.6.1 Early Dynamics Predicts Duration of Plateau

For a general input covariance matrix, the full time-course solution to two-layer fully-connected linear networks is currently unavailable. Nonetheless, the training dynamics is well understood and we can analyze the early phase dynamics to estimate the duration of the loss plateau.

In the early phase of training when the loss plateaus, the weights have not moved much away from their small initialization. The training dynamics of $\boldsymbol{W}_1$ is mainly driven by the first term in Equation (13a), and similarly for $\boldsymbol{w}_2$ in Equation (13b)

$$\tau \dot{\boldsymbol{W}}_1 = \boldsymbol{w}_2 \left(\mathbb{E}\left(y_q \boldsymbol{z}^\top \right) - \boldsymbol{w}_2^\top \boldsymbol{W}_1 \mathbb{E}\left(\boldsymbol{z}\boldsymbol{z}^\top \right) \right) = \boldsymbol{w}_2 \mathbb{E}\left(y_q \boldsymbol{z}^\top \right) + O(w_{\text{init}}^3),$$
$$\tau \dot{\boldsymbol{w}}_2 = \boldsymbol{W}_1 \left(\mathbb{E}\left(y_q \boldsymbol{z}^\top \right) - \boldsymbol{w}_2^\top \boldsymbol{W}_1 \mathbb{E}\left(\boldsymbol{z}\boldsymbol{z}^\top \right) \right)^\top = \boldsymbol{W}_1 \mathbb{E}\left(y_q \boldsymbol{z} \right) + O(w_{\text{init}}^3).$$

Thus, the early training dynamics is well approximated by the linear dynamical system

$$\tau \dot{\boldsymbol{W}}_1 = \boldsymbol{w}_2 \mathbb{E}\left(y_q \boldsymbol{z}^\top \right), \quad \tau \dot{\boldsymbol{w}}_2 = \boldsymbol{W}_1 \mathbb{E}\left(y_q \boldsymbol{z} \right).$$

In the case of nonwhite covariance, the change of variable in Equation (44) is valid in the early phase of training but no longer valid when the loss starts to decrease appreciably (Atanasov et al. 2022). For the early training dynamics, we apply the change of variable in Equation (44) and obtain

$$\tau \dot{\boldsymbol{w}}_2 = \boldsymbol{w}_2 \boldsymbol{m}^\top \mathbb{E}\left(y_q \boldsymbol{z} \right) = \gamma \boldsymbol{w}_2.$$

Recall that $s = \boldsymbol{w}_2^\top \boldsymbol{w}_2$. The early phase dynamics of $s(t)$ is approximately

$$\tau \dot{s} = 2\gamma s.$$

We solve the differential equation and obtain

$$t = \frac{\tau}{2\gamma} (\ln s(t) - \ln s(0)).$$

Due to small initialization, $\ln s(t)$ at the end of the plateau is much smaller compared to $-\ln s(0)$. Hence, the duration of the initial plateau of loss, t_{plateau}, is

$$t_{\text{plateau}} \approx \frac{\tau}{2\gamma} \ln \frac{1}{s(0)}. \tag{49}$$

Here, the scalar γ is

$$\begin{aligned} \gamma \equiv \| \mathbb{E}(y_q \boldsymbol{z}) \| = \left\| \mathbb{E}\left(\boldsymbol{w}^\top \boldsymbol{x}_q \text{vec}(\boldsymbol{\beta} \boldsymbol{x}_q^\top) \right) \right\| &= \left\| \mathbb{E}\left(\boldsymbol{w}^\top \boldsymbol{x}_q \boldsymbol{\beta} \boldsymbol{x}_q^\top \right) \right\|_{\text{F}} \\ &= \left\| \mathbb{E}\left(\hat{\boldsymbol{\Lambda}} \boldsymbol{w} \boldsymbol{w}^\top \boldsymbol{x}_q \boldsymbol{x}_q^\top \right) \right\|_{\text{F}} \\ &= \left\| \mathbb{E}\left(\hat{\boldsymbol{\Lambda}} \right) \mathbb{E}_{\boldsymbol{w}}\left(\boldsymbol{w} \boldsymbol{w}^\top \right) \mathbb{E}_{\boldsymbol{x}_q}\left(\boldsymbol{x}_q \boldsymbol{x}_q^\top \right) \right\|_{\text{F}} \\ &= \left\| \boldsymbol{\Lambda}^2 \right\|_{\text{F}} \end{aligned} \tag{50}$$

Substituting Equation (50) into Equation (49), we obtain the approximate duration of the loss plateau

$$t_{\text{plateau}} \approx \frac{\tau}{2 \left\| \boldsymbol{\Lambda}^2 \right\|_{\text{F}}} \ln \frac{1}{s(0)} \approx \frac{\tau}{\left\| \boldsymbol{\Lambda}^2 \right\|_{\text{F}}} \ln \frac{1}{w_{\text{init}}}, \tag{51}$$

where we used the definition $s(0) = \| \boldsymbol{w}_2(0) \|^2 = w_{\text{init}}^2$.

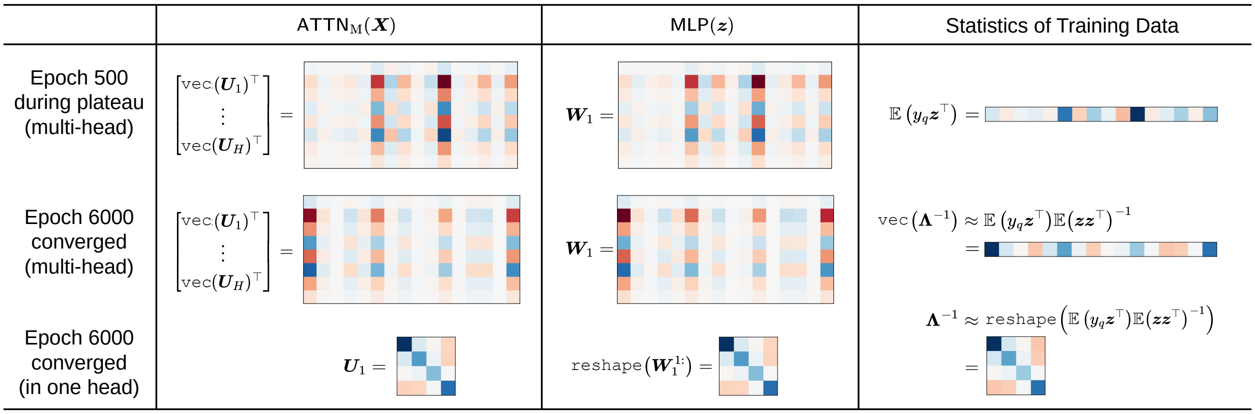

Figure 6: The dynamics of weights in multi-head linear attention with merged key and query can be predicted with statistics of the training dataset. We plot the weights at different times in training, corresponding to the loss trajectories in Figure 1 (right). The weights in linear attention (first column) stay close to the weights in the fully-connected linear network (second column) throughout training. During the initial plateau, the vectorized key-query weights in attention $\texttt{vec}(\boldsymbol{U}_1), \cdots, \texttt{vec}(\boldsymbol{U}_i)$ and the first-layer weight in the fully-connected network $\boldsymbol{W}_1$ are rank-one and align with the correlation between the output and the cubic feature input $\mathbb{E}\left(y_q \boldsymbol{z}^\top\right)$ (top row). At convergence, $\texttt{vec}(\boldsymbol{U}_1), \cdots, \texttt{vec}(\boldsymbol{U}_i)$ in attention and $\boldsymbol{W}_1$ in the fully-connected linear network are rank-one and align with the linear regression solution in the cubic feature space $\mathbb{E}\left(y_q \boldsymbol{z}^\top\right)\mathbb{E}\left(\boldsymbol{z}\boldsymbol{z}^\top\right)^{-1}$ (middle row), which is also the in-context linear regression solution in the original token space $\boldsymbol{\Lambda}^{-1}$ (bottom row) as described by Equation (16). The approximate equality in the third column is exact when the sequence length $N \to \infty$.

C.6.2 Weights Dynamics

For a white input covariance, the training dynamics reduces to a scalar ordinary differential equation about $s(t)$ given in Equation (45). For a general input covariance, the vector $\boldsymbol{m}$ in the change of variable defined in Equation (44) rotates during training. As shown in the top row of Figure 6, during the initial loss plateau, the rows of the first-layer weight align with the input-output correlation $\mathbb{E}\left(y_q \boldsymbol{z}^\top\right)$ but do not change appreciably in scale (Atanasov et al. 2022). Later, when the loss decreases rapidly, the first-layer weight grows in scale and rotates to align with the global minimum solution, $\mathbb{E}\left(y_q \boldsymbol{z}^\top\right)\mathbb{E}\left(\boldsymbol{z}\boldsymbol{z}^\top\right)^{-1}$. The alignment and rotation behaviors apply to the rows of the first-layer weight in the fully-connected network, corresponding to the merged key-query weights in the different heads in linear attention, as shown in Figure 6.

D Linear Attention with Separate Rank-One Key and Query

D.1 Justification for Zero Blocks Assumption

This is a special case of linear attention with separate rank-R key and query. The proof for the more general rank-R case can be found in Appendix E.1.

D.2 Gradient Flow Equations

We here derive the gradient flow dynamics for linear attention with separate rank-one key and query introduced in Equation (19).

Based on the gradient flow training rule in Equation (10), the gradient flow dynamics for the value, key, and query weights in the i-th head are

$$\tau \dot{v}_i = \boldsymbol{k}_i^\top \mathbb{E}\left(\boldsymbol{\beta}(y_q - \hat{y}_q)\boldsymbol{x}_q^\top\right) \boldsymbol{q}_i, \tag{52a}$$

$$\tau \dot{\boldsymbol{k}}_i = v_i \mathbb{E}\left(\boldsymbol{\beta}(y_q - \hat{y}_q)\boldsymbol{x}_q^\top\right) \boldsymbol{q}_i, \tag{52b}$$

$$\tau \dot{\boldsymbol{q}}_i = v_i \mathbb{E}\left(\boldsymbol{x}_q(y_q - \hat{y}_q)\boldsymbol{\beta}^\top\right) \boldsymbol{k}_i. \tag{52c}$$

We calculate the common term in Equation (52), that is

$$\begin{aligned}
\mathbb{E}\left(\boldsymbol{\beta}(y_q - \hat{y}_q)\boldsymbol{x}_q^\top\right) &= \mathbb{E}\left[\boldsymbol{\beta}\left(\boldsymbol{w}^\top \boldsymbol{x}_q - \sum_{i=1}^H v_i \boldsymbol{\beta}^\top \boldsymbol{k}_i \boldsymbol{q}_i^\top \boldsymbol{x}_q\right) \boldsymbol{x}_q^\top\right] \\
&= \mathbb{E}\left[\hat{\boldsymbol{\Lambda}} \boldsymbol{w}\boldsymbol{w}^\top \left(\boldsymbol{I} - \sum_{i=1}^H v_i \hat{\boldsymbol{\Lambda}} \boldsymbol{k}_i \boldsymbol{q}_i^\top\right) \boldsymbol{x}_q \boldsymbol{x}_q^\top\right] \\
&= \mathbb{E}\left(\hat{\boldsymbol{\Lambda}}\right) \mathbb{E}_{\boldsymbol{w}}\left(\boldsymbol{w}\boldsymbol{w}^\top\right) \mathbb{E}_{\boldsymbol{x}_q}\left(\boldsymbol{x}_q \boldsymbol{x}_q^\top\right) - \mathbb{E}\left(\hat{\boldsymbol{\Lambda}} \boldsymbol{w}\boldsymbol{w}^\top \hat{\boldsymbol{\Lambda}}\right) \sum_{i=1}^H v_i \boldsymbol{k}_i \boldsymbol{q}_i^\top \mathbb{E}_{\boldsymbol{x}_q}\left(\boldsymbol{x}_q \boldsymbol{x}_q^\top\right) \\
&= \boldsymbol{\Lambda}^2 - \mathbb{E}\left(\hat{\boldsymbol{\Lambda}}^2\right) \sum_{i=1}^H v_i \boldsymbol{k}_i \boldsymbol{q}_i^\top \boldsymbol{\Lambda}
\end{aligned} \tag{53}$$

Substituting Equation (53) into Equation (52), we arrive at the same equations as Equation (19) in the main text

$$\begin{aligned}
\tau \dot{v}_i &= \boldsymbol{k}_i^\top \left(\boldsymbol{\Lambda}^2 - \mathbb{E}\left(\hat{\boldsymbol{\Lambda}}^2\right) \sum_{i'=1}^H v_{i'} \boldsymbol{k}_{i'} \boldsymbol{q}_{i'}^\top \boldsymbol{\Lambda}\right) \boldsymbol{q}_i, \\
\tau \dot{\boldsymbol{k}}_i &= v_i \left(\boldsymbol{\Lambda}^2 - \mathbb{E}\left(\hat{\boldsymbol{\Lambda}}^2\right) \sum_{i'=1}^H v_{i'} \boldsymbol{k}_{i'} \boldsymbol{q}_{i'}^\top \boldsymbol{\Lambda}\right) \boldsymbol{q}_i, \\
\tau \dot{\boldsymbol{q}}_i &= v_i \left(\boldsymbol{\Lambda}^2 - \boldsymbol{\Lambda} \sum_{i'=1}^H v_{i'} \boldsymbol{k}_{i'} \boldsymbol{q}_{i'}^\top \mathbb{E}\left(\hat{\boldsymbol{\Lambda}}^2\right)\right) \boldsymbol{k}_i.
\end{aligned}$$

where the data statistics $\mathbb{E}\left(\hat{\boldsymbol{\Lambda}}^2\right)$ is calculated in Equation (31).

D.3 Validity of Fixed Points

We prove that the fixed points given in Equation (21) are valid.

Proof. When the model is at a fixed point in set $\mathcal{M}(\mathcal{S}_m)$, it satisfies Equation (23). Equation (23) can be rewritten using a_d (defined in Equation (32)) as

$$\sum_{i=1}^H v_i \boldsymbol{k}_i \boldsymbol{q}_i^\top = \sum_{d \in \mathcal{S}_m} \frac{\lambda_d}{a_d} \boldsymbol{e}_d \boldsymbol{e}_d^\top. \tag{55}$$

Using Equations (33) and (55), we can simplify a common term in the gradient descent dynamics in Equation (19) to

$$
\begin{aligned}
\boldsymbol{\Lambda}^2 - \mathbb{E}\left(\hat{\boldsymbol{\Lambda}}^2\right) \sum_{i=1}^{H} v_i \boldsymbol{k}_i \boldsymbol{q}_i^\top \boldsymbol{\Lambda} &= \sum_{d=1}^{D} \lambda_d^2 \boldsymbol{e}_d \boldsymbol{e}_d^\top - \sum_{d'=1}^{D} a_{d'} \boldsymbol{e}_{d'} \boldsymbol{e}_{d'}^\top \sum_{d \in \mathcal{S}_m} \frac{\lambda_d}{a_d} \boldsymbol{e}_d \boldsymbol{e}_d^\top \boldsymbol{\Lambda} \\
&= \sum_{d=1}^{D} \lambda_d^2 \boldsymbol{e}_d \boldsymbol{e}_d^\top - \sum_{d \in \mathcal{S}_m} \lambda_d \boldsymbol{e}_d \boldsymbol{e}_d^\top \boldsymbol{\Lambda} \\
&= \sum_{d \notin \mathcal{S}_m} \lambda_d^2 \boldsymbol{e}_d \boldsymbol{e}_d^\top . \qquad (56)
\end{aligned}
$$

Substituting Equation (56) into Equation (19), we obtain the gradient flow dynamics when the model is at a fixed point in $\mathcal{M}(\mathcal{S}_m)$

$$
\tau \dot{v}_i = \boldsymbol{k}_i^\top \left(\sum_{d \notin \mathcal{S}_m} \lambda_d^2 \boldsymbol{e}_d \boldsymbol{e}_d^\top \right) \boldsymbol{q}_i, \qquad (57a)
$$

$$
\tau \dot{\boldsymbol{k}}_i = v_i \left(\sum_{d \notin \mathcal{S}_m} \lambda_d^2 \boldsymbol{e}_d \boldsymbol{e}_d^\top \right) \boldsymbol{q}_i, \qquad (57b)
$$

$$
\tau \dot{\boldsymbol{q}}_i = v_i \left(\sum_{d \notin \mathcal{S}_m} \lambda_d^2 \boldsymbol{e}_d \boldsymbol{e}_d^\top \right) \boldsymbol{k}_i. \qquad (57c)
$$

(i) For the heads with a nonzero value weight, $v_i \neq 0$, the key and query weights at a fixed point satisfy condition (C2) for Equation (21), that is the key and query weights lie in the span of $\{\boldsymbol{e}_d\}_{d \in \mathcal{S}_m}$ and thus can be written as

$$
\boldsymbol{k}_i = \sum_{d \in \mathcal{S}_m} b_d \boldsymbol{e}_d, \quad b_d \in \mathbb{R}, \qquad (58a)
$$

$$
\boldsymbol{q}_i = \sum_{d \in \mathcal{S}_m} c_d \boldsymbol{e}_d, \quad c_d \in \mathbb{R}. \qquad (58b)
$$

Substituting Equation (58) into the gradient flow dynamics given in Equation (57), we obtain

$$
\begin{aligned}
\tau \dot{v}_i &= \boldsymbol{k}_i^\top \left(\sum_{d \notin \mathcal{S}_m} \lambda_d^2 \boldsymbol{e}_d \boldsymbol{e}_d^\top \right) \sum_{d' \in \mathcal{S}_m} c_{d'} \boldsymbol{e}_{d'} = 0, \\
\tau \dot{\boldsymbol{k}}_i &= v_i \left(\sum_{d \notin \mathcal{S}_m} \lambda_d^2 \boldsymbol{e}_d \boldsymbol{e}_d^\top \right) \sum_{d' \in \mathcal{S}_m} c_{d'} \boldsymbol{e}_{d'} = \boldsymbol{0}, \\
\tau \dot{\boldsymbol{q}}_i &= v_i \left(\sum_{d \notin \mathcal{S}_m} \lambda_d^2 \boldsymbol{e}_d \boldsymbol{e}_d^\top \right) \sum_{d' \in \mathcal{S}_m} b_{d'} \boldsymbol{e}_{d'} = \boldsymbol{0},
\end{aligned}
$$

where we have used the fact that $\boldsymbol{e}_d^\top \boldsymbol{e}_{d'} = 0$ if $d \neq d'$, because eigenvectors of the covariance matrix $\boldsymbol{\Lambda}$ are orthogonal.

(ii) For the heads with a zero value weight, $v_i = 0$, the gradients of the key and query weights in Equations (57b) and (57c) contain v_i and are thus zero, $\dot{\boldsymbol{k}}_i = \mathbf{0}, \dot{\boldsymbol{q}}_i = \mathbf{0}$. Further, the key and query weights of a head with a zero value weight satisfy condition (C3) for Equation (21). Without loss of generality, suppose that $\boldsymbol{q}_i$ lies in the span of $\{\boldsymbol{e}_d\}_{d\in\mathcal{S}_m}$, that is $\boldsymbol{q}_i$ satisfies Equation (58b). Substituting Equation (58b) into the gradient of v_i given in Equation (57a), we obtain

$$\dot{v}_i = \boldsymbol{k}_i^\top \left(\sum_{d\notin\mathcal{S}_m} \lambda_d^2 \boldsymbol{e}_d \boldsymbol{e}_d^\top \right) \sum_{d'\in\mathcal{S}_m} c_{d'} \boldsymbol{e}_{d'} = 0,$$

where we have again used the fact that eigenvectors of $\mathbf{\Lambda}$ are orthogonal.

Hence, when the model has weights specified in Equation (21), the gradients of the weights are zero, meaning that the fixed points are valid. ■

D.4 Loss Value at A Fixed Point

We derive the loss when the model is at a fixed point in set $\mathcal{M}(\mathcal{S}_m)$, where the loss is given by

$$\mathcal{L}(\mathcal{M}(\mathcal{S}_m)) = \mathtt{tr}(\mathbf{\Lambda}) - \sum_{d\in\mathcal{S}_m} \lambda_d \left(1 + \frac{1 + \mathtt{tr}(\mathbf{\Lambda})/\lambda_d}{N} \right)^{-1}. \tag{59}$$

Equation (24) in the main text follows directly from Equation (59) when taking $S_m = \{1, 2, \cdots, m\}$.

Proof. We substitute Equations (33) and (55) into the mean square loss and obtain

$$\begin{aligned}
\mathcal{L}(\mathcal{M}(\mathcal{S}_m)) &= \mathbb{E}(y_q - \hat{y}_q)^2 \\
&= \mathbb{E}\left(\boldsymbol{w}^\top \boldsymbol{x}_q - \sum_{d\in\mathcal{S}_m} \frac{\lambda_d}{a_d} \boldsymbol{w}^\top \hat{\mathbf{\Lambda}} \boldsymbol{e}_d \boldsymbol{e}_d^\top \boldsymbol{x}_q \right)^2 \\
&= \mathbb{E}\left[\boldsymbol{x}_q^\top \left(\boldsymbol{I} - \sum_{d\in\mathcal{S}_m} \frac{\lambda_d}{a_d} \hat{\mathbf{\Lambda}} \boldsymbol{e}_d \boldsymbol{e}_d^\top \right) \mathbb{E}_{\boldsymbol{w}}(\boldsymbol{w}\boldsymbol{w}^\top) \left(\boldsymbol{I} - \sum_{d\in\mathcal{S}_m} \frac{\lambda_d}{a_d} \hat{\mathbf{\Lambda}} \boldsymbol{e}_d \boldsymbol{e}_d^\top \right) \boldsymbol{x}_q \right] \\
&= \mathbb{E}\left[\boldsymbol{x}_q^\top \left(\boldsymbol{I} - \sum_{d\in\mathcal{S}_m} \frac{\lambda_d}{a_d} \hat{\mathbf{\Lambda}} \boldsymbol{e}_d \boldsymbol{e}_d^\top \right) \left(\boldsymbol{I} - \sum_{d\in\mathcal{S}_m} \frac{\lambda_d}{a_d} \hat{\mathbf{\Lambda}} \boldsymbol{e}_d \boldsymbol{e}_d^\top \right) \boldsymbol{x}_q \right] \\
&= \mathbb{E}\left[\boldsymbol{x}_q^\top \left(\boldsymbol{I} - 2 \sum_{d\in\mathcal{S}_m} \frac{\lambda_d}{a_d} \hat{\mathbf{\Lambda}} \boldsymbol{e}_d \boldsymbol{e}_d^\top + \left(\sum_{d\in\mathcal{S}_m} \frac{\lambda_d}{a_d} \hat{\mathbf{\Lambda}} \boldsymbol{e}_d \boldsymbol{e}_d^\top \right)^2 \right) \boldsymbol{x}_q \right].
\end{aligned} \tag{60}$$

Since $\hat{\mathbf{\Lambda}}$ is independent of $\boldsymbol{x}_q$, we can calculate the expectation of the purple and teal terms first,

$$\mathbb{E}\left(\sum_{d\in\mathcal{S}_m}\frac{\lambda_d}{a_d}\hat{\mathbf{\Lambda}}\boldsymbol{e}_d\boldsymbol{e}_d^\top\right)=\sum_{d\in\mathcal{S}_m}\frac{\lambda_d}{a_d}\mathbf{\Lambda}\boldsymbol{e}_d\boldsymbol{e}_d^\top=\sum_{d\in\mathcal{S}_m}\frac{\lambda_d^2}{a_d}\boldsymbol{e}_d\boldsymbol{e}_d^\top,$$

$$\begin{aligned}\mathbb{E}\left[\left(\sum_{d\in\mathcal{S}_m}\frac{\lambda_d}{a_d}\hat{\mathbf{\Lambda}}\boldsymbol{e}_d\boldsymbol{e}_d^\top\right)^2\right]&=\mathbb{E}\left[\sum_{d\in\mathcal{S}_m}\frac{\lambda_d^2}{a_d^2}\boldsymbol{e}_d\boldsymbol{e}_d^\top\hat{\mathbf{\Lambda}}\hat{\mathbf{\Lambda}}\boldsymbol{e}_d\boldsymbol{e}_d^\top+\sum_{d,d'\in\mathcal{S}_m,d\neq d'}\frac{\lambda_d\lambda_{d'}}{a_da_{d'}}\hat{\mathbf{\Lambda}}\boldsymbol{e}_d\boldsymbol{e}_d^\top\boldsymbol{e}_{d'}\boldsymbol{e}_{d'}^\top\hat{\mathbf{\Lambda}}\right]\\&=\sum_{d\in\mathcal{S}_m}\frac{\lambda_d^2}{a_d^2}\boldsymbol{e}_d\boldsymbol{e}_d^\top\mathbb{E}\left(\hat{\mathbf{\Lambda}}\hat{\mathbf{\Lambda}}\right)\boldsymbol{e}_d\boldsymbol{e}_d^\top+\mathbf{0}\\&=\sum_{d\in\mathcal{S}_m}\frac{\lambda_d^2}{a_d^2}\boldsymbol{e}_d\boldsymbol{e}_d^\top\sum_{d'=1}^{D}a_{d'}\boldsymbol{e}_{d'}\boldsymbol{e}_{d'}^\top\boldsymbol{e}_d\boldsymbol{e}_d^\top\\&=\sum_{d\in\mathcal{S}_m}\frac{\lambda_d^2}{a_d}\boldsymbol{e}_d\boldsymbol{e}_d^\top.\end{aligned}$$

Substituting them back into Equation (60), we get

$$\begin{aligned}\mathcal{L}(\mathcal{M}(\mathcal{S}_m))&=\mathbb{E}\left[\boldsymbol{x}_q^\top\left(\boldsymbol{I}-2\sum_{d\in\mathcal{S}_m}\frac{\lambda_d^2}{a_d}\boldsymbol{e}_d\boldsymbol{e}_d^\top+\sum_{d\in\mathcal{S}_m}\frac{\lambda_d^2}{a_d}\boldsymbol{e}_d\boldsymbol{e}_d^\top\right)\boldsymbol{x}_q\right]\\&=\mathbb{E}\left[\boldsymbol{x}_q^\top\left(\boldsymbol{I}-\sum_{d\in\mathcal{S}_m}\frac{\lambda_d^2}{a_d}\boldsymbol{e}_d\boldsymbol{e}_d^\top\right)\boldsymbol{x}_q\right]\\&=\mathbb{E}\left(\boldsymbol{x}_q^\top\boldsymbol{x}_q\right)-\sum_{d\in\mathcal{S}_m}\frac{\lambda_d^2}{a_d}\mathbb{E}\left(\boldsymbol{x}_q^\top\boldsymbol{e}_d\boldsymbol{e}_d^\top\boldsymbol{x}_q\right)\\&=\mathtt{tr}(\mathbf{\Lambda})-\sum_{d\in\mathcal{S}_m}\frac{\lambda_d^2}{a_d}\boldsymbol{e}_d^\top\mathbf{\Lambda}\boldsymbol{e}_d\\&=\mathtt{tr}(\mathbf{\Lambda})-\sum_{d\in\mathcal{S}_m}\frac{\lambda_d^3}{a_d}\end{aligned}$$

We plug in the definition of a_d in Equation (32) and arrive at the desired result:

$$\begin{aligned}\mathcal{L}(\mathcal{M}(\mathcal{S}_m))&=\mathtt{tr}(\mathbf{\Lambda})-\sum_{d\in\mathcal{S}_m}\lambda_d^3\frac{1}{\lambda_d^2}\left(1+\frac{1+\mathtt{tr}(\mathbf{\Lambda})/\lambda_d}{N}\right)^{-1}\\&=\mathtt{tr}(\mathbf{\Lambda})-\sum_{d\in\mathcal{S}_m}\lambda_d\left(1+\frac{1+\mathtt{tr}(\mathbf{\Lambda})/\lambda_d}{N}\right)^{-1}.\end{aligned}$$

■

D.5 Saddle-to-Saddle Dynamics: From $\mathcal{M}_0$ to $\mathcal{M}_1$

We denote the time at which the loss has just undergone the d-th abrupt drop as $t_d\,(d=1,\ldots,D)$, as illustrated in Figure 7.

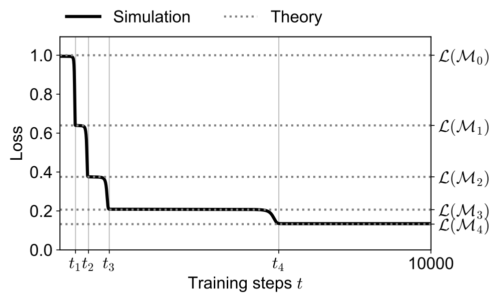

Figure 7: Illustration of $t_1, \cdots, t_D$. The loss trajectory plotted is one of the trajectories of linear attention with separate rank-one key and query in Figure 3a. The time $t_d \, (d = 1, \ldots, D)$ denotes the time when the loss has just undergone the d-th abrupt drop.

D.5.1 Alignment During the Plateau.

In the initial loss plateau, the weights have not moved much away from their small initialization and thus the training dynamics are mainly driven by the first terms in Equation (19), which are

$$\tau \dot{v}_i = \boldsymbol{k}_i^\top \boldsymbol{\Lambda}^2 \boldsymbol{q}_i + O(w_{\text{init}}^5), \tag{61a}$$

$$\tau \dot{\boldsymbol{k}}_i = v_i \boldsymbol{\Lambda}^2 \boldsymbol{q}_i + O(w_{\text{init}}^5), \tag{61b}$$

$$\tau \dot{\boldsymbol{q}}_i = v_i \boldsymbol{\Lambda}^2 \boldsymbol{k}_i + O(w_{\text{init}}^5). \tag{61c}$$

With a small initialization scale w_{init}, the key and query weights in a head evolve approximately as

$$\tau \frac{\mathrm{d}}{\mathrm{d}t} \begin{bmatrix} \boldsymbol{k}_i \\ \boldsymbol{q}_i \end{bmatrix} = v_i \begin{bmatrix} \mathbf{0} & \boldsymbol{\Lambda}^2 \\ \boldsymbol{\Lambda}^2 & \mathbf{0} \end{bmatrix} \begin{bmatrix} \boldsymbol{k}_i \\ \boldsymbol{q}_i \end{bmatrix}. \tag{62}$$

The matrix $\begin{bmatrix} \mathbf{0} & \boldsymbol{\Lambda}^2 \\ \boldsymbol{\Lambda}^2 & \mathbf{0} \end{bmatrix} \in \mathbb{R}^{2D \times 2D}$ has eigenvalues $\{\lambda_d^2, -\lambda_d^2\}_{d=1}^D$, corresponding to eigenvectors

$$\begin{bmatrix} \mathbf{0} & \boldsymbol{\Lambda}^2 \\ \boldsymbol{\Lambda}^2 & \mathbf{0} \end{bmatrix} \begin{bmatrix} \boldsymbol{e}_d \\ \boldsymbol{e}_d \end{bmatrix} = \lambda_d^2 \begin{bmatrix} \boldsymbol{e}_d \\ \boldsymbol{e}_d \end{bmatrix}, \quad \begin{bmatrix} \mathbf{0} & \boldsymbol{\Lambda}^2 \\ \boldsymbol{\Lambda}^2 & \mathbf{0} \end{bmatrix} \begin{bmatrix} \boldsymbol{e}_d \\ -\boldsymbol{e}_d \end{bmatrix} = -\lambda_d^2 \begin{bmatrix} \boldsymbol{e}_d \\ -\boldsymbol{e}_d \end{bmatrix}, \quad d = 1, \cdots, D.$$

where recall that $\lambda_d, \boldsymbol{e}_d (d = 1, \cdots, D)$ are eigenvalues and eigenvectors of $\boldsymbol{\Lambda}$. Hence, the solution to Equation (62) takes the following form

$$\begin{aligned} \begin{bmatrix} \boldsymbol{k}_i(t) \\ \boldsymbol{q}_i(t) \end{bmatrix} = & \frac{1}{2} \sum_{d=1}^D \boldsymbol{e}_d^\top \left(\boldsymbol{k}_i(0) + \boldsymbol{q}_i(0) \right) \exp\left(\frac{\lambda_d^2}{\tau} \int_0^t v_i(t') \mathrm{d}t' \right) \begin{bmatrix} \boldsymbol{e}_d \\ \boldsymbol{e}_d \end{bmatrix} \\ & + \frac{1}{2} \sum_{d=1}^D \boldsymbol{e}_d^\top \left(\boldsymbol{k}_i(0) - \boldsymbol{q}_i(0) \right) \exp\left(-\frac{\lambda_d^2}{\tau} \int_0^t v_i(t') \mathrm{d}t' \right) \begin{bmatrix} \boldsymbol{e}_d \\ -\boldsymbol{e}_d \end{bmatrix}. \end{aligned} \tag{63}$$

If $v_i > 0$, the first summation term in Equation (63) grows and the second summation term decays. The key and query weights $\boldsymbol{k}_i, \boldsymbol{q}_i$ both grow in size along the directions of the eigenvectors $\boldsymbol{e}_d$. If $v_i < 0$, the first summation term in Equation (63) decays and the second summation term grows. The key and query weights $\boldsymbol{k}_i, \boldsymbol{q}_i$ grow in opposite directions, $\boldsymbol{e}_d$ and $-\boldsymbol{e}_d$ respectively. In either case, the multiplication $v_i \boldsymbol{k}_i \boldsymbol{q}_i^\top$ grows along $\boldsymbol{e}_d \boldsymbol{e}_d^\top$.

D.5.2 Reduction to Scalar Dynamics with An Alignment Ansatz.

The dominating term in Equation (63) is the term with the largest positive eigenvalue. In other words, the key and query weights grow the fastest along the first eigenvector $\boldsymbol{e}_1$ and thus are approximately aligned with $\boldsymbol{e}_1$. Motivated by this insight, we make an ansatz that the key and query weights in a head are exactly aligned with $\boldsymbol{e}_1$ and the rest of the heads are zero[4]:

$$\boldsymbol{k}_1 = \boldsymbol{q}_1 = v_1 \boldsymbol{e}_1, \tag{64a}$$

$$\boldsymbol{k}_i = \boldsymbol{q}_i = \boldsymbol{0}, v_i = 0, \ i = 2, \cdots, H. \tag{64b}$$

Note that Equation (64) also assumes that the ℓ^2 norms of $\boldsymbol{k}_1, \boldsymbol{q}_1, v_1$ are equal, which is true under vanishing initialization due to the conservation law in Equation (79). This ansatz can greatly simplify the training dynamics and provide a good approximation of the true dynamics, where weights in one of the heads grow in scale with the key and query weights aligning with $\boldsymbol{e}_1$, while the rest of the heads remain near zero from time 0 to t_1.

We substitute the ansatz into the training dynamics in Equation (19) to reduce the high-dimensional dynamics to a one-dimensional ordinary differential equation. To do that, we first calculate the common expectation term in the training dynamics with the ansatz,

$$\boldsymbol{\Lambda}^2 - \mathbb{E}\left(\hat{\boldsymbol{\Lambda}}^2\right) \sum_{i=1}^{H} v_i \boldsymbol{k}_i \boldsymbol{q}_i^\top \boldsymbol{\Lambda} = \boldsymbol{\Lambda}^2 - \sum_{d=1}^{D} a_d \boldsymbol{e}_d \boldsymbol{e}_d^\top v_1^3 \boldsymbol{e}_1 \boldsymbol{e}_1^\top \boldsymbol{\Lambda} = \boldsymbol{\Lambda}^2 - \lambda_1 a_1 \boldsymbol{e}_1 \boldsymbol{e}_1^\top v_1^3 \tag{65}$$

where a_1 is the first eigenvalue of $\mathbb{E}(\hat{\boldsymbol{\Lambda}}^2)$ defined in Equation (32). Substituting Equations (64) and (65) into Equation (19), we find that the training dynamics of the first head simplify and the dynamics of the rest of the heads are zero

$$\begin{aligned}
\tau \dot{v}_1 &= v_1^2 \boldsymbol{e}_1^\top \left(\boldsymbol{\Lambda}^2 - \lambda_1 a_1 \boldsymbol{e}_1 \boldsymbol{e}_1^\top v_1^3\right) \boldsymbol{e}_1 = \lambda_1^2 v_1^2 - \lambda_1 a_1 v_1^5, \\
\tau \dot{\boldsymbol{k}}_1 &= v_1^2 \left(\boldsymbol{\Lambda}^2 - \lambda_1 a_1 \boldsymbol{e}_1 \boldsymbol{e}_1^\top v_1^3\right) \boldsymbol{e}_1 = \lambda_1^2 v_1^2 \boldsymbol{e}_1 - \lambda_1 a_1 v_1^5 \boldsymbol{e}_1, \\
\tau \dot{\boldsymbol{q}}_1 &= v_1^2 \left(\boldsymbol{\Lambda}^2 - \lambda_1 a_1 \boldsymbol{e}_1 \boldsymbol{e}_1^\top v_1^3\right) \boldsymbol{e}_1 = \lambda_1^2 v_1^2 \boldsymbol{e}_1 - \lambda_1 a_1 v_1^5 \boldsymbol{e}_1, \\
\dot{v}_i &= 0, \dot{\boldsymbol{k}}_i = \boldsymbol{0}, \dot{\boldsymbol{q}}_i = \boldsymbol{0}, \ i = 2, \cdots, H.
\end{aligned}$$

We further substitute in $\dot{\boldsymbol{k}}_1 = \dot{v}_1 \boldsymbol{e}_1, \dot{\boldsymbol{q}}_1 = \dot{v}_1 \boldsymbol{e}_1$ and find that the high-dimensional training dynamics reduce to one-dimensional dynamics about $v_1(t)$

$$\begin{cases} \tau \dot{v}_1 = \lambda_1^2 v_1^2 - \lambda_1 a_1 v_1^5 \\ \tau \dot{v}_1 \boldsymbol{e}_1 = \lambda_1^2 v_1^2 \boldsymbol{e}_1 - \lambda_1 a_1 v_1^5 \boldsymbol{e}_1 \\ \tau \dot{v}_1 \boldsymbol{e}_1 = \lambda_1^2 v_1^2 \boldsymbol{e}_1 - \lambda_1 a_1 v_1^5 \boldsymbol{e}_1 \end{cases} \quad \Rightarrow \quad \tau \dot{v}_1 = \lambda_1^2 v_1^2 - \lambda_1 a_1 v_1^5 \tag{66}$$

Equation (66) is a separable ordinary differential equation. By separating variables and integrating both sides, we can solve t in terms of v_1

$$\begin{aligned}
\frac{\lambda_1^2}{\tau} t &= \int \frac{1}{v_1^2 - \frac{a_1}{\lambda_1} v_1^2} \mathrm{d}v_1 \\
&= \frac{\sqrt[3]{\frac{a_1}{\lambda_1}}}{6} \left[\ln \left(\frac{\sqrt[3]{\frac{a_1^2}{\lambda_1^2}} v_1^2 + \sqrt[3]{\frac{a_1}{\lambda_1}} v_1 + 1}{\sqrt[3]{\frac{a_1^2}{\lambda_1^2}} v_1^2 - 2\sqrt[3]{\frac{a_1}{\lambda_1}} v_1 + 1} \right) - 2\sqrt{3} \tan^{-1} \left(\frac{2\sqrt[3]{\frac{a_1}{\lambda_1}} v_1 + 1}{\sqrt{3}} \right) \right] - \frac{1}{v_1}.
\end{aligned} \tag{67}$$

[4] We trivially let the head aligned with $\boldsymbol{e}_1$ to have index 1.

Since Equation (67) does not have a straight-forward inverse, we cannot obtain a general analytical solution of $v_1(t)$ in terms of t. Nonetheless, we can readily generate numerical solutions and obtain approximate analytical solutions when v_1 is near its small initialization to estimate the duration of the first loss plateau.

When v_1 is small, the dominating term in Equation (66) is $\lambda_1^2 v_1^2$ and thus the dynamics can be approximated by

$$\tau \dot{v}_i = \lambda_1^2 v_i^2 \quad \Rightarrow \quad t = \frac{\tau}{\lambda_1^2}\left(\frac{1}{v_i(0)} - \frac{1}{v_i(t)}\right).$$

At the end of the plateau, $v_1(t)$ has grown to be much larger than $v_1(0)$. Hence, the duration of the first loss plateau, t_1, is

$$t_1 \approx \frac{\tau}{\lambda_1^2 v_1(0)}. \tag{68}$$

D.6 Saddle-to-Saddle Dynamics: From $\mathcal{M}_m$ to $\mathcal{M}_{m+1}$

In Appendix D.5, we have analyzed the training dynamics from time 0 to t_1, during which the model moves from saddle $\mathcal{M}_0$ to saddle $\mathcal{M}_1$. We now analyze the general saddle-to-saddle dynamics from time t_m to t_{m+1} $(m = 0, \cdots, D-1)$, during which the model moves from $\mathcal{M}_m$ to $\mathcal{M}_{m+1}$.

D.6.1 Alignment During the Plateau.

Based on our dynamics analysis from time 0 to t_1 and by induction, the weights during the m-th plateau are approximately described by Equation (25). Namely, there are m heads whose key and query weights have grown and become aligned with the first m eigenvectors while weights in the rest of the heads have not moved much from their small initialization. Thus, similarly to Equation (57), the heads that are near small initialization have the following training dynamics

$$\begin{aligned}
\tau \dot{v}_i &= \boldsymbol{k}_i^\top \left(\sum_{d=m+1}^{D} \lambda_d^2 \boldsymbol{e}_d \boldsymbol{e}_d^\top\right) \boldsymbol{q}_i + O(w_{\text{init}}^5), \\
\tau \dot{\boldsymbol{k}}_i &= v_i \left(\sum_{d=m+1}^{D} \lambda_d^2 \boldsymbol{e}_d \boldsymbol{e}_d^\top\right) \boldsymbol{q}_i + O(w_{\text{init}}^5), \\
\tau \dot{\boldsymbol{q}}_i &= v_i \left(\sum_{d=m+1}^{D} \lambda_d^2 \boldsymbol{e}_d \boldsymbol{e}_d^\top\right) \boldsymbol{k}_i + O(w_{\text{init}}^5).
\end{aligned}$$

With a small initialization scale w_{init}, the key and query weights in this head evolve approximately as

$$\tau \frac{\mathrm{d}}{\mathrm{d}t}\begin{bmatrix} \boldsymbol{k}_i \\ \boldsymbol{q}_i \end{bmatrix} = v_i \begin{bmatrix} \mathbf{0} & \boldsymbol{\Omega} \\ \boldsymbol{\Omega} & \mathbf{0} \end{bmatrix} \begin{bmatrix} \boldsymbol{k}_i \\ \boldsymbol{q}_i \end{bmatrix}, \quad \text{where } \boldsymbol{\Omega} = \sum_{d=m+1}^{D} \lambda_d^2 \boldsymbol{e}_d \boldsymbol{e}_d^\top. \tag{69}$$

The matrix $\begin{bmatrix} \mathbf{0} & \boldsymbol{\Omega} \\ \boldsymbol{\Omega} & \mathbf{0} \end{bmatrix} \in \mathbb{R}^{2D \times 2D}$ has $2m$ zero eigenvalues and $(2D - 2m)$ nonzero eigenvalues, which are $\{\lambda_d^2, -\lambda_d^2\}_{d=m+1}^{D}$. The nonzero eigenvalues correspond to eigenvectors

$$\begin{bmatrix} \mathbf{0} & \boldsymbol{\Omega} \\ \boldsymbol{\Omega} & \mathbf{0} \end{bmatrix} \begin{bmatrix} \boldsymbol{e}_d \\ \boldsymbol{e}_d \end{bmatrix} = \lambda_d^2 \begin{bmatrix} \boldsymbol{e}_d \\ \boldsymbol{e}_d \end{bmatrix}, \quad \begin{bmatrix} \mathbf{0} & \boldsymbol{\Omega} \\ \boldsymbol{\Omega} & \mathbf{0} \end{bmatrix} \begin{bmatrix} \boldsymbol{e}_d \\ -\boldsymbol{e}_d \end{bmatrix} = -\lambda_d^2 \begin{bmatrix} \boldsymbol{e}_d \\ -\boldsymbol{e}_d \end{bmatrix}, \quad d = m+1, \cdots, D.$$

Hence, the solution to Equation (69) takes the following the form

$$\begin{aligned}\begin{bmatrix}\boldsymbol{k}_i(t)\\ \boldsymbol{q}_i(t)\end{bmatrix} &= \frac{1}{2}\sum_{d=m+1}^{D} \boldsymbol{e}_d^\top \left(\boldsymbol{k}_i(t_m)+\boldsymbol{q}_i(t_m)\right)\exp\left(\frac{\lambda_d^2}{\tau}\int_{t_m}^{t} v_i(t')\mathrm{d}t'\right)\begin{bmatrix}\boldsymbol{e}_d\\ \boldsymbol{e}_d\end{bmatrix}\\ &+\frac{1}{2}\sum_{d=m+1}^{D} \boldsymbol{e}_d^\top \left(\boldsymbol{k}_i(t_m)-\boldsymbol{q}_i(t_m)\right)\exp\left(-\frac{\lambda_d^2}{\tau}\int_{t_m}^{t} v_i(t')\mathrm{d}t'\right)\begin{bmatrix}\boldsymbol{e}_d\\ -\boldsymbol{e}_d\end{bmatrix}\\ &+\sum_{d=1}^{m} \boldsymbol{e}_d^\top \left(\boldsymbol{k}_i(t_m)+\boldsymbol{q}_i(t_m)\right)\begin{bmatrix}\boldsymbol{e}_d\\ \boldsymbol{e}_d\end{bmatrix}.\end{aligned} \tag{70}$$

For $v_i > 0$, the first term grows and the second term decays with time. The third term does not change with respect to time.

D.6.2 Reduction to Scalar Dynamics with An Alignment Ansatz.

The dominating term in Equation (70) is the term with the largest positive eigenvalue. In other words, during the $(m+1)$-th plateau, the key and query weights that are still near small initialization grow the fastest along the $(m+1)$-th eigenvector $\boldsymbol{e}_{m+1}$. Based on this insight, we make the ansatz in Equation (25). This ansatz can reduce the high-dimensional training dynamics to a one-dimensional ordinary differential equation and provides a good approximation of the true dynamics, where weights in one of the heads grow in scale with the key and query weights aligning with $\boldsymbol{e}_{m+1}$, while the rest of the heads do not change much from time t_m to t_{m+1}.

To calculate the training dynamics in Equation (19) with the ansatz, we first calculate a common term with the ansatz

$$\begin{aligned}\boldsymbol{\Lambda}^2 - \mathbb{E}\left(\hat{\boldsymbol{\Lambda}}^2\right)\sum_{i=1}^{H} v_i \boldsymbol{k}_i \boldsymbol{q}_i^\top \boldsymbol{\Lambda} &= \boldsymbol{\Lambda}^2 - \sum_{d=1}^{D} a_d \boldsymbol{e}_d \boldsymbol{e}_d^\top \left(\sum_{i=1}^{m}\frac{\lambda_d}{a_d}\boldsymbol{e}_i\boldsymbol{e}_i^\top + v_{m+1}^3 \boldsymbol{e}_{m+1}\boldsymbol{e}_{m+1}^\top\right)\boldsymbol{\Lambda}\\ &= \boldsymbol{\Lambda}^2 - \sum_{d=1}^{m}\lambda_d^2 \boldsymbol{e}_d\boldsymbol{e}_d^\top - \lambda_{m+1} a_{m+1} \boldsymbol{e}_{m+1}\boldsymbol{e}_{m+1}^\top v_{m+1}^3\end{aligned} \tag{71}$$

By substituting Equations (25) and (71) into Equation (19), we find that the dynamics for the heads with index $i \neq m+1$ are zero

$$\dot{v}_i = 0, \dot{\boldsymbol{k}}_i = \boldsymbol{0}, \dot{\boldsymbol{q}}_i = \boldsymbol{0},\ i \neq m+1.$$

For the head with index $i = m+1$, the dynamics reduce to one-dimensional dynamics about $v_i(t)$

$$\begin{aligned}
\tau \dot{v}_i &= v_i^2 \boldsymbol{e}_{m+1}^\top \left(\boldsymbol{\Lambda}^2 - \sum_{d=1}^{m} \lambda_d^2 \boldsymbol{e}_d \boldsymbol{e}_d^\top - \lambda_{m+1} a_{m+1} \boldsymbol{e}_{m+1} \boldsymbol{e}_{m+1}^\top v_i^3 \right) \boldsymbol{e}_{m+1} \\
&= \lambda_{m+1}^2 v_i^2 - \lambda_{m+1} a_{m+1} v_i^5 \\
\tau \dot{\boldsymbol{k}}_i = \tau \dot{v}_i \boldsymbol{e}_{m+1} &= v_i^2 \left(\boldsymbol{\Lambda}^2 - \sum_{d=1}^{m} \lambda_d^2 \boldsymbol{e}_d \boldsymbol{e}_d^\top - \lambda_{m+1} a_{m+1} \boldsymbol{e}_{m+1} \boldsymbol{e}_{m+1}^\top v_i^3 \right) \boldsymbol{e}_{m+1} \\
&= \lambda_{m+1}^2 v_i^2 \boldsymbol{e}_{m+1} - \lambda_{m+1} a_{m+1} v_i^5 \boldsymbol{e}_{m+1} \\
\tau \dot{\boldsymbol{q}}_i = \tau \dot{v}_i \boldsymbol{e}_{m+1} &= v_i^2 \left(\boldsymbol{\Lambda}^2 - \sum_{d=1}^{m} \lambda_d^2 \boldsymbol{e}_d \boldsymbol{e}_d^\top - \lambda_{m+1} a_{m+1} \boldsymbol{e}_{m+1} \boldsymbol{e}_{m+1}^\top v_i^3 \right) \boldsymbol{e}_{m+1} \\
&= \lambda_{m+1}^2 v_i^2 \boldsymbol{e}_{m+1} - \lambda_{m+1} a_{m+1} v_i^5 \boldsymbol{e}_{m+1} \\
\Rightarrow \quad \tau \dot{v}_i &= \lambda_{m+1}^2 v_i^2 - \lambda_{m+1} a_{m+1} v_i^5
\end{aligned} \tag{72}$$

Equation (72) is the same ordinary differential equation as Equation (66) modulo the constant coefficients. Therefore, with the same analysis, we can estimate the duration of the $(m+1)$-th loss plateau.

When v_{m+1} is small, the dominating term in Equation (72) is $\lambda_{m+1}^2 v_i^2$ and thus the dynamics is well approximated by

$$\tau \dot{v}_{m+1} = \lambda_{m+1}^2 v_{m+1}^2 \quad \Rightarrow \quad t - t_m = \frac{\tau}{\lambda_{m+1}^2} \left(\frac{1}{v_{m+1}(t_m)} - \frac{1}{v_{m+1}(t)} \right).$$

At the end of the plateau, $v_{m+1}(t_{m+1})$ has grown to be much larger than $v_{m+1}(t_m)$. Hence, the duration of the $(m+1)$-th loss plateau is

$$t_{m+1} - t_m \approx \frac{\tau}{\lambda_{m+1}^2 v_{m+1}(t_m)}. \tag{73}$$

We note that the Equation (73) involves $v_{m+1}(t_m)$, which depends on the random initialization and the dynamics from time 0 to t_m. This explains why we observe the variance of t_m increases with a larger m, that is the timing of a later abrupt loss drop varies more across random seeds as shown in Figure 3a.

D.7 Weight Configuration with Minimal L2 Norm

We prove that Equation (25) with $v_{m+1} = 0$ is the weight configuration with minimal ℓ^2 norm that satisfies Equation (23). To do this, we find the weight configuration with minimal ℓ^2 norm satisfying a general equality constrain and apply the solution to Equation (23).

Consider the equality constrained optimization problem

$$\begin{aligned}
\text{minimize} \; & \sum_{i=1}^{H} v_i^2 + \|\boldsymbol{k}_i\|^2 + \|\boldsymbol{q}_i\|^2 \\
\text{subject to} \; & \sum_{i=1}^{H} v_i \boldsymbol{k}_i \boldsymbol{q}_i^\top = \boldsymbol{A}
\end{aligned}$$

where $\boldsymbol{A}$ is a positive semi-definite matrix.

Proof. We use Lagrange multiplier to solve this equality constrained optimization problem. First, we construct the Lagrangian function $L(\boldsymbol{M})$ where the Lagrange multiplier $\boldsymbol{M} \in \mathbb{R}^{D\times D}$ is a symmetric matrix

$$\begin{aligned}L(\boldsymbol{M}) &= \frac{1}{2}\sum_{i=1}^{H}\left(v_i^2 + \|\boldsymbol{k}_i\|^2 + \|\boldsymbol{q}_i\|^2\right) + \texttt{vec}(\boldsymbol{M})^\top \texttt{vec}\left(\boldsymbol{A} - \sum_{i=1}^{H} v_i \boldsymbol{k}_i \boldsymbol{q}_i^\top\right)\\ &= \frac{1}{2}\sum_{i=1}^{H}\left(v_i^2 + \|\boldsymbol{k}_i\|^2 + \|\boldsymbol{q}_i\|^2\right) + \texttt{tr}\left[\boldsymbol{M}\left(\boldsymbol{A} - \sum_{i=1}^{H} v_i \boldsymbol{k}_i \boldsymbol{q}_i^\top\right)\right]\end{aligned}$$

Differentiating the Lagrangian with respect to all the variables and setting them to zero, we get

$$\frac{\partial L}{\partial v_i} = v_i - \boldsymbol{k}_i^\top \boldsymbol{M}\boldsymbol{q}_i = 0 \tag{74a}$$

$$\frac{\partial L}{\partial \boldsymbol{k}_i} = \boldsymbol{k}_i - v_i \boldsymbol{M}\boldsymbol{q}_i = \boldsymbol{0} \tag{74b}$$

$$\frac{\partial L}{\partial \boldsymbol{q}_i} = \boldsymbol{q}_i - v_i \boldsymbol{M}\boldsymbol{k}_i = \boldsymbol{0} \tag{74c}$$

$$\frac{\partial L}{\partial \boldsymbol{M}} = \boldsymbol{A} - \sum_{i=1}^{H} v_i \boldsymbol{k}_i \boldsymbol{q}_i^\top = 0 \tag{74d}$$

One possible solution is that the value, key, and query weights in a head are all zero

$$v_i = 0, \boldsymbol{k}_i = \boldsymbol{q}_i = \boldsymbol{0}. \tag{75}$$

If the weights are not zero, we can substitute Equation (74c) into Equation (74b) and get

$$\boldsymbol{k}_i = v_i \boldsymbol{M}\boldsymbol{q}_i = v_i^2 \boldsymbol{M}^2 \boldsymbol{k}_i,$$

which implies that $\boldsymbol{k}_i$ is an eigenvector of $\boldsymbol{M}^2$ and thus an eigenvector of $\boldsymbol{M}$. Let us denote $\boldsymbol{k}_i = \|\boldsymbol{k}_i\|\boldsymbol{e}$ where $\boldsymbol{e}$ is a normalized eigenvector of $\boldsymbol{M}$ with eigenvalue η. Substituting $\boldsymbol{k}_i = \|\boldsymbol{k}_i\|\boldsymbol{e}$ into Equations (74b) and (74c) and rearranging, we get

$$\boldsymbol{k}_i = \boldsymbol{q}_i = v_i \boldsymbol{e},\; v_i = \frac{1}{\eta}. \tag{76}$$

We now try to solve the Lagrange multiplier $\boldsymbol{M}$. Multiplying Equation (74c) by $\boldsymbol{q}_i^\top$ on the right and summing over $i = 1, \cdots, H$, we get

$$\sum_{i=1}^{H} \boldsymbol{q}_i \boldsymbol{q}_i^\top = \sum_{i=1}^{H} v_i \boldsymbol{M}\boldsymbol{k}_i \boldsymbol{q}_i^\top = \boldsymbol{M}\boldsymbol{A}. \tag{77}$$

Suppose that the query weight $\boldsymbol{q}_j$ in the j-th head is nonzero and aligns with a different eigenvector of $\boldsymbol{M}$ than $\boldsymbol{q}_i$. By multiplying Equation (77) by $\boldsymbol{q}_j^\top$ on the left, we find that $\boldsymbol{q}_j$ is an eigenvector of $\boldsymbol{A}$

$$\begin{aligned}\boldsymbol{q}_j^\top \sum_{i=1}^{H} \boldsymbol{q}_i \boldsymbol{q}_i^\top = \boldsymbol{q}_j^\top \boldsymbol{M}\boldsymbol{A} \quad \Rightarrow \quad \|\boldsymbol{q}_j\|^2 \boldsymbol{q}_j^\top &= \eta \boldsymbol{q}_j^\top \boldsymbol{A}\\ v_i^3 \boldsymbol{q}_j^\top &= \boldsymbol{q}_j^\top \boldsymbol{A}\end{aligned}$$

where we have used the fact that eigenvectors of a symmetric matrix are orthogonal to each other. Hence, Equation (76) suggests that the nonzero key and query weights are eigenvectors of matrix $\boldsymbol{A}$ and v_i^3 is equal to the corresponding eigenvalue.

For the optimization problem, the weights in each head must satisfy either Equation (75) or Equation (76). The optimal solution is that there are $H - \texttt{rank}(\boldsymbol{A})$ heads with zero weights and $\texttt{rank}(\boldsymbol{A})$ heads with nonzero weights. The nonzero heads have weights

$$\boldsymbol{k}_i = \boldsymbol{q}_i = v_i \boldsymbol{e}_i,\ v_i = \xi_i^{\frac{1}{3}}, \quad i = 1, \cdots, \texttt{rank}(\boldsymbol{A}), \tag{78}$$

where $\xi_i, \boldsymbol{e}_i$ are eigenvalues and eigenvectors of $\boldsymbol{A}$. The indices of heads can be trivially permuted. The signs of any two among $v_i, \boldsymbol{k}_i, \boldsymbol{q}_i$ can be flipped without affecting the optimization problem. ■

We apply the solution in Equation (78) to find a weight configuration with the minimal ℓ^2 norm that satisfies Equation (23). Equation (23) can be rewritten as Equation (55), namely

$$\sum_{i=1}^{H} v_i \boldsymbol{k}_i \boldsymbol{q}_i^\top = \sum_{d \in \mathcal{S}_m} \frac{\lambda_d}{a_d} \boldsymbol{e}_d \boldsymbol{e}_d^\top.$$

The matrix on the right hand side has rank m and eigenvalues and eigenvectors $\lambda_d / a_d, \boldsymbol{e}_d\ (d \in \mathcal{S}_m)$. Thus, the weight configuration with minimal ℓ^2 norm has $(H - m)$ heads with zero weights and m heads with nonzero weights. The nonzero heads have weights

$$\boldsymbol{k}_i = \boldsymbol{q}_i = v_i \boldsymbol{e}_i,\ v_i = \left(\frac{\lambda_d}{a_d}\right)^{\frac{1}{3}} = \lambda_i^{-\frac{1}{3}} \left(1 + \frac{1 + \texttt{tr}(\boldsymbol{\Lambda})/\lambda_i}{N}\right)^{-\frac{1}{3}}, \quad i = 1, \cdots, m.$$

This is the same weight configuration as Equation (25) with $v_{m+1} = 0$.

D.8 Conservation Law

The gradient flow dynamics of linear attention with separate rank-one key and query in Equation (19) implies a conservation law. The value, key, and query weights in a head obey

$$\frac{\mathrm{d}}{\mathrm{d}t}\left(\boldsymbol{k}_i^\top \boldsymbol{k}_i - \boldsymbol{q}_i^\top \boldsymbol{q}_i\right) = \boldsymbol{0}, \quad \frac{\mathrm{d}}{\mathrm{d}t}\left(\boldsymbol{k}_i^\top \boldsymbol{k}_i - v_i^2\right) = 0, \tag{79}$$

Under small initialization, the quantities $\boldsymbol{k}_i^\top \boldsymbol{k}_i - \boldsymbol{q}_i^\top \boldsymbol{q}_i \approx \boldsymbol{0}$ and $\boldsymbol{k}_i^\top \boldsymbol{k}_i - v_i^2 \approx 0$ are small at initialization and remain small throughout training. Thus, the conservation law enforces the ℓ^2 norms of the value, key, and query to be approximately the same throughout training, $\|\boldsymbol{k}_i\|^2 \approx \|\boldsymbol{q}_i\|^2 \approx v_i^2$.

We here prove that Equation (79) holds regardless of the choice of the loss function.

Proof. We can use the generic gradient flow equation in Equation (10) to calculate the gradients of $\boldsymbol{k}_i^\top \boldsymbol{k}_i, \boldsymbol{q}_i^\top \boldsymbol{q}_i$, and v_i^2,

$$\begin{aligned}
\frac{\mathrm{d}\boldsymbol{k}_i^\top \boldsymbol{k}_i}{\mathrm{d}t} &= 2\boldsymbol{k}_i^\top \frac{\mathrm{d}\boldsymbol{k}_i}{\mathrm{d}t} = 2\mathbb{E}\left(-\boldsymbol{k}_i^\top \frac{\mathrm{d}\mathcal{L}}{\mathrm{d}\hat{y}_q} \frac{\mathrm{d}\hat{y}_q}{\mathrm{d}\boldsymbol{k}_i}\right) = 2\mathbb{E}\left(-\frac{\mathrm{d}\mathcal{L}}{\mathrm{d}\hat{y}_q} v_i \boldsymbol{k}_i^\top \boldsymbol{\beta} \boldsymbol{q}_i^\top \boldsymbol{x}_q\right) \\
\frac{\mathrm{d}\boldsymbol{q}_i^\top \boldsymbol{q}_i}{\mathrm{d}t} &= 2\boldsymbol{q}_i^\top \frac{\mathrm{d}\boldsymbol{q}_i}{\mathrm{d}t} = 2\mathbb{E}\left(-\boldsymbol{q}_i^\top \frac{\mathrm{d}\mathcal{L}}{\mathrm{d}\hat{y}_q} \frac{\mathrm{d}\hat{y}_q}{\mathrm{d}\boldsymbol{q}_i}\right) = 2\mathbb{E}\left(-\frac{\mathrm{d}\mathcal{L}}{\mathrm{d}\hat{y}_q} v_i \boldsymbol{q}_i^\top \boldsymbol{x}_q \boldsymbol{k}_i^\top \boldsymbol{\beta}\right) \\
\frac{\mathrm{d}v_i^2}{\mathrm{d}t} &= 2v_i \frac{\mathrm{d}v_i}{\mathrm{d}t} = 2\mathbb{E}\left(-v_i \frac{\mathrm{d}\mathcal{L}}{\mathrm{d}\hat{y}_q} \frac{\mathrm{d}\hat{y}_q}{\mathrm{d}v_i}\right) = 2\mathbb{E}\left(-\frac{\mathrm{d}\mathcal{L}}{\mathrm{d}\hat{y}_q} v_i \boldsymbol{\beta}^\top \boldsymbol{k}_i \boldsymbol{q}_i^\top \boldsymbol{x}_q\right)
\end{aligned}$$

We see that the gradients of $\boldsymbol{k}_i^\top \boldsymbol{k}_i, \boldsymbol{q}_i^\top \boldsymbol{q}_i$, and v_i^2 are equal, regardless of the specific choice of the loss function $\mathcal{L}$. Hence, the following conservation law holds for any loss function:

$$\frac{\mathrm{d}}{\mathrm{d}t}\left(\boldsymbol{k}_i^\top \boldsymbol{k}_i - \boldsymbol{q}_i^\top \boldsymbol{q}_i\right) = \boldsymbol{0}, \quad \frac{\mathrm{d}}{\mathrm{d}t}\left(\boldsymbol{k}_i^\top \boldsymbol{k}_i - v_i^2\right) = 0.$$

■

E Linear Attention with Separate Low-Rank Key and Query

E.1 Justification for Zero Blocks Assumption

We initialize $\boldsymbol{v}_i = \boldsymbol{0}, k_{i,r} = 0\,(i = 1, \cdots, H, r = 1, \cdots, R)$, and prove that they will stay zero throughout training.

Proof. The bottom right entry of the output of linear attention with separate rank-R key and query is

$$\begin{aligned}
\hat{y}_q &\equiv \mathsf{ATTN}_{\mathsf{S}}(\boldsymbol{X})_{D+1,N+1} \\
&= \sum_{i=1}^{H} \begin{bmatrix} \boldsymbol{v}_i^\top & v_i \end{bmatrix} \begin{bmatrix} \frac{1}{N}\left(\boldsymbol{x}_q \boldsymbol{x}_q^\top + \sum_n \boldsymbol{x}_n \boldsymbol{x}_n^\top\right) & \frac{1}{N}\sum_n \boldsymbol{x}_n y_n \\ \frac{1}{N}\sum_n y_n \boldsymbol{x}_n^\top & \frac{1}{N}\sum_n y_n^2 \end{bmatrix} \begin{bmatrix} \boldsymbol{k}_{i,1} & \cdots & \boldsymbol{k}_{i,R} \\ k_{i,1} & \cdots & k_{i,R} \end{bmatrix} \begin{bmatrix} \boldsymbol{q}_{i,1}^\top \\ \vdots \\ \boldsymbol{q}_{i,R}^\top \end{bmatrix} \boldsymbol{x}_q \\
&= \sum_{i=1}^{H} \left(\boldsymbol{v}_i^\top \left(\hat{\boldsymbol{\Lambda}} + \frac{1}{N}\boldsymbol{x}_q \boldsymbol{x}_q^\top\right) \sum_{r=1}^{R} \boldsymbol{k}_{i,r} \boldsymbol{q}_{i,r}^\top + v_i \boldsymbol{\beta}^\top \sum_{r=1}^{R} \boldsymbol{k}_{i,r} \boldsymbol{q}_{i,r}^\top + \boldsymbol{v}_i^\top \boldsymbol{\beta} \sum_{r=1}^{R} k_{i,r} \boldsymbol{q}_{i,r}^\top + v_i \boldsymbol{w}^\top \hat{\boldsymbol{\Lambda}} \boldsymbol{w} \sum_{r=1}^{R} k_{i,r} \boldsymbol{q}_{i,r}^\top \right) \boldsymbol{x}_q
\end{aligned}$$

If we initialize $\boldsymbol{v}_i = \boldsymbol{0}, k_{i,r} = 0$, $\hat{y}_q$ is

$$\hat{y}_q = \sum_{i=1}^{H} \sum_{r=1}^{R} v_i \boldsymbol{\beta}^\top \boldsymbol{k}_{i,r} \boldsymbol{q}_{i,r}^\top \boldsymbol{x}_q = \boldsymbol{w}^\top \hat{\boldsymbol{\Lambda}} \sum_{i=1}^{H} \sum_{r=1}^{R} v_i \boldsymbol{k}_{i,r} \boldsymbol{q}_{i,r}^\top \boldsymbol{x}_q.$$

We now calculate the gradient updates of $\boldsymbol{v}_i = \boldsymbol{0}, k_{i,r} = 0$ and prove their gradients are zero if their initialization is zero. The gradient update of $\boldsymbol{v}_i$ contains $\mathbb{E}(\boldsymbol{w})$, which is zero as defined in Equation (3). Similarly to Equation (39), we have

$$\begin{aligned}
\tau \dot{\boldsymbol{v}}_i &= \mathbb{E}\left[(y_q - \hat{y}_q) \left(\left(\hat{\boldsymbol{\Lambda}} + \frac{1}{N}\boldsymbol{x}_q \boldsymbol{x}_q^\top\right) \sum_{r=1}^{R} \boldsymbol{k}_{i,r} \boldsymbol{q}_{i,r}^\top + \boldsymbol{\beta} \sum_{r=1}^{R} k_{i,r} \boldsymbol{q}_{i,r}^\top \right) \boldsymbol{x}_q \right] \\
&= \mathbb{E}\left[\left(\boldsymbol{w}^\top \boldsymbol{x}_q - \boldsymbol{w}^\top \hat{\boldsymbol{\Lambda}} \sum_{i=1}^{H} \sum_{r=1}^{R} v_i \boldsymbol{k}_{i,r} \boldsymbol{q}_{i,r}^\top \boldsymbol{x}_q \right) \left(\hat{\boldsymbol{\Lambda}} + \frac{1}{N}\boldsymbol{x}_q \boldsymbol{x}_q^\top\right) \sum_{r=1}^{R} \boldsymbol{k}_{i,r} \boldsymbol{q}_{i,r}^\top \boldsymbol{x}_q \right] \\
&= \mathbb{E}_{\boldsymbol{w}}(\boldsymbol{w})^\top \mathbb{E}\left[\left(\boldsymbol{x}_q - \hat{\boldsymbol{\Lambda}} \sum_{i=1}^{H} \sum_{r=1}^{R} v_i \boldsymbol{k}_{i,r} \boldsymbol{q}_{i,r}^\top \boldsymbol{x}_q \right) \left(\hat{\boldsymbol{\Lambda}} + \frac{1}{N}\boldsymbol{x}_q \boldsymbol{x}_q^\top\right) \sum_{r=1}^{R} \boldsymbol{k}_{i,r} \boldsymbol{q}_{i,r}^\top \boldsymbol{x}_q \right] \\
&= \boldsymbol{0}.
\end{aligned}$$

The gradient update of $k_{i,r}$ contains $\mathbb{E}_{\boldsymbol{w}}\left(\boldsymbol{w}^\top \hat{\boldsymbol{\Lambda}} \boldsymbol{w} \boldsymbol{w}^\top\right)$, whose entries are linear combinations of third moments the zero-mean normal random variable $\boldsymbol{w}$, and are thus zero. Similarly to Equation (40), we have

$$\begin{aligned}
\tau \dot{k}_{i,r} &= \mathbb{E}\left[\left(\boldsymbol{v}_i^\top \boldsymbol{\beta} + v_i \boldsymbol{w}^\top \hat{\boldsymbol{\Lambda}} \boldsymbol{w}\right)(y_q - \hat{y}_q)\boldsymbol{q}_{i,r}^\top \boldsymbol{x}_q\right] \\
&= \mathbb{E}\left[v_i \boldsymbol{w}^\top \hat{\boldsymbol{\Lambda}} \boldsymbol{w}\left(\boldsymbol{w}^\top \boldsymbol{x}_q - \boldsymbol{w}^\top \hat{\boldsymbol{\Lambda}} \sum_{i=1}^{H}\sum_{r'=1}^{R} v_i \boldsymbol{k}_{i,r'} \boldsymbol{q}_{i,r'}^\top \boldsymbol{x}_q\right)\boldsymbol{q}_{i,r}^\top \boldsymbol{x}_q\right] \\
&= \mathbb{E}_{\boldsymbol{w}}\left(\boldsymbol{w}^\top \hat{\boldsymbol{\Lambda}} \boldsymbol{w}\boldsymbol{w}^\top\right)\mathbb{E}\left[v_i\left(\boldsymbol{x}_q - \hat{\boldsymbol{\Lambda}} \sum_{i=1}^{H}\sum_{r'=1}^{R} v_i \boldsymbol{k}_{i,r'} \boldsymbol{q}_{i,r'}^\top \boldsymbol{x}_q\right)\boldsymbol{q}_{i,r}^\top \boldsymbol{x}_q\right] \\
&= \mathbf{0}.
\end{aligned}$$

■

E.2 Gradient Flow Equations

Based on the gradient flow training rule in Equation (10), the gradient flow dynamics of linear attention with separate rank-R key and query is

$$\tau \dot{v}_i = \sum_{r=1}^{R} \boldsymbol{k}_{i,r}^\top \mathbb{E}\left(\boldsymbol{\beta}(y_q - \hat{y}_q)\boldsymbol{x}_q^\top\right)\boldsymbol{q}_{i,r} = \sum_{r=1}^{R} \boldsymbol{k}_{i,r}^\top \left(\boldsymbol{\Lambda}^2 - \mathbb{E}\left(\hat{\boldsymbol{\Lambda}}^2\right)\sum_{i=1}^{H}\sum_{r'=1}^{R} v_i \boldsymbol{k}_{i,r'} \boldsymbol{q}_{i,r'}^\top \boldsymbol{\Lambda}\right)\boldsymbol{q}_{i,r}, \tag{80a}$$

$$\tau \dot{\boldsymbol{k}}_{i,r} = v_i \mathbb{E}\left(\boldsymbol{\beta}(y_q - \hat{y}_q)\boldsymbol{x}_q^\top\right)\boldsymbol{q}_{i,r} = v_i\left(\boldsymbol{\Lambda}^2 - \mathbb{E}\left(\hat{\boldsymbol{\Lambda}}^2\right)\sum_{i=1}^{H}\sum_{r'=1}^{R} v_i \boldsymbol{k}_{i,r'} \boldsymbol{q}_{i,r'}^\top \boldsymbol{\Lambda}\right)\boldsymbol{q}_{i,r}, \tag{80b}$$

$$\tau \dot{\boldsymbol{q}}_{i,r} = v_i \boldsymbol{k}_{i,r}^\top \mathbb{E}\left(\boldsymbol{\beta}(y_q - \hat{y}_q)\boldsymbol{x}_q\right) = v_i\left(\boldsymbol{\Lambda}^2 - \boldsymbol{\Lambda}\sum_{i=1}^{H}\sum_{r'=1}^{R} v_i \boldsymbol{q}_{i,r'} \boldsymbol{k}_{i,r'}^\top \mathbb{E}\left(\hat{\boldsymbol{\Lambda}}^2\right)\right)\boldsymbol{k}_{i,r}. \tag{80c}$$

where $i = 1, \cdots, H$, $r = 1, \cdots, R$, and the data statistics $\mathbb{E}\left(\hat{\boldsymbol{\Lambda}}^2\right)$ is calculated in Equation (31).

E.3 Fixed Points

We use $\mathcal{M}(\mathcal{S}_m)$ to denote a set of fixed points that correspond to learning m ($m = 0, 1, \cdots, D$) out of the D eigenvectors,

$$\mathcal{M}(\mathcal{S}_m) = \left\{ v_{1:H}, \boldsymbol{W}_{1:H}^K, \boldsymbol{W}_{1:H}^Q \middle| \text{conditions (C1)-(C3) are met} \right\}, \tag{81}$$

where the set $\mathcal{S}_m$ specifies the indices of the learned eigenvectors,

$$\mathcal{S}_m \subseteq \{1, 2, \cdots, D\},\ |\mathcal{S}_m| = m. \tag{82}$$

The three conditions for Equation (81) are:

(C1) The heads sum up to fit the eigenvectors with indices $\mathcal{S}_m$

$$\sum_{i=1}^{H}\sum_{r=1}^{R} v_i \boldsymbol{k}_{i,r} \boldsymbol{q}_{i,r}^\top = \sum_{d \in \mathcal{S}_m} \lambda_d^{-1}\left(1 + \frac{1 + \mathrm{tr}(\boldsymbol{\Lambda})/\lambda_d}{N}\right)^{-1} \boldsymbol{e}_d \boldsymbol{e}_d^\top. \tag{83}$$

(C2) For heads with a nonzero value weight, $v_i \neq 0$, $\boldsymbol{k}_{i,r}, \boldsymbol{q}_{i,r}$ ($r = 1, \cdots, R$) all lie in the span of $\{\boldsymbol{e}_d\}_{d \in \mathcal{S}_m}$.

(C3) For heads with a zero value weight, $v_i = 0$,

$$\sum_{r=1}^{R} \sum_{d \notin \mathcal{S}_m} \lambda_d^2 \boldsymbol{k}_{i,r}^\top \boldsymbol{e}_d \boldsymbol{e}_d^\top \boldsymbol{q}_{i,r} = 0. \tag{84}$$

With the same reasoning as Appendix D.3, one can show the weights satisfying these three conditions have zero gradients and thus are fixed points. Though conditions (C1,C3) do not explicitly specify the weights, they are feasible conditions. One possible weight configuration that satisfies all three conditions is to let $\boldsymbol{k}_{i,r}, \boldsymbol{q}_{i,r}$ $(r \neq 1)$ be zero and let $v_i, \boldsymbol{k}_{i,1}, \boldsymbol{q}_{i,1}$ be the same as the fixed point for linear attention with rank-one key query, where the low-rank case falls back into the rank-one case. Therefore, the fixed points described in Equation (81) are valid and feasible. Linear attention with separate rank-R key and query has the same 2^D fixed points in the function space as its rank-one counterpart.

E.4 Saddle-to-Saddle Dynamics

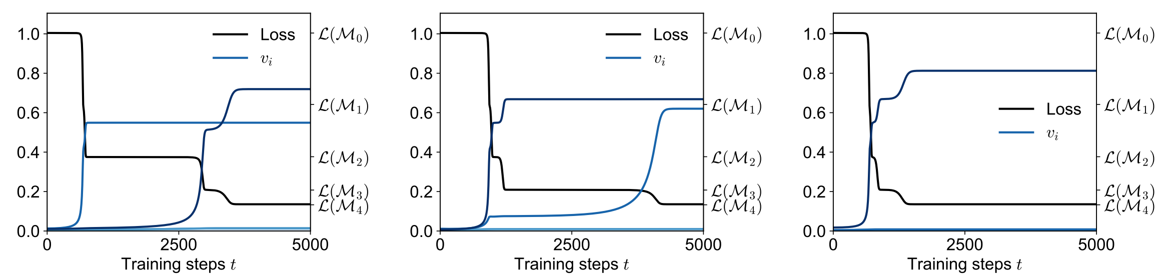

(a) $R = 2$ (b) $R = 3$ (c) $R = 4$

Figure 8: Loss and value weights trajectories. The setting is the same as Figure 3b except different ranks $R = 2, 3, 4$. In the rank-one case in Figure 3b, value weights in four heads grow, each corresponding to an abrupt loss drop from $\mathcal{L}(\mathcal{M}_m)$ to $\mathcal{L}(\mathcal{M}_{m+1})$ $(m = 0, 1, 2, 3)$. In the rank-R case, a new value weight grows big from small initialization when the loss decreases from $\mathcal{L}(\mathcal{M}_m)$ to $\mathcal{L}(\mathcal{M}_{m+1})$ for m that divides R. Here $D = 4, N = 32, H = 5$, and $\boldsymbol{\Lambda}$ has eigenvalues $0.4, 0.3, 0.2, 0.1$.

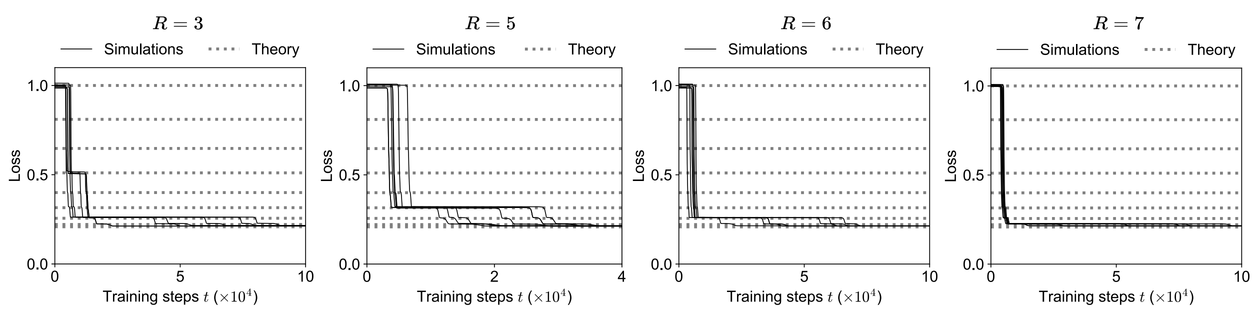

Figure 9: Loss trajectories. Same as Figure 4 but with ranks $R = 3, 5, 6, 7$. Here $D = 8, N = 32, H = 9$, $\boldsymbol{\Lambda}$ has trace 1 and eigenvalues $\lambda_d \propto d^{-1}$.

For linear attention with rank-R key and query, the gradient updates of the key and query weights in Equation (80), $\dot{\boldsymbol{k}}_{i,r}, \dot{\boldsymbol{q}}_{i,r}$, include the factor v_i, which is the shared across ranks $r = 1, \cdots, R$ but unique to each head. In linear attention with rank-one key and query initialized with small weights, the weights in a head, $v_i, \boldsymbol{k}_i, \boldsymbol{q}_i$, escape from the unstable zero fixed point to drive the first abrupt drop of loss. Similarly, in the rank-R model, the value weight v_i and a pair of key and query weights $\boldsymbol{k}_{i,r}, \boldsymbol{q}_{i,r}$ in a head escape from the zero fixed point to drive the first abrupt drop of loss.

However, the subsequent dynamics differ between the the rank-one and rank-R models. In the rank-one model, the loss will undergo a conspicuous plateau until weights in a new head, $v_{i'}, \boldsymbol{k}_{i'}, \boldsymbol{q}_{i'}$ $(i' \neq i)$, escape from the zero fixed point to grow. By contrast, in the rank-R model ($R > 1$), the loss will plateau briefly or not plateau because a new pair of key and query weights in the same i-th head, $\boldsymbol{k}_{i,r'}, \boldsymbol{q}_{i,r'}$ $(r' \neq r)$, can quickly grow to drive the loss drop. A new pair of key and query weights in the i-th head grows faster than the key and query weights in a new head, because the value weight in the i-th head, v_i, has already grown during the first abrupt loss drop. Since the gradient updates of all key and query weights in the i-th head include the factor v_i, a larger value weight leads to larger gradient updates for the associated key and query weights. We plot the value weights with $D = 4$ and ranks $R = 1, 2, 3, 4$ in Figures 3b and 8 to show: the loss drop after a conspicuous plateau corresponds to a new value weight escaping from zero, while the loss drop after a brief plateau does not.

We plot the loss trajectories with $D = 8$ and different ranks in Figure 9 to complement Figure 4 in the main text.

E.5 Conservation Law

The gradient flow dynamics of linear attention with separate key and query in Equation (80) implies a conservation law. The value, key, and query weights in a head obey

$$\frac{\mathrm{d}}{\mathrm{d}t}\left(\boldsymbol{k}_{i,r}^\top \boldsymbol{k}_{i,r} - \boldsymbol{q}_{i,r}^\top \boldsymbol{q}_{i,r}\right) = \boldsymbol{0}, \quad \frac{\mathrm{d}}{\mathrm{d}t}\left(\sum_{r=1}^{R} \boldsymbol{k}_{i,r}^\top \boldsymbol{k}_{i,r} - v_i^2\right) = 0. \tag{85}$$

We here prove that Equation (85) holds regardless of the choice of the loss function.

Proof. We can use the generic gradient flow equation in Equation (10) to calculate the relevant gradients

$$\frac{\mathrm{d}\boldsymbol{k}_{i,r}^\top \boldsymbol{k}_{i,r}}{\mathrm{d}t} = 2\boldsymbol{k}_{i,r}^\top \frac{\mathrm{d}\boldsymbol{k}_{i,r}}{\mathrm{d}t} = 2\mathbb{E}\left(-\boldsymbol{k}_i^\top \frac{\mathrm{d}\mathcal{L}}{\mathrm{d}\hat{y}_q}\frac{\mathrm{d}\hat{y}_q}{\mathrm{d}\boldsymbol{k}_{i,r}}\right) = 2\mathbb{E}\left(-\frac{\mathrm{d}\mathcal{L}}{\mathrm{d}\hat{y}_q} v_i \boldsymbol{k}_{i,r}^\top \boldsymbol{\beta} \boldsymbol{q}_{i,r}^\top \boldsymbol{x}_q\right) \tag{86a}$$

$$\frac{\mathrm{d}\boldsymbol{q}_{i,r}^\top \boldsymbol{q}_{i,r}}{\mathrm{d}t} = 2\boldsymbol{q}_{i,r}^\top \frac{\mathrm{d}\boldsymbol{q}_{i,r}}{\mathrm{d}t} = 2\mathbb{E}\left(-\boldsymbol{q}_i^\top \frac{\mathrm{d}\mathcal{L}}{\mathrm{d}\hat{y}_q}\frac{\mathrm{d}\hat{y}_q}{\mathrm{d}\boldsymbol{q}_{i,r}}\right) = 2\mathbb{E}\left(-\frac{\mathrm{d}\mathcal{L}}{\mathrm{d}\hat{y}_q} v_i \boldsymbol{q}_{i,r}^\top \boldsymbol{x}_q \boldsymbol{k}_{i,r}^\top \boldsymbol{\beta}\right) \tag{86b}$$

$$\frac{\mathrm{d}v_i^2}{\mathrm{d}t} = 2v_i \frac{\mathrm{d}v_i}{\mathrm{d}t} = 2\mathbb{E}\left(-v_i \frac{\mathrm{d}\mathcal{L}}{\mathrm{d}\hat{y}_q}\frac{\mathrm{d}\hat{y}_q}{\mathrm{d}v_i}\right) = 2\sum_{r=1}^{R}\mathbb{E}\left(-\frac{\mathrm{d}\mathcal{L}}{\mathrm{d}\hat{y}_q} v_i \boldsymbol{\beta}^\top \boldsymbol{k}_{i,r} \boldsymbol{q}_{i,r}^\top \boldsymbol{x}_q\right) \tag{86c}$$

Comparing Equations (86a) and (86b), we see that the following holds regardless of the specific choice of the loss function $\mathcal{L}$

$$\frac{\mathrm{d}\boldsymbol{k}_{i,r}^\top \boldsymbol{k}_{i,r}}{\mathrm{d}t} = \frac{\mathrm{d}\boldsymbol{q}_{i,r}^\top \boldsymbol{q}_{i,r}}{\mathrm{d}t}.$$

Similarly, comparing Equations (86a) and (86b) with Equation (86c), we obtain

$$\sum_{r=1}^{R} \frac{\mathrm{d}\boldsymbol{k}_{i,r}^\top \boldsymbol{k}_{i,r}}{\mathrm{d}t} = \frac{\mathrm{d}v_i^2}{\mathrm{d}t}.$$

∎

F Training Dynamics of In-Context and In-Weight Learning

For the in-context linear regression task we focused on in the main text, we sample the task vectors for all training sequences from a standard normal distribution, $\boldsymbol{w} \sim \mathcal{N}(\mathbf{0}, \boldsymbol{I})$. In this case, the linear attention model only develops in-context learning ability as shown in Figure 10a.

In Figure 10, we let the task vector for some of the training sequences be fixed and sample the rest from a standard normal distribution to elicit in-weight learning ability. We plot the training loss, in-context learning test loss, and in-weight learning test loss for varying portions of fixed task vectors in Figure 10. Unlike Figure 10a, the dynamics of in-context and in-weight learning dynamics interact and possibly compete when there are training sequences with a fixed task vector.

Technically, the consequence of fixing some of the task vectors is that Equations (39) and (40) break. In other words, we cannot assume the certain blocks of the value and the merged key-query matrices are zero as in Appendix C.1. Without the zero block assumption, the linear attention model implements

$$\hat{y}_q = \sum_{i=1}^{H} \left(\boldsymbol{v}_i^\top \left(\hat{\boldsymbol{\Lambda}} + \frac{1}{N} \boldsymbol{x}_q \boldsymbol{x}_q^\top \right) \boldsymbol{U}_i + v_i \boldsymbol{\beta}^\top \boldsymbol{U}_i + \boldsymbol{v}_i^\top \boldsymbol{\beta} \boldsymbol{u}_i^\top + v_i \frac{1}{N} \sum_{n=1}^{N} y_n^2 \boldsymbol{u}_i^\top \right) \boldsymbol{x}_q. \tag{87}$$

Equation (87) include not only a linear map of the cubic feature $\boldsymbol{z} = \texttt{vec}(\boldsymbol{\beta} \boldsymbol{x}_q^\top)$ but also linear maps of additional features, $\left(\hat{\boldsymbol{\Lambda}} + \frac{1}{N} \boldsymbol{x}_q \boldsymbol{x}_q^\top \right) \otimes \boldsymbol{x}_q$, $\frac{1}{N} \sum_{n=1}^{N} y_n^2 \boldsymbol{x}_q$. Future work could analyze the gradient descent dynamics of the model described by Equation (87), building on our results on the dynamics of in-context learning to incorporate the dynamics of in-weight learning.

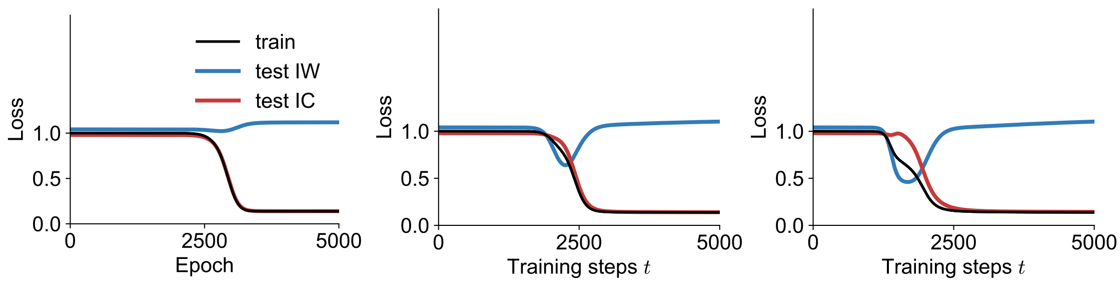

(a) 0% fixed task (in-context) (b) 20% fixed tasks (c) 40% fixed tasks

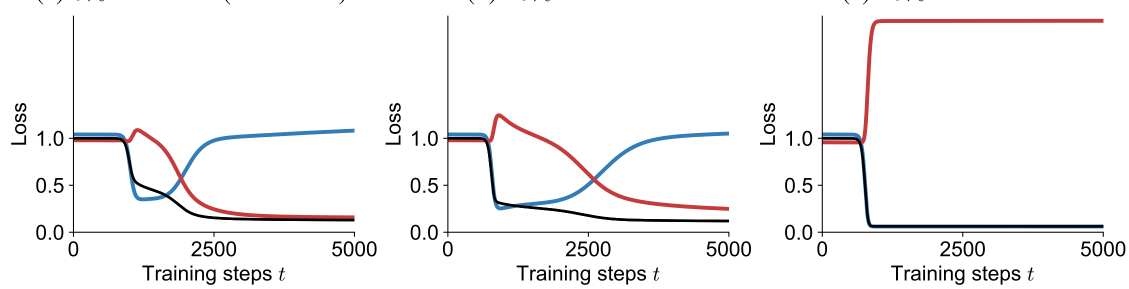

(d) 60% fixed tasks (e) 80% fixed tasks (f) 100% fixed tasks (in-weight)

Figure 10: Training loss, in-weight learning test loss, and in-context learning test loss of linear attention with merged key and query corresponding to Figure 5. The training set is the same as the in-context linear regression task described in Section 2.1 except that a portion of the task vectors $\boldsymbol{w}$ are fixed. The portion of fixed task vectors indicates how much training samples can be fitted with the in-weight learning solution, that is memorizing the fixed task vector. The in-context learning test loss is evaluated on test sequences whose task vectors are all sampled from $\mathcal{N}(\mathbf{0}, \boldsymbol{I})$. The in-weight learning test loss is evaluated on test sequences whose task vector is the same fixed task vector from the training set. Here $D = 4, N = 32, H = 8, \boldsymbol{\Lambda} = \boldsymbol{I}/D$.